Post-transcriptional regulation of the pro-apoptotic BH3-only gene *egl-1* in *C. elegans*

Yanwen Jiang

Department of Cell and Developmental Biology
Division of Biosciences
University College London

Supervisor: Prof. Barbara Conradt

A thesis submitted for the degree of
Doctor of Philosophy
University College London
November 2023

Declaration

I, Yanwen Jiang, confirm that this thesis was composed by myself and that the work presented here is my own. Where information has been derived from other sources, I confirm that this has been indicated in the thesis.

Yanwen Jiang

Abstract

During *Caenorhabditis elegans* (*C. elegans*) development, 1090 somatic cells are generated of which 131 reproducibly die, mostly through apoptosis. Apoptosis during *C. elegans* development is dependent on the conserved central apoptosis pathway, whose most upstream component is the pro-apoptotic BH3-only gene *egl-1*. Its overexpression can cause ectopic apoptosis. Unlike the other components of the central apoptosis pathway (i.e. *ced-9* BCL-2, *ced-4* Apaf-1, and *ced-3* caspase), which are broadly expressed, *egl-1* is predominantly expressed in 'cell death lineages'. It was previously demonstrated that *egl-1* BH3-only transcription is controlled by transcription factors in a 'lineage-specific' manner and initiated in mothers of cells programmed to die. After mother cell division, the number of *egl-1* transcripts increases in the daughter that is programmed to die and decreases in the daughter that survives. In addition, post-transcriptional regulation has been demonstrated to play a critical role in fine-tuning *egl-1* expression. For example, the miR-35 and miR-58 families of microRNAs repress *egl-1* expression in the mother of cells programmed to die by binding to their binding sites located in the *egl-1* 3′ UTR. The loss of these microRNAs causes precocious mother cell deaths due to the up-regulation of *egl-1* expression in mother cells.

Considering the critical roles of 3′ UTRs of mRNAs in post-transcriptional gene regulation, this study first investigates the sequence features of the *egl-1* 3′ UTR. In addition to the binding elements for miR-35 and miR-58 microRNAs, this study identifies other elements that are evolutionarily conserved among species, including four FBF-binding elements (FBEs) and a 3′ terminal element (TPTE). Mutation in any of these *cis*-acting elements leads to de-repression of the *egl-1* 3′ UTR reporter (P_{mai-2}*gfp::h2b::egl-1 3′ UTR*) whose expression is under the control of the *egl-1* 3′ UTR. Besides, the disruption of the TPTE in the endogenous *egl-1* gene causes the appearance of large cell corpses during embryo development, which is indicative of precocious mother cell death or ectopic cell death. These results indicate that the *cis*-acting elements in the *egl-1* 3′ UTR contribute to the modulation of *egl-1* expression.

Additionally, I perform a genetic screen, in which 660 genes predicted to encode RNA-binding proteins (RBPs) are individually knocked down by RNA interference (RNAi),

to identify RBPs that could be involved in the regulation of *egl-1* expression. Through this screen, five repressor candidates and two activator candidates of *egl-1* were identified. The loss of the repressor candidates up-regulates the expression of the *egl-1* 3′ UTR reporter (P_{mai-2}*gfp::h2b::egl-1 3′ UTR*) and results in the appearance of large cell corpses, which are indicative of precocious/ectopic cell death. The loss of activator candidates down-regulates the expression of the *egl-1* 3′ UTR reporter (P_{mai-2}*gfp::h2b::egl-1 3′ UTR*) and causes the survival of cells that normally die via apoptosis.

Finally, the present study describes the development of a novel method, based on the SunTag system, for the live imaging of the translation of an individual *egl-1* mRNA in real time. The SunTag system amplifies signals from the protein of interest by recruiting multiple copies of the fluorescent protein to a polypeptide scaffold that is fused to the protein of interest. Taking advantage of this method, *egl-1* mRNA translation is visualized with a high sensitivity, and the potential spatiotemporal expression pattern of *egl-1* in specific lineages where apoptotic cell death occurs is investigated.

In summary, the data presented in this work contributes to our understanding of the control of *egl-1* expression and apoptosis. In addition, the development of a method to visualize *egl-1* mRNA translation *in vivo* in developing *C. elegans* enables future research on the control of the spatiotemporal expression of *egl-1* BH3-only gene.

Impact Statement

The work described in the thesis suggests that the evolutionarily conserved elements within the 3′ untranslated region (UTR) of the mRNA of the pro-apoptotic BH3-only gene *egl-1* and RNA-binding proteins (RBPs) contribute to the control of *egl-1* expression and apoptosis in *C. elegans*. Additionally, through establishing a signal amplification method for live imaging single protein molecules, this study reveals the spatiotemporal synthesis of the BH3-only protein EGL-1 in live cells during *C. elegans* development.

This study provides valuable information for the field. First, my results add to our understanding of the control of apoptosis in *C. elegans*. *egl-1* BH3-only is the key activator of apoptotic cell death, which specifies which cells will die. Previous studies have revealed that *egl-1* transcription is regulated by transcription factors in a lineage-specific manner and that EGL-1 protein synthesis can be regulated at the post-transcriptional level by miR-35 and miR-58 families of miRNAs. As complementation, my work shows that RBPs might also contribute to the regulation of *egl-1* expression, possibly through interacting with the *egl-1* 3′ UTR.

Second, while several signal amplification methods for live imaging single protein molecules have been established in human cells cultured *in vitro* and in *Drosophila* embryos, currently there is no such method established in *C. elegans* yet. In this study, I successfully adapted and deployed the SunTag system for *C. elegans* and imaged *egl-1* mRNA translation in live cells. Visualizing a protein with low abundances in a cell (e.g., EGL-1) is always challenging. Through recruiting 18 copies of GFP at a single EGL-1 protein, this approach creates bright fluorescent signals for single-molecule EGL-1 protein imaging. This system could be utilized for other *C. elegans* proteins, which would allow the investigation of translation dynamics and subcellular localization of a given protein with a low abundance.

Outside of the field, as my study contributes to the understanding of the control of apoptotic cell death, there is a potential impact on developing treatment strategies for human diseases, such as tumors. The EGL-1 protein is a homolog of human BH3-only proteins, such as BID, BIM, and BIK, which play a crucial role in the killing of tumor cells. The combination of the delivery of BH3-only mRNA agents and the targeted

synthesis of BH3-only proteins in tumor cells could be a potential therapy for certain types of cancers.

In addition to the impact of this study in and outside the field, I would also state here that there is a big impact from the COVID-19 pandemic on my research. My lab work was disrupted in 2020 for several months during the lockdown times. Even after the lockdown periods, my work was delayed because the lab was not operating at full capacity until the summer of 2021.

Acknowledgements

Time flies, my PhD journey is nearing the end. Throughout my PhD studies, so many people have helped and influenced me.

My most profound appreciation goes to Prof. Barbara Conradt, for her time, effort, and understanding in helping me learn how to be a better researcher. Thank you, Barbara, for mentoring me over these past years both intellectually and emotionally! It has been a difficult time due to the COVID-19 pandemic when we just moved to UCL. You were so helpful! And Eric, thank you for the wise advice and great discussions! You always have an open door whenever I need help!

To my Thesis Committee: Prof. Andres Ramos and Prof. Susan Evans, thank you for your valuable direction and help with my PhD upgrade and thesis outline.

To UCL image facility: Christopher, Mike, and Alan, thank you for giving me a hand when I was encountering problems during Confocal imaging.

To other UCL people: Michael and Debbie, thank you for dealing with my concerns about my registration and degree examination!

To each member of the lab both in Munich and in London: you have made my years in Munich and London the best of my life. Thank you, Jimei, Adi, Ioannis, Jens, Madiha, Louisa and Minjia, I have spent most hours with you during my PhD time and I could not ask for a better group of colleagues. Especially Ioannis, I will never forget those evenings you stayed with me beside the confocal microscope to help me image QL.p cell divisions. And Hai, Simon, Fabian, Ryan, Stéphane, Nadin, Nadja, it has been nice time spent with you when I was in Munich. Special thanks also to the other ‘worm people’ who are not mentioned by their names!

To my closest friends in London: Haoyu, Pin, Junjie, Vincy, Jeremy, Fangjia and Jiayi, et al., I knew you guys because of playing badminton but finally we became friends. You made my life in London a lot of fun!

To my family: Dad, Mom, and Yanyue, thank you for your unwavering support and understanding over all these years, especially during my difficult time. I am grateful to have you in my life.

Contents

Introduction

Chapter 1 Introduction

1.1 Overview of programmed cell death

The word ‘death’ often brings up negative feelings. Within the human body, however, tens of billions of cells are dying every day and are replaced by new cells generated by cell division, to maintain tissue homeostasis and replace damaged cells (Nagata, 2018). Regulated cell death is often beneficial for human life. This kind of regulated cell death, including apoptosis, necroptosis, and pyroptosis, is termed programmed cell death (PCD).

1.1.1 Programmed cell death in health and disease

PCD is a crucial biological process for the elimination of unwanted or damaged cells in multicellular organisms. It plays critical roles in embryonic development, organ sculpture and maintenance, as well as the coordination of immune responses. During development, the coordinated removal of large numbers of cells provides a way for sculpting tissues and organs without disturbing neighboring constitutive cells. For example, the individualization of digits requires the elimination of the interdigital webs, which is realized through PCD (**Fig. 1.1**) (Perez-Garijo and Steller, 2015). Dysregulation of this cell death program could result in developmental disorders (Ameisen, 2002). In many organs, such as the nervous, immune, and reproductive systems, cells are overproduced and must be subsequently removed by PCD. In the developing nervous system, as many as 50% of neurons are eliminated through apoptosis and the remaining surviving neurons form neural circuits (Dekkers et al., 2013; Okouchi et al., 2007). In females, the majority of oocytes that are generated from primordial germ cells (PGCs) are culled through apoptosis or other PCD (Baum et al., 2005). Similar cases also happen in other biological processes, such as spermatogenesis (Shukla et al., 2012) and mammary morphogenesis.

PCD acts as a protective process by deleting cells that present abnormalities and are potentially dangerous. Genomic integrity is constantly threatened by DNA damage arising from environmental (e.g., UV exposure) and intrinsic (errors during

chromosome segregation) sources. Failure to repair DNA damage can cause mutations and tumors (Surova and Zhivotovsky, 2013). In this scenario, DNA damage-induced apoptosis is critical for eliminating these dangerous cells. Evading or resisting apoptotic cell death has been considered a hallmark of tumorigenesis (**Fig. 1.1**) (Goldblatt et al., 2021; Letai, 2017). T lymphocytes (T-cells) are crucial components of the immune system, which are responsible for the clearance of infected or damaged cells in the body. During T-cell maturation, any ineffective or self-reactive T-cells are removed through apoptotic cell death (Opferman and Korsmeyer, 2003). In this manner, apoptosis removes self-reactive cells to prevent autoimmunity.

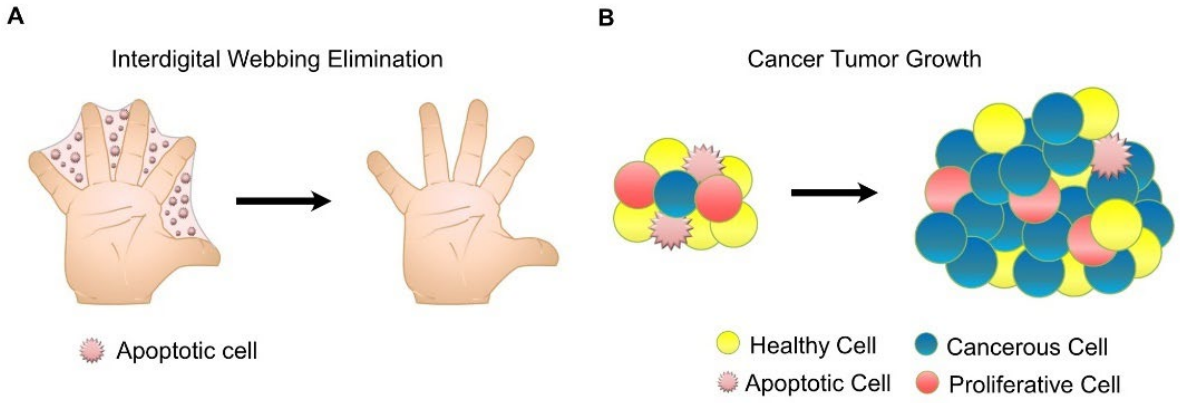

Figure 1.1 Crucial roles of apoptosis in health and disease. (A) During human embryonic development, apoptosis helps separate digits in the hands and feet. (B) Healthy tissues have a balance between mitosis and apoptosis; by contrast, the cancerous cells evading apoptosis result in tumorigenesis. Image adapted from (Goldblatt et al., 2021).

1.1.2 Classification of programs governing programmed cell death

Genetically encoded programs of PCD have been revealed in many species, including nematodes, flies, and mammals (Bender et al.. 2012). So far, many types of PCD have been revealed, including apoptosis, necroptosis, and pyroptosis, as well as others. In contrast to necrosis, which occurs in an uncontrolled manner, all types of PCD occur under the control of distinct molecular pathways.

Apoptosis is the first PCD discovered and the best-understood form of PCD. The concept of apoptosis was forged in 1972, and it was first supposed as an opposite force to mitosis to control cell populations (Kerr et al., 1972). Sulston (1976) noticed a similar type of cell death that occurs during the neuronal development of *C. elegans*. When meticulously tracking the cell lineages, he and colleagues noted that, among 1090 somatic cells generated, 131 cells died reproducibly in specific invariant lineages in developing *C. elegans* (Sulston and Horvitz, 1977; Sulston et al., 1983). In subsequent studies, Horvitz and colleagues identified a molecular genetic pathway (introduced in **section 1.2.3**) that is required for the control of cell death in *C. elegans* through the forward genetic screen (Conradt and Horvitz, 1998; Ellis and Horvitz, 1986; Hengartner et al., 1992). In parallel, *BCL-2* (B-cell lymphoma 2) gene damage was identified at the t(14;18) translocation breakpoint in human follicular B cell lymphoma (Bakhshi et al., 1985; Cleary and Sklar, 1985; Mcdonnell and Korsmeyer, 1991; Rowley, 1973, 1988; Tsujimoto et al., 1984). BCL-2 was later demonstrated to prevent apoptosis (Hockenbery et al., 1990; Vaux et al., 1988). These works provide the first evidence that PCD pathways are genetically programmed. Since then, more and more regulators of apoptosis have been uncovered.

In mammals, apoptosis is a noninflammatory cell suicide process, which is often activated by *intrinsic* factors, such as DNA damage, hypoxia, and metabolic stress (Fuchs and Steller, 2015). In this scenario, the cellular stress signals activate one or more pro-apoptotic BCL-2 homology domain 3 (BH3)-only proteins either transcriptionally, post-transcriptionally, or through post-translational modifications. Activated BH3-only proteins bind and inhibit the anti-apoptotic multi-BH BCL-2 like proteins (e.g., BCL-2, BCL-X_L, and MCL-1), thereby activating the cell death activator BAX/BAK (pro-apoptotic multi-BH proteins). Of note, certain BH3-only proteins (BID, BIM, and PUMA) can interact directly with BAX/BAK to lead to their conformational

activation (Roufayel et al., 2022). The activated BAX or BAK assembles into large complexes and forms pores on the outer mitochondrial membrane (OMM), which causes OMM permeabilization and the release of some mitochondrial proteins (e.g., cytochrome C) into the cytoplasm. These leaked mitochondrial proteins together with apoptotic adaptor Apaf-1 form the apoptosome, which induces activation of caspases, which are a class of aspartate-specific cysteine proteases. Because the activation of the canonical intrinsic apoptosis pathway is mediated by mitochondrial proteins, it is also known as the mitochondrial pathway. *Extrinsic* factors, such as tumor necrosis factor (TNF), also induce apoptosis by involving membrane receptors such as TNF receptor 1 (TNFR1), death receptors, or Toll-Like Receptors (TLRs). These two pathways converge on caspase activation. The activated caspases eventually dismantle the dying cell, resulting in irreversible cell suicide. Apoptosis in mammals has characteristic cellular changes, including plasma membrane blebbing, nuclear condensation, and the formation of apoptotic bodies (Taylor et al., 2008). Eventually, the apoptotic cell bodies are engulfed by phagocytes.

In addition to apoptosis, several other types of PCD have been discovered. Pyroptosis and necroptosis are two major examples of regulated necrosis, which are primarily described in mammalian systems. Distinct from apoptosis, they are considered inflammatory due to the release of proinflammatory intracellular contents into the extracellular space. The molecular basis of these non-apoptotic programmed cell death has been extensively reviewed (Bertheloot et al., 2021; Fuchs and Steller, 2015; Tang et al., 2019). Because they are not relevant to my study, I am not introducing them in detail here.

1.1.3 BH3-only proteins: sentinels for apoptotic cell death

The BCL-2 family of proteins represents a critical cellular checkpoint for the activation of apoptosis. The BCL-2 family includes not only anti-apoptotic members but also pro-apoptotic ones, which are classified by the homology of amino acid sequence in four α-helical regions known as BH1–BH4 (**Fig. 1.2**) (Gimenez-Cassina and Danial, 2015; Gross and Katz, 2017; Gross et al., 1999). Most of the anti-apoptotic members (e.g., BCL-2, BCL-X_L, and BCL-w) possess all four BH domains, whereas a few of them contain BH1–BH3 but not BH4. The BH1–BH3 domains in BCL-2 proteins form a hydrophobic pocket that can bind the BH3 domain present on other BCL-2 family proteins. Most of the pro-apoptotic members contain only the BH3 domain, such as BID and BIM, which are known as BH3-only proteins. In fewer cases, they contain three BH domains BH1–BH3, for example, BAX and BAK.

The list of BH3-only proteins has been expanded substantially (**Fig. 1.2**) (Lomonosova and Chinnadurai, 2008; Roufayel et al., 2022). BH3-only proteins are the initiators in the canonical intrinsic apoptosis pathway. They exert their pro-apoptotic functions by activating pro-apoptotic BAX/BAK, which is inhibited by anti-apoptotic BCL-2 proteins (Lomonosova and Chinnadurai, 2008). Of note, although most (if not all) BH3-only proteins activate BAX/BAK through binding and neutralizing anti-apoptotic BCL-2 proteins, certain (only a few) BH3-only proteins (e.g., BID, BIM, and PUMA) can also interact directly with BAX and BAK to induce their conformational activation (Roufayel et al., 2022). While BH3-only proteins have distinct binding selectivity to multi-BH proteins in different contexts, there is no doubt that their pro-apoptotic function is dependent on their BH3 domains (Chen et al., 2005).

BH3-only proteins act as initial sensors of diverse cytotoxic stress signals that stimulate apoptosis and are stringently regulated at multiple levels. For example, *Puma* and *Noxa* transcription is up-regulated by tumor suppressor p53 protein in response to various physiological and pathological stimuli (Oda et al., 2000; Wu et al., 2007; Yoo et al., 2008). The modulation of mRNA levels of the BH3-only gene at the post-transcriptional level is another regulatory mechanism for BH3-only protein production. For example, the stability of *Bim* and *Hrk* mRNA was demonstrated to be regulated by an AU-rich element (ARE) in the 3′ untranslated region (UTR) (Hughes et al., 2011; Inohara et al., 1997; Matsui et al., 2007). In a few cases, the post-

transcriptional modifications are also involved in the modulation of BH3-only protein activity or functional mode. Certain BH3-only proteins are constitutively expressed, such as BID and BAD (Danial, 2008; Yin, 2006). However, they are usually located in certain parts of the cell to exert their non-apoptotic functions (e.g., cell cycle regulation and glucose metabolism) (Chattopadhyay et al., 2001; Danial et al., 2003; Danial et al., 2008; Mok et al., 1999) and would not activate apoptosis unless they are post-translationally modified. For example, ATM and ATR kinases phosphorylate BID upon DNA damage or replicative stress (Kamer et al., 2005; Zinkel et al., 2005). In addition, phosphorylation at multiple sites modifies the BH3 region of BAD, through which it gains a higher affinity for anti-apoptotic BCL-2 family proteins (Datta et al., 2000; Lizcano et al., 2000; Tan et al., 2000; Zha et al., 1996). Similar case was also observed for human BIK (Verma et al., 2001). Overall, the current model for apoptosis activation is that various cell death stimuli activate one or more BH3-only proteins transcriptionally and/or post-transcriptionally, which integrate and transmit the cell death signal through the apoptosis pathway and eventually lead to the cell's demise.

After activation, localization of BH3-only proteins to membranes (e.g., mitochondrial and/or ER membranes) appears to be necessary for the proper activation of apoptosis (Lomonosova and Chinnadurai, 2008; Roufayel et al., 2022). Several BH3-only proteins, including BIM, BIK, and HRK, have a C-terminal hydrophobic transmembrane domain (TM) (**Fig. 1.2**), which is implicated in targeting them to membranes. Other BH3-only proteins, such as BID, BAD, and NOXA, do not harbor an obvious membrane-localization sequence. Localization of these BH3-only proteins to the mitochondria may be dependent on their interaction with BCL-2 and/or BAX/BAK located on the mitochondrial membrane.

Taken together, the activity of BH3-only proteins is spatiotemporally regulated by multiple mechanisms to ensure proper response to cell death signals. They are sentinels that connect the various stress stimuli with apoptosis activation. Studying BH3-only proteins and manipulating the apoptosis activation represents an important modality of anti-cancer drug discovery. Several BH3-mimetics have been developed for cancer therapeutics, such as Navitoclax (Tse et al., 2008) and Venetoclax (Souers et al., 2013).

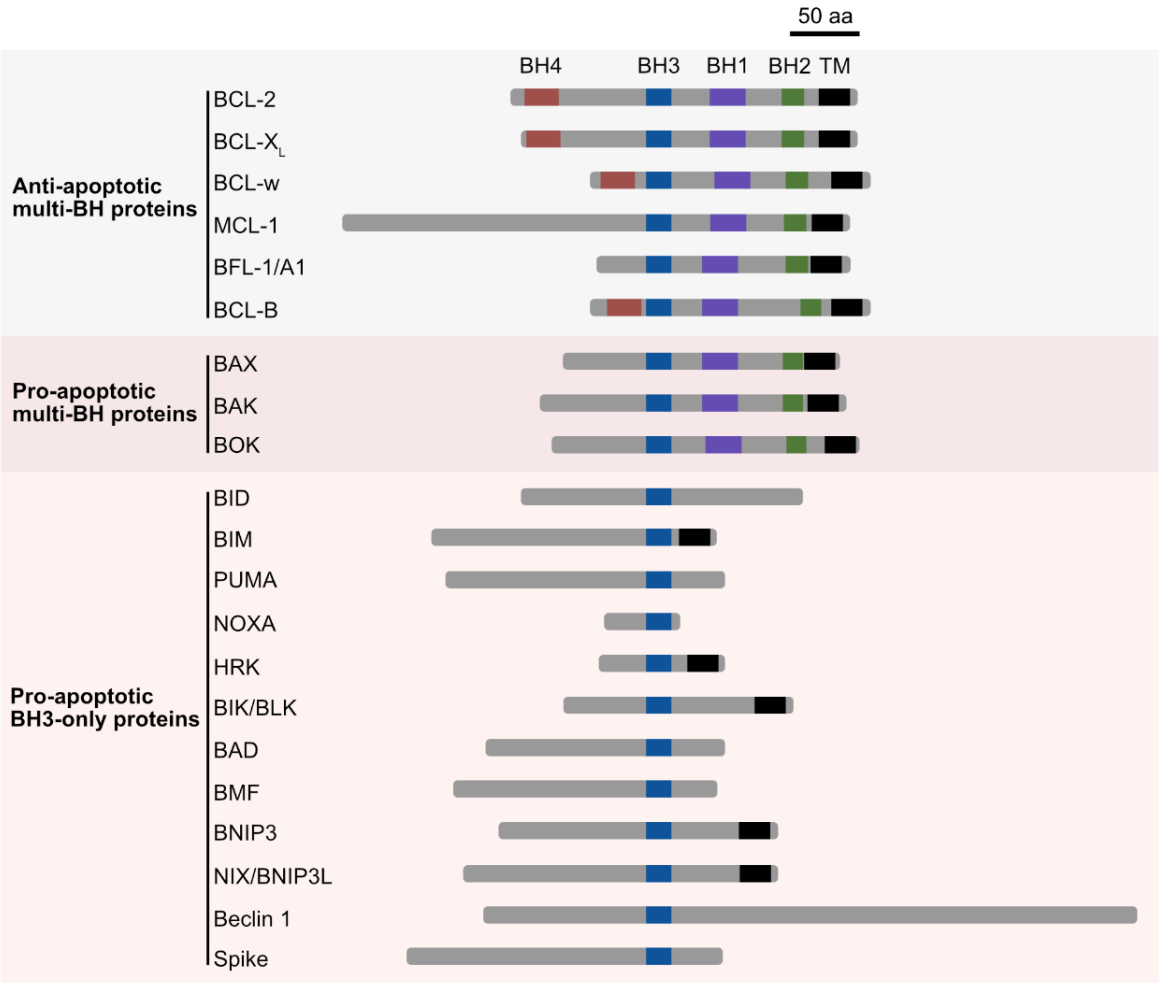

Figure 1.2 Structural and functional classification of BCL-2 family proteins in mammals. BCL-2 family proteins can be categorized into three groups based on their function and BCL-2 homology (BH) domains: anti-apoptotic multi-BH proteins (Top), pro-apoptotic multi-BH proteins (Middle), and pro-apoptotic BH3-only proteins (Bottom). Image modified from (Gimenez-Cassina and Danial, 2015).

Abbreviations: BAD, BCL-2 Associated agonist of cell Death; BAK, BCL-2 homologous Antagonist/Killer; BAX, BCL-2-Associated X protein (also known as BCL-2-like protein 4); BH, BCL-2 Homology domain; BID, BH3 Interacting-Domain death agonist; BIK, BCL-2 Interacting Killer; BIM, BCL-2 Interacting Mediator of cell death (also known as BCL-2-like protein 11); BLK, B-Lymphoid tyrosine Kinase; BMF, BCL-2 Modifying Factor; BOK, BCL-2 related Ovarian Killer; BCL-2, B-Cell Lymphoma 2; BCL-B (BCL2L10), BCL-2 Like protein 10; BCL-w (BCL2L2), BCL-2 Like protein 2; BCL-X_L, B-Cell Lymphoma-extra Large; BFL-1/A1 (BCL2L5), BCL-2 Like protein 5; BNIP3, BCL-2 interacting protein 3; HRK, Harakiri; NOXA (PMAIP1), Phorbol-12-Myristate-13-Acetate-Induced Protein 1; MCL-1, Myeloid Cell Leukemia sequence 1; PUMA, P53 Upregulated Modulator of Apoptosis; TM, TransmeMbrane domain.

1.2 *C. elegans*, an excellent model organism for studying apoptosis

1.2.1 *C. elegans* as a model organism

C. elegans is a soil nematode and is significantly simpler than a human both anatomically and genetically. However, it does share many similarities at the molecular level, for example, about 83% of the proteome was found to have human orthologs (Lai et al., 2000). In addition, it has numerous other advantages to being a model organism for delineating human gene function and elucidating biological processes.

First, it is easy to handle. *C. elegans* adults are about 1 mm in length and 65 μm in diameter. Because of their small size, a large population of *C. elegans* can be maintained in the laboratory easily in a petri-dish containing a growth medium (NGM) on which *Escherichia coli* (*E. coli*) is growing, as their natural diet is bacteria. It is also convenient to store *C. elegans* in a "starved" state for months or freeze it at -80°C or in liquid nitrogen. Second, it is powerful for genetic manipulation. The life cycle of *C. elegans* is around 3–4 days, which is quite short compared to other organisms. The self-fertilizing hermaphrodite can propagate in high numbers quickly but does not need a mate. Males can also be easily obtained for performing genetic crosses. These properties provide a unique opportunity for isolating different mutants after mutagenesis. Besides, it is quite easy to generate transgenic stains through microinjection. Moreover, *C. elegans* is transparent throughout the entire life cycle, which makes it possible to observe individual cells and their divisions, migrations, and fates using Nomarski differential interference contrast (DIC) microscopy. It has a relatively short time course of embryogenesis, which takes about 840 minutes. Due to these benefits, the complete lineage for cells generated during *C. elegans* development has been established, and it turns out to be invariant between individuals (**Fig. 1.3**) (Sulston and Horvitz, 1977; Sulston et al., 1983). This makes it possible to follow and observe individual cells using DIC microscopy to study their fate.

In addition to the above advantages, *C. elegans* has a particular benefit for studying the molecular mechanisms governing apoptosis during animal development. Apoptosis is not essential for the development of *C. elegans*, which provides a unique opportunity for identifying the activators of apoptosis by looking for extra cells (survival of cells that normally undergo apoptosis during development) after mutagenesis.

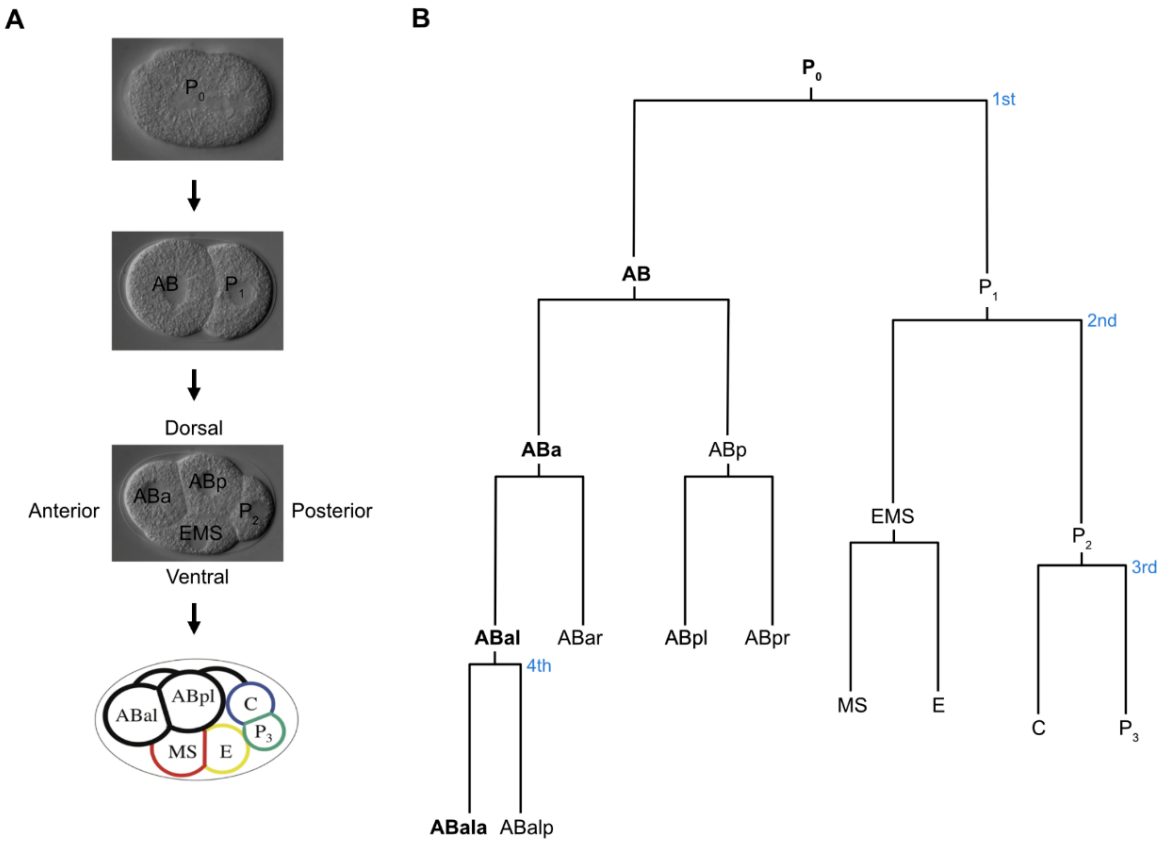

Figure 1.3 Conventional naming scheme for the invariant cell lineage during *C. elegans* development. (A) Cell positions and their lineage naming during early embryogenesis. In all images, the anterior is to the left, posterior to the right, dorsal is up, and ventral is down. The daughter cells are named by their position, e.g., ABa is the anterior daughter of AB. (B) Representative cell lineage diagram for early embryogenesis. The horizontal lines connect sibling cells; the vertical lines indicate cell cycle duration. Image modified from (Rose and Gonczy, 2014).

1.2.2 Programmed cell death during *C. elegans* development

Apoptosis during *C. elegans* development occurs in a highly reproducible pattern (**Fig. 1.4**). Sulston and colleagues followed individual cell lineages during the development of *C. elegans*, noting very reproducible somatic cell lineage trees (Sulston and Horvitz, 1977; Sulston et al., 1983). They demonstrated that, among 1090 somatic cells that are generated during *C. elegans* hermaphrodite development, precisely 131 of them are eliminated by PCD, 113 during embryogenesis and 18 during larval stages. During *C. elegans* development, nearly all PCD is achieved by apoptosis; except for the death of the male-specific linker cell, which occurs in a caspase-independent manner (Abraham et al., 2007). Most of these apoptotic cells are generated through asymmetric neuroblast divisions, which produce the larger daughter cells that normally survive and the smaller daughter cells that undergo apoptosis (Sulston et al., 1983). About 20 minutes after the mother cell division, the smaller daughter has already undergone cell death. It is rounded up and forms a cell corpse, which is refractile under the DIC microscope, making them distinguishable from surrounding surviving cells. The dead cell eventually is engulfed (internalized) and digested by a neighboring cell (**Fig. 1.5**).

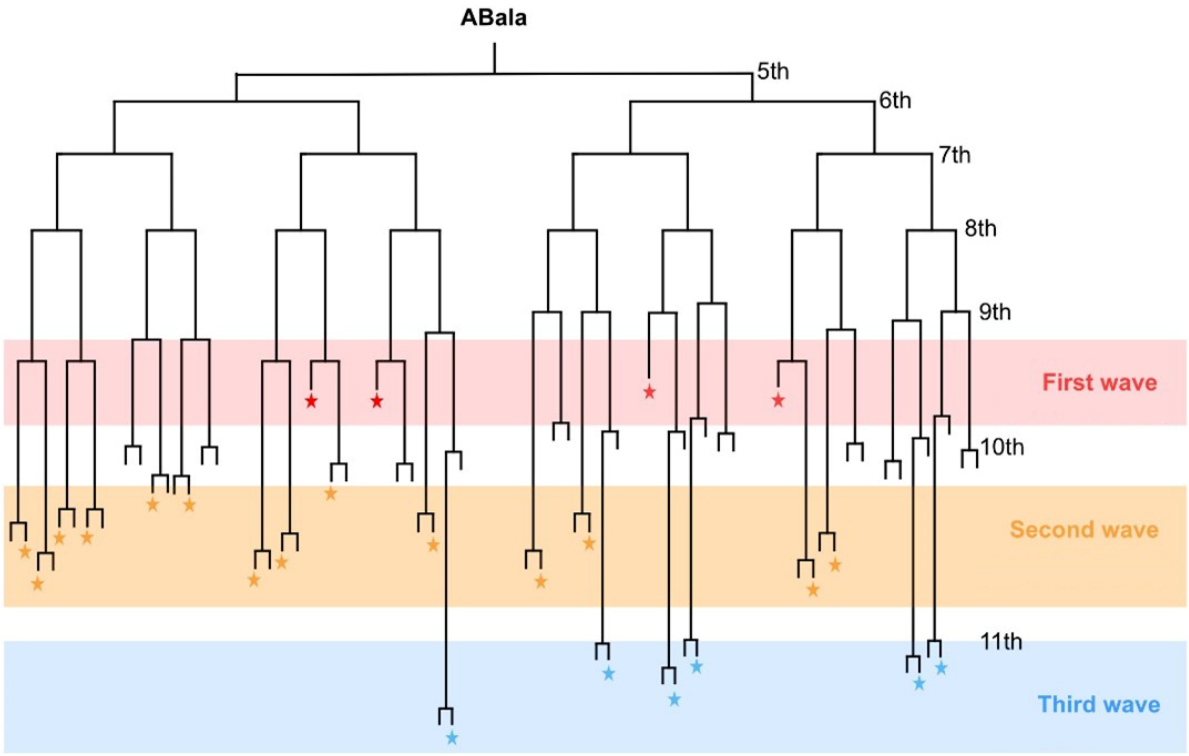

Figure 1.4 Diagram showing the apoptotic cells generated in the Abala sub-lineage during *C. celegans* embryogenesis. Cells that undergo apoptosis are indicated by colorful stars. Those that die following the 9th, 10th, and 11th embryonic cell divisions are categorized as the first wave (Red color), second wave (Yellow color), and third wave (Blue color) of cell deaths, respectively. Image made by Ryan Sherrard based on (Sulston and Horvitz, 1977; Sulston et al., 1983).

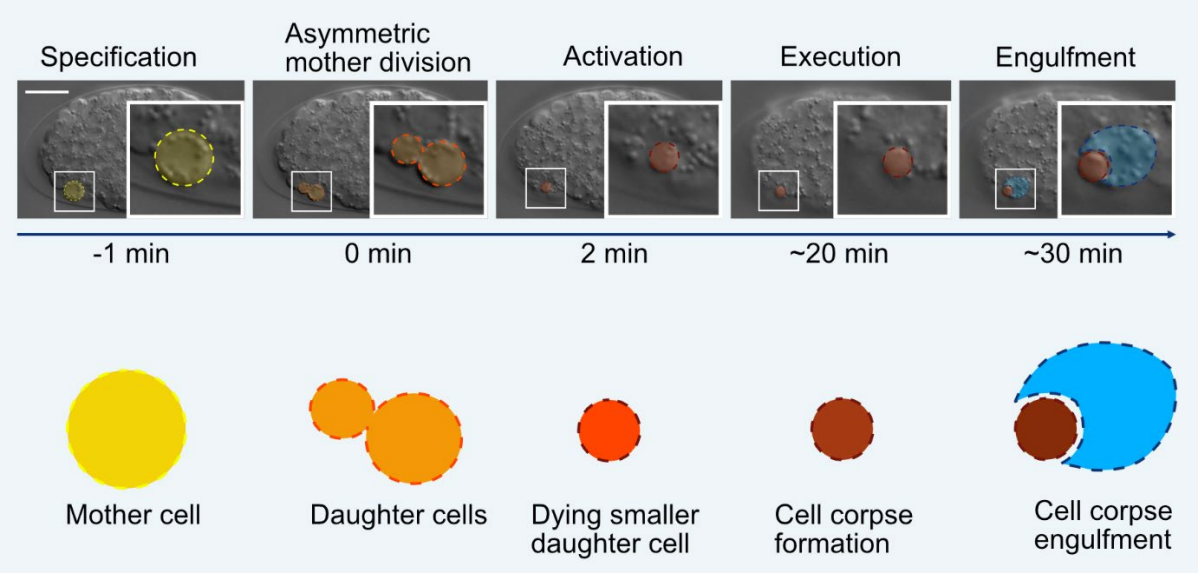

Figure 1.5 Generation and clearance of cells programmed to die during *C. celegans* development. The apoptotic cells during *C. elegans* development are mostly generated from asymmetric cell divisions. Soon after their birth, they round up and form refractile cell corpses, which are later engulfed and digested by neighboring cells. DIC images of embryos (Top) and diagrams (Bottom) are shown. Insets show 3x enlarged images. Scale bar: 10 μm.

1.2.3 Apoptosis pathway in *C. elegans*

Due to the numerus advantages of *C. elegans*, the genetic control of PCD was first evidenced by groundbreaking genetic studies in this organism. Following the observation of invariant cell death pattern in developing *C. elegans* in 1978, Horvitz and co-workers isolated the genes and established the genetic pathway responsible for this highly reproducible apoptotic cell death. This work is recognized by the Nobel Prize in Physiology or Medicine 2002. This apoptotic pathway initially established in *C. elegans* was later found highly conserved in different organisms (**Fig. 1.6**). The *C. elegans* apoptosis pathway consists of four core component genes: *egl-1* (**eg**g **l**aying defective gene **1**) encoding a BH3-only protein, *ced-9* (**ce**ll **d**eath abnormality gene **9**) encoding an anti-apoptotic BCL-2 like protein, *ced-4* encoding an Apaf-1 like protein, and *ced-3* encoding a caspase (Conradt and Horvitz, 1998; Ellis and Horvitz, 1986; Hengartner et al., 1992). In cells that normally survive, the production of the pro-apoptotic BH3-only protein EGL-1 is suppressed. The anti-apoptotic CED-9 BCL-2 protein, which resides on the OMM (Chen et al., 2000), physically sequesters the CED-4 Apaf-1 homodimer and blocks CED-4 Apaf-1 activity (Chinnaiyan et al., 1997; Yan et al., 2005). In cells destined to die, EGL-1 BH3-only protein is synthesized, and it binds and neutralizes CED-9 BCL-2 (Conradt and Horvitz, 1998). Thus, CED-4 Apaf-1 is displaced, thereby allowing CED-4 Apaf-1 to form the octameric apoptosome, which promotes the autoproteolytic activation of the CED-3 caspase (Chinnaiyan et al., 1997). Activated CED-3 caspase cleaves multiple substrates, ultimately leading to cell death execution (Conradt et al., 2016; Horvitz, 1999; Nehme and Conradt, 2008). During *C. elegans* development, *egl-1* activation is the most important step for the specification of cell death and the activation of the apoptosis program. Deregulation of *egl-1* results in ectopic activation of apoptotic cell death (Chen et al., 2000). Therefore, it is strictly controlled to avoid any ectopic cell death. Of note, in the germline, more than half of germ cells undergo apoptosis through a stochastic process without fixed cell fate specification, and *egl-1* activity is thought to be dispensable for this process (Bailly and Gartner, 2013; Gumienny et al., 1999). Nevertheless, *egl-1* is the key initiator of apoptosis activation in somatic tissues during *C. elegans* development.

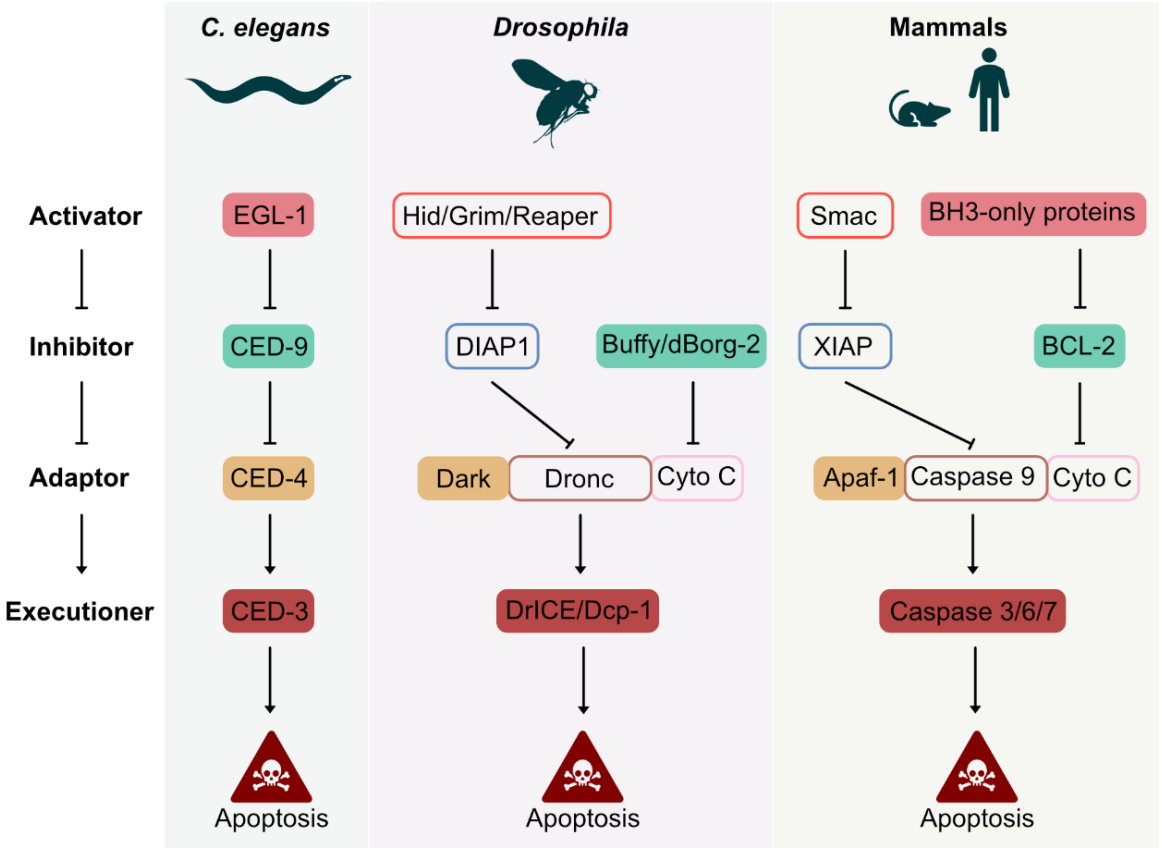

Figure 1.6 Conserved intrinsic apoptosis pathway in *C. elegans*, *Drosophila*, and mammals. In *C. elegans*, EGL-1 BH3-only protein (Light red color shapes) is synthesized in apoptotic cells, and it binds to CED-9 BCL-2 like protein (Green color shapes), thereby displacing the dimer of CED-4 Apaf-1 like protein (Yellow color shapes) from the CED-9/CED-4 complex on the outer mitochondrial membrane (OMM). CED-4 Apaf-1 forms the CED-4 octameric apoptosome, which facilitates autocatalytic activation of CED-3 caspase (Dark red color shapes). Activated CED-3 caspase cleaves multiple substrates, ultimately leading to apoptosis. The components in this pathway are largely conserved in *C. elegans*, *Drosophila*, and mammals. Other apoptosis regulators that are not identified in *C. elegans* are indicated by outlines with different colors. Of note, no BH3-only proteins have been identified in *Drosophila* so far.

Abbreviations: Apaf-1, Apoptotic Peptidase Activating Factor 1; BH, B-cell lymphoma 2 (BCL-2) Homology domain; Caspase, Cysteine-dependent ASPartate-directed proteASE; CED, Cell Death Defect; Cyto C, Cytochrome C; Dark, *Drosophila* Apaf-1 Related Killer; Dcp-1, *Drosophila* CasPase-1; DIAP1, Death-associated Inhibitor of Apoptosis Protein 1; DrICE, Death Related Interleukin-1beta-Converting Enzyme (ICE)-like caspase; Dronc, Death Regulator Nedd2-like caspase; EGL, Egg-Laying Defect; Smac, Second Mitochondria-derived Activator of Caspase; XIAP, X-linked Inhibitor of Apoptosis Protein.

1.3 Regulation of *egl-1* BH3-only expression pattern

The apoptotic pathway is highly regulated to ensure proper cell death. Unlike the other three genes (*ced-9* BCL-2, *ced-4* Apaf-1, and *ced-3* caspase) in the apoptosis pathway, which are broadly expressed, BH3-only gene *egl-1* is predominantly expressed in the cell death lineages (Conradt et al., 2016).

1.3.1 Transcriptional regulation of *egl-1* BH3-only expression

The regulation of gene expression in eukaryotes is complex, involving mechanisms that act at multiple layers from the transcription of DNA at the genomic locus (gene) to the translation of the messenger RNA (mRNA) to produce a functional protein. It has been demonstrated that *egl-1* expression is controlled extensively at the transcriptional level by transcription factors (i.e., *trans*-acting factors) (**Fig. 1.7**) (Conradt et al., 2016). It seems that *egl-1* transcription is not controlled universally by a same set of transcription factors across different cells programmed to die. Instead, each cell death lineage uses its own transcription factors to control the activation of *egl-1* transcription. The genomic locus of the *egl-1* gene has evolved to be large and complex. The *cis*-acting elements in the *egl-1* locus reported so far are found both up- and downstream of the *egl-1* coding region, even spanning beyond the neighboring genes. A comparative analysis of the genomic sequence in this region among different *Caenorhabditis* species demonstrated several conserved regions span ~14.5 kb in distance (**Fig. 1.7**). All the *cis*-acting elements of *egl-1* reported to date are within these regions (Conradt et al., 2016).

In the hermaphrodite-specific neurons (HSNs) in hermaphrodites, the zinc-finger transcription factor TRA-1 shows a higher level compared to males (Hodgkin, 1987). TRA-1 prevents the death of HSNs by directly binding to an element located 5.6 kb downstream of the *egl-1* coding region and repressing the transcription of *egl-1* in the HSNs (Conradt and Horvitz, 1999). As a result, HSNs survive in hermaphrodites. By contrast, the HSN cells die via apoptosis in males during development because the TRA-1 level is low. Mutations in the TRA-1-binding element in the *egl-1* locus result in the de-repression of *egl-1* transcription in the HSNs and causes the inappropriate

death of HSNs in hermaphrodites with a penetrance as high as 100%. In addition, a loss-of-function (lf) mutation *e1099* of *tra-1* results in a high rate (89%) of inappropriate death of HSNs in hermaphrodites. By contrast, a dominant gain-of-function (gf) mutation *e1575* of *tra-1* leads to the inappropriate survival of HSNs (up to 82%) in heterozygous males. Thus, TRA-1 modulates the transcriptional activity of *egl-1* and thereby determines the sexually dimorphic cell death fate of HSNs.

A heterodimer formed by bHLH (helix-loop-helix) proteins HLH-2/HLH-3 promotes the death of the sister cells of the neurosecretory motorneurons (NSM) (Thellmann et al., 2003). HLH-2/HLH-3 activates *egl-1* transcription by directly binding to four E boxes/Snail binding sites located 3.0 kb downstream of the *egl-1* coding region. In surviving cells, the Snail-like Zn-finger transcription factor CES-1 prevents the transcriptional activation of *egl-1* by competing with HLH-2/HLH-3 heterodimer for binding to the *egl-1* locus (Hatzold and Conradt, 2008; Thellmann et al., 2003). Knocking down *hlh-2* by RNAi leads to the inappropriate survival of NSM sister cells (up to 15%). In addition, a dominant gain-of-function (gf) mutation *n703* of *ces-1* prevents the death of the NSM sister cells (up to 100%) by blocking the HLH-2/HLH-3–dependent activation of *egl-1* transcription.

The Collier/Olf1/EBF1 (COE) transcription factor UNC-3 promotes the death of the sister cell of the dopaminergic RID neuron by directly binding to a region located 1.0 kb downstream of the *egl-1* coding region and activating *egl-1* transcription (Wang et al., 2015). A loss-of-function (lf) mutation *xd86* of *unc-3* causes the inappropriate survival of the RID sister cell (~70%).

The Six family homeodomain protein CEH-34 and the Eyes absent ortholog EYA-1 promote the death of the sister cell of the M4 motor neuron (Hirose et al., 2010). CEH-34 activates *egl-1* transcription by physically interacting with EYA-1 and binding directly to an element located 4.9 kb upstream of the *egl-1* start codon. Mutation in this binding element causes the survival of M4 sister cell (80%). Similarly, the loss of either *ceh-34* or *eya-1* also leads to the survival of M4 sister cell with a penetrance of 38% in *ceh-34*(lf) and 49% in *eya-1*(lf), respectively.

Sp1 family transcription factor SPTF-3 promotes the programmed cell death of the M4 sister and AQR sister by directly binding to an element immediately upstream of the

egl-1 start codon and activating *egl-1* transcription in a cell-specific manner (Hirose and Horvitz, 2013). A partial loss-of-function mutation *n4850* of *sptf-3* causes the survival of the M4 sister (34%) and AQR sister (18%).

A complex formed by the Hox protein MAB-5 and the Pbx homolog CEH-20 promotes the programmed cell death of the P11.aaap cell by directly binding to an element located 6 kb downstream of the *egl-1* start codon and activating *egl-1* transcription (Liu et al., 2006). Mutations in this element or in *ceh-20* or *mab-5* lead to a failure to activate *egl-1* transcription in the P11.aaap cell and cause the survival of the P11.aaap cell.

ETS domain-containing transcription factor LIN-1 promotes the death of specific cells, including the g1A sister cells (Jiang and Wu, 2014). LIN-1 directly activates the transcription of *egl-1* in these cells by binding to an element located 4 kb downstream of the *egl-1* stop codon. The loss of *lin-1* causes the survival of the g1A sisters with a penetrance of 15%.

These transcription factors often have other targets and play non-apoptotic roles during development. TRA-1 is required for sex determination (Hodgkin, 1987). CES-1 is required for the asymmetric cell division of the NSM neuroblast by targeting the MELK gene *pig-1* (Hatzold and Conradt, 2008; Wei et al., 2017) and it also modulates cell cycle progression by targeting the cyclin A gene *cya-1* (Yan et al., 2013). SPTF-3 also targets *pig-1* (Hirose and Horvitz, 2013). UNC-3 functions in neuronal differentiation, including but not limited to the RID neuron (Kim et al., 2005; Kratsios et al., 2012; Richard et al., 2011; Wang et al., 2015).

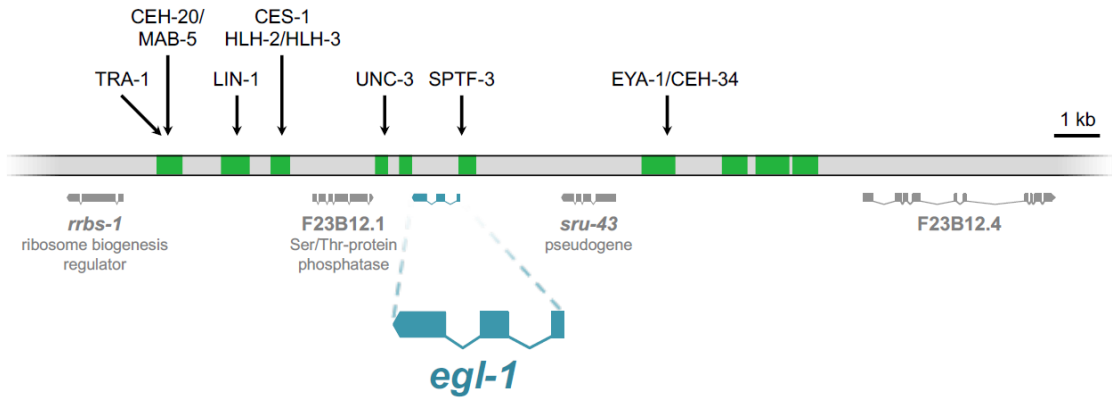

Figure 1.7 Transcriptional regulation of *egl-1* expression. The *egl-1* locus is on the minus strand of chromosome V (i.e., linkage group V, LGV). The *egl-1* coding region (1050 bp) is enlarged and colored blue. Upstream and downstream genes are shown in grey. Sequences conserved in other *Caenorhabditis* species are indicated in green. Transcription factors that have been reported to directly regulate *egl-1* transcription are indicated above their respective binding elements. Image from (Conradt et al., 2016).

Abbreviations: CEH-20, *C. Elegans* Homeobox 20; CEH-34, *C. Elegans* Homeobox 34; CES-1, CEll death Specification 1; EYA-1, *Drosophila* EYes Absent homolog 1; LIN-1, abnormal cell LINeage 1; MAB-5, Male ABnormal 5; SPTF-3, Specificity ProteinTranscription Factor 3; TRA-1, TRAnsformer 1; UNC-3, UNCoordinated 3;

1.3.2 Post-transcriptional regulation of *egl-1* BH3-only expression

In addition to transcriptional regulation, the regulation of *egl-1* expression at the post-transcriptional level is also crucial for the control of apoptotic cell death. Our lab and others have recently demonstrated that miR-35 clusters (eight members, collectively referred to as miR-35-42) and miR-58 clusters (six members miR-80, miR-58.1, miR-81, miR-82, miR-58.2 and miR-2209.1) can cooperate to repress *egl-1* expression. By binding to the binding elements in the 3′ untranslated region (UTR) of the *egl-1* mRNA, the miR-35 and miR-58 families of miRNAs repress *egl-1* expression in 'mothers' of apoptotic cells and prevent precocious mother cell death during *C. elegans* embryogenesis (Sherrard et al., 2017; Yang et al., 2020). The loss of these microRNAs results in an increase in *egl-1* mRNA levels in mother cells and causes a low rate of precocious mother cell death, indicated by the presence of large cell corpses in developing embryos. 4.6 and 10.7 large cell corpses per embryo were observed in *mir-35* and *mir-35 mir-58* double embryos, respectively. Totally, about 118 cells die via apoptosis during embryogenesis. Thus, the penetrance of the *mir-35 mir-58* double is only ~9%, which is very low compared to the penetrance of mutations in genes encoding transcriptional regulators of *egl-1*.

In addition, our lab has noticed that mutations in several sites in the *egl-1* 3′ UTR up-regulate the expression of a reporter, in which GFP expression is under the control of the *egl-1* 3′ UTR. Thus, the *egl-1* 3′ UTR and its associated RBPs may contribute to the control of *egl-1* expression at the post-transcriptional level. Our preliminary findings from the single-molecule RNA FISH experiment have shown that the *egl-1* mRNA is already transcribed in mothers of apoptotic cells in certain cell lineages, for example in the MSpaap cell and RID neuroblast. The repression by regulators, such as miRNAs, is necessary to keep the translation of the EGL-1 protein below the threshold that can trigger cell death in mothers. After mother cell division, *egl-1* mRNA copy number increases in the small daughter cell that consequently dies. The increase in *egl-1* mRNA levels is proposed to be caused by a combination of increased transcription and mRNA stabilization. By contrast, *egl-1* mRNAs are removed, possibly through degradation, in larger sibling cells that should normally survive.

1.4 Post-transcriptional regulation of gene expression

Post-transcriptional regulation of gene expression occurs at all aspects from mRNA maturation in the nucleus to translation in the cytoplasm (**Fig. 1.8**). These processes rely on interactions of the mRNA with RNA binding proteins (RBPs) and noncoding RNAs (ncRNAs), which together form a dynamic RNA-protein complex called ribonucleoprotein (RNP).

1.4.1 Regulation of mRNA splicing and polyadenylation

The nascent precursor mRNAs (pre-mRNAs) transcribed from the genome are bound by various regulatory factors and undergo a complex maturation process in the nucleus. The processing starts when the mRNA is still undergoing transcription elongation (Bentley, 2014). In eukaryotes, pre-mRNA processing begins with capping, through which a N^7-methyl-guanylate (m^7G) is added to the first nucleotide at the 5′ end. Capping is crucial not only for the splicing and export of mRNA from the nucleus but also for mRNA stability regulation and translation initiation in the cytoplasm (Jurado et al., 2014; Ramanathan et al., 2016).

Following transcription, the pre-mRNA undergoes splicing. Constitutive splicing removes intervening introns in pre-mRNAs and joins remaining exons together in the order in which they appear in a gene. However, in alternative splicing, exons might be skipped during the ligation and joined in different combinations, resulting in diverse mRNA isoforms from the same gene and thereby generating different protein products (Ast, 2004). About 90% of human protein-coding genes can undergo alternative mRNA splicing, which is much higher compared to 45% in *Drosophila* and 25% in *C. elegans* (Lee and Rio, 2015; Pan et al., 2008; Wang et al., 2008). Thus, alternative splicing provides a significant expansion of the functional proteome. The machinery that conducts pre-mRNA splicing is called the spliceosome, which comprises uridine-rich small nuclear ribonucleoprotein complexes (U snRNP) (Wahl et al., 2009). Besides, more than 150 additional regulatory proteins are involved in this process, such as SR proteins, RBM proteins, CELF proteins, and heterogeneous nuclear ribonucleoproteins (hnRNPs). All these RNPs together recognize the splice sites and

catalyze intron excision (Rogalska et al., 2023; Wahl et al., 2009). These splicing regulators are largely conserved from *C. elegans* to mammals.

Following splicing, the 3′ end of the pre-mRNA is cleaved and a poly(A) tail of 100–300 nt adenine bases is added after the cleavage site. The poly(A) tail is thought to help in mRNA export from the nucleus and to protect the mRNA from degradation by nucleases (Eckner et al., 1991; Hilleren et al., 2001). The cleavage site is usually specified by the polyadenylation signal (PAS, commonly known as AAUAAA) which is 10–30 nt upstream of it and a GU-rich element that is 20–40 nt downstream of it. These two elements and their interactors not only determine where the poly(A) tail is added but also control the length of the tail (Colgan and Manley, 1997; Elkon et al., 2013). A large complex of factors participates in the regulation of mRNA cleavage and polyadenylation. First, the cleavage/polyadenylation specificity factor (CPSF) complex recognizes and binds to the PAS in a pre-mRNA, which is enhanced by the cleavage stimulation factor (CstF). The CPSF complex recruits poly(A) polymerases (PAP) to catalyze the polyadenylation reaction (Colgan and Manley, 1997). Surprisingly, recent advances in transcriptome-wide techniques have demonstrated that a large class of mRNAs have more than one cleavage/polyadenylation site. (Shi, 2012; Wang et al., 2008). These mRNA isoforms differ in their 3′ ends. Thus, alternative polyadenylation (APA) is a common regulatory mechanism to produce mRNA isoforms with different 3′ UTRs. The usage of polyadenylation sites in an mRNA is highly tissue-specific (Sandberg et al., 2008). For example, mRNAs in neurons preferentially use distal polyadenylation sites, resulting in longer 3′ UTR isoforms whereas, mRNAs in the placenta and blood prefer to use those proximal sites, resulting in shorter 3′ UTRs (Zhang et al., 2005). Distinct 3′ UTRs interact with different regulatory factors and, thus, differentially regulate mRNA stability and translation. APA thereby extends the complexity of the transcriptome and provides an important layer of control of temporal and spatial gene regulation in diverse tissues.

Diverse mechanisms have been demonstrated to regulate APA, including *cis*-acting signals in an mRNA and *trans*-acting factors. Generally, distal polyadenylation sites prefer the canonical PAS (AAUAAA), whereas proximal polyadenylation sites preferentially use alternative PAS variants. In addition, the usage of proximal polyadenylation sites could be positively correlated with the distance between two

polyadenylation sites and negatively correlated with the transcription elongation speed (Bentley, 2014; Maniatis and Reed, 2002; Pinto et al., 2011; Shi, 2012). Moreover, certain splicing factors are involved in APA modulation, such as NOVA2 (NOVA alternative splicing regulator 2), a neuron-specific RBP (Licatalosi et al., 2008). In addition, RBPs binding near those proximal cleavage/polyadenylation sites are also involved in the modulation of APA. For example, poly(A) binding protein nuclear 1 (PABPN1), as well as ELAV proteins (e.g., HUB, HUC, and HUD) interact with proximal cleavage/polyadenylation sites, thereby repressing the cleavage and use of these proximal sites (Mansfield and Keene, 2012; Zhu et al., 2007). In contrast to PABPN1 and ELAV proteins, cytoplasmic polyadenylation element binding protein 1 (CPEB1), which is the key regulator responsible for cytoplasmic polyadenylation, was also reported to enhance the usage of proximal cleavage/polyadenylation sites during nuclear mRNA processing by binding closely to those sites and recruiting poly(A) polymerases (Bava et al., 2013). A growing body of studies has exceedingly expanded the annotation of potential polyadenylation sites genome-widely. However, the biological importance of APA is still not fully uncovered. APA did not substantially alter the mRNA stability of the genes affected and their expression level (Sandberg et al., 2008).

1.4.2 Regulation of mRNA localization, stability, and translation

Following transcription and nuclear processing, the mRNAs are exported through nuclear pores to the cytoplasm to be translated. Through the interaction with poly(A) binding proteins (PABPs), which are bound to the 3′ Poly(A) tail, and the eIF4F complex, which is bound to the 5′ cap, mRNAs maintain a stable closed-loop structural state (**Fig. 1.9**), which is crucial for the initiation of translation and the regulation of mRNA stability. These regulatory factors interact with mRNAs through RNA recognition motifs (RRM), which allow binding to a specific sequence or secondary structure of the transcript, typically in the 5′ and 3′ UTRs of the transcript. RBPs and ncRNAs are thought to regulate diverse fates of mRNAs, including localization, stability, and translation (Glisovic et al., 2008; Matoulkova et al., 2012; Shimabukuro et al., 2014). The control of mRNA localization, stability, and translation are coupled processes involving a number of regulators.

The subcellular localization of an mRNA is not only a common and efficient way to target gene products to specific regions in a cell but is also a key mechanism for cytoplasmic mRNA processing and storage (Martin and Ephrussi, 2009). The localization of mRNA is determined by the *cis*-acting elements located in the mRNA molecule. These sequence or structure elements, which are usually present in the 3′ UTR, associate with *trans*-acting regulatory factors. So far, all *trans*-acting factors that are involved in the mRNA localization process have been identified as proteins. However, this does not rule out that other regulators such as small RNAs may play a role in this process. The interaction between mRNAs and regulatory factors forms a large RNP granule. The protein factors bound to the mRNA recognize and interact with the proper subcellular structure to direct it to its destination through the use of molecular motors. Staufen protein is one of the best-characterized RBPs that regulate mRNA localization in diverse cell types (Roegiers and Jan, 2000). For example, during *Drosophila* oogenesis, Staufen associates with *oskar* mRNA and directs its localization to the posterior pole. Staufen also plays such a role in somatic cells. For example, it binds *prospero* mRNA and directs its localization during the asymmetric divisions of neuroblasts. These multiple functions of Staufen are mediated by its different RNA binding domains (RBDs). Staufen proteins have been conserved throughout evolution and harbor five double-strand RNA (dsRNA)-binding domains which appear to bind stem regions of mRNAs non-specifically. These RBDs in Staufen not only mediate the binding to RNAs but also interact with microtubules to direct RNP transport along microtubule. In addition to the famous Staufen, some other RBPs have also been identified to regulate mRNA localization, such as mammalian hnRNP A2, which has been reported to regulate the transport of mRNAs in the dendrites of neurons (Shan et al., 2003).

Localized mRNAs are open localized into large complexes containing many RNAs and proteins, called RNA granules, such as stress granules, RNA processing bodies (P-bodies), and germ granules (also known as P granules in *C. elegans*) (Anderson and Kedersha, 2009). Stress-induced translational repression allows translating ribosomes to run off the mRNAs, thereby allowing mRNAs to form stress granules (Anderson and Kedersha, 2008) or P-bodies (Franks and Lykke-Andersen, 2008). The RBPs TIA1 and TIAR contribute to stress-induced translational repression and stress granule formation (Gilks et al., 2004; Kedersha et al., 1999). Stress granules and P-bodies

share certain proteins and can contain the same species of mRNA. The major difference is that stress granules contain components of the translation initiation machinery, such as eIF3 and PABP1, whereas P-bodies contain components of the mRNA degradation machinery, such as decapping enzymes DCP1/2 and PAT1 as well as RNA-induced silencing complexes (RISCs) (Anderson and Kedersha, 2009). P granules found in the *C. elegans* P lineage and in germ cells typically contain the PGL-1 protein, which along with other constitutive components contributes to the storage and translational repression of maternal mRNAs (Gallo et al., 2008).

Modulating mRNA levels largely contributes to the regulation of protein levels. Cytoplasmic mRNA levels represent a balance between transcription and mRNA turnover. The modulation of mRNA degradation is a major regulation point in gene expression. The stabilization of mRNAs usually provides an expanded translational window for genes that need to be expressed at high levels; by contrast, mRNAs of genes expressed in short bursts in response to developmental or environmental cues have short half-lives (Guhaniyogi and Brewer, 2001). The mRNA degradation machinery consists of decapping enzymes (e.g., DCP1), deadenylases (e.g., CCR4–NOT complex), as well as 5′–3′ and 3′–5′ exoribonucleases. Many RBPs are involved in the control of mRNA degradation. AU-rich elements (AREs)-binding proteins, including AUF1, ELAV proteins (e.g., HuR), and tristetraprolin (TTP), are the major regulatory RBPs of the turnover of ARE-containing mRNAs (Chen et al., 2001). Small RNAs, such as microRNAs (miRNAs), endogenous small interfering RNA (endo-siRNA), and PIWI-interacting RNAs (piRNAs), also regulate mRNA degradation by forming the RISCs (Ramat and Simonelig, 2021; Valencia-Sanchez et al., 2006). In addition, recent discoveries have highlighted a crucial role of cellular RNA modifications in mRNA stability (Boo and Kim, 2020). To date, several RNA modifications, including N^6-methyladenosine (m^6A), $N^{6,2'}$-*O*-dimethyladenosine (m^6Am), 8-oxo-7,8-dihydroguanosine (8-oxoG), pseudouridine (Ψ), 5-methylcytidine (m^5C), and N^4-acetylcytidine (ac^4C), have been reported to regulate mRNA stability. The fate of an mRNA is determined by the coordinated actions of writer enzymes, reader RBPs, and eraser enzymes (Nachtergaele and He, 2018). All these regulatory mechanisms synergistically control the fate of an mRNA regarding mRNA decay.

Translation of mRNA into protein products can be divided into three stages, namely, initiation, elongation, and termination. The elongation and termination stages involve limited factors; however, translation initiation in eukaryotes is a complex process, which involves tens of factors (Pestova et al., 2001). Eukaryotic translation initiation factor 4G (eIF4G) interacts both with eIF4E, which is bound to the 5′ cap of the mRNA, and poly(A)-binding protein 1 (PABP1), which is bound to the poly(A) tail at the 3′ end. through these interactions, the mRNA molecule forms a circular state (**Fig. 1.9**). The eIF4G–eIF4E complex associates with eIF4A to form the cap-binding complex eIF4F, which binds to the 40S ribosomal subunit to allow translation initiation. The accessibility of eIF4E is regulated by the phosphorylation of eIF4E and eIF4E-binding proteins, such as 4E-BP. The Akt–mTOR–eIF4E axis has been reported to phosphorylate 4E-BP. Phosphorylated 4E-BP dissociates from eIF4E to allow eIF4F complex assembly (Susor et al., 2015). In addition, miRNAs extensively participate in the repression of mRNA translation by directly binding to their binding elements located in the target mRNA (Filipowicz et al., 2008). miRNAs together with Argonaute proteins form RISCs on the target mRNA and thereby promote polysome disassembly from the mRNA. Furthermore, the translation status is controlled by mRNA localization and associated RBPs. For example, during the oocyte meiotic maturation process, a large population of maternal mRNAs is translationally repressed in various RNA granules until they are needed for translation (Jiang et al., 2023). In neurons and germ cells, the switch between the active or inactive stage of an mRNA is predominantly controlled by the shortening or lengthening of the poly(A) tail, which is regulated by CPEB1 and associated factors. Thus, the translation activity of an mRNA is regulated by the coordinated actions of different mechanisms.

1.4.3 3′ UTR plays a key role in post-transcriptional regulation

UTRs are the noncoding parts of mRNAs and are less conserved than the coding sequence (CDS). However, 3′ UTRs still contain some highly conserved sequences, which are often elements required for the binding of miRNAs and RBPs. This makes the 3′ UTR a hotspot of post-transcriptional regulation and a key element in the determination of an mRNA's fate. The regulatory potential of the 3′ UTR is determined by the composition of its *cis*-acting elements (sequence and secondary structure),

which defines which and how *trans*-acting factors interact with them. The 3′ UTR has been well-known to control diverse fates of an mRNA, such as localization, destabilization, and translation. However, they may also act like noncoding RNAs as the whole 3′ UTR and/or cleaved fragments (El Mouali and Balsalobre, 2019; Mayr, 2017). All these functions of the 3′ UTR are mediated by effector proteins recruited by RBPs that bind to the 3′ UTR.

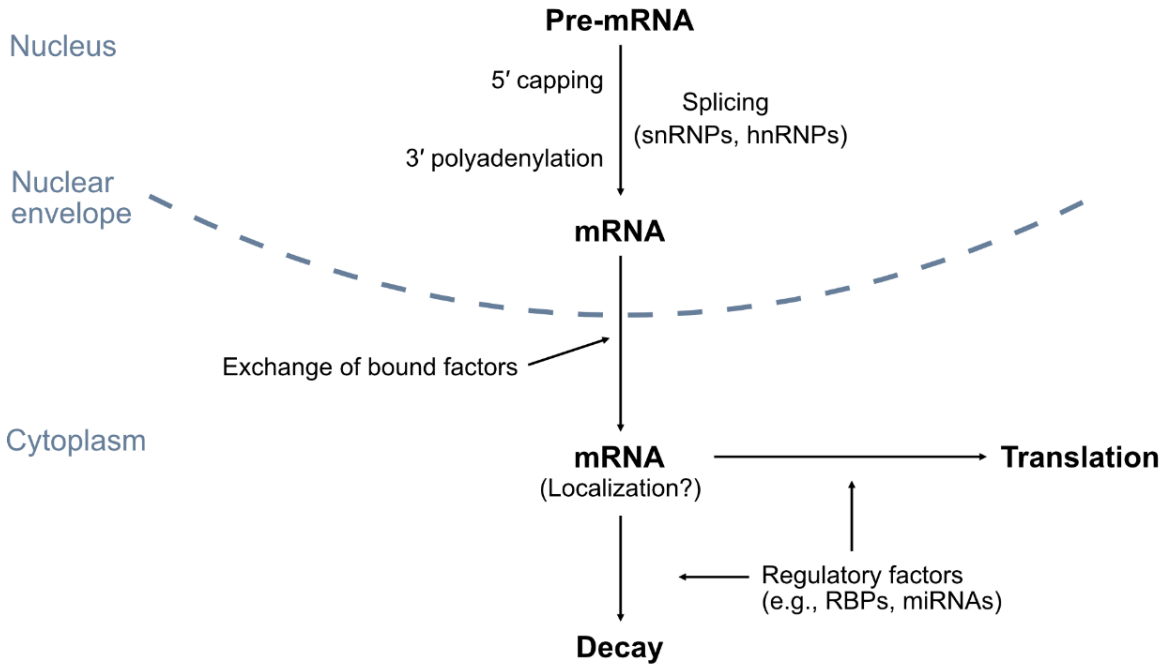

Figure 1.8 Model of post-transcriptional regulation of gene expression. Pre-mRNAs undergo capping at the 5′ end and polyadenylated at the 3′ end along with the splicing in the nucleus. Mature mRNAs are then exported from the nucleus to the cytoplasm and bound by cytoplasmic regulatory factors to regulate their localization, stability, and translation. Each of these steps is highly regulated, which relies on regulatory factors bound to the mRNA.

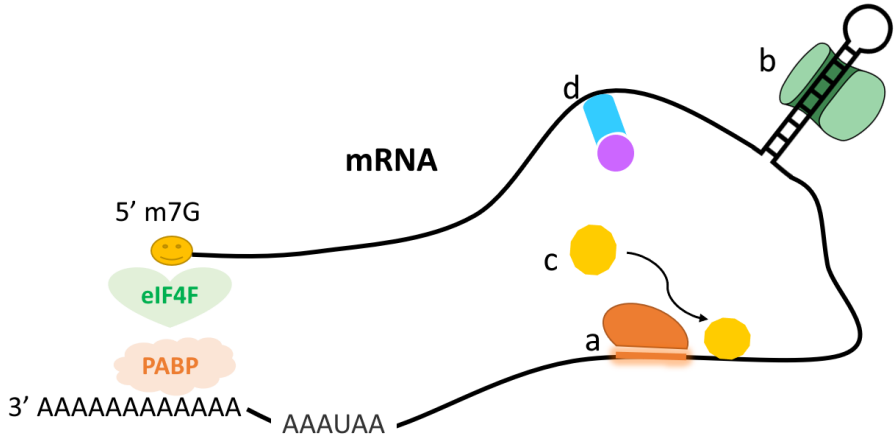

Figure 1.9 The generic structure of a eukaryotic mRNA and interactions with RNA-binding proteins (RBPs). There are four conventional ways by which RBPs bind to target mRNA: (a) direct binding to the binding elements on the target mRNA; (b) binding to a secondary structural element, such as hairpin region; (c) recruitment by a RBP currently bound on the mRNA; and (d) association with a currently bound RBP on the mRNA or binding to target mRNA as a complex (protein-protein/protein-RNA). The mRNA maintains a closed-loop structure through the interaction of RBPs bound on the 5′ cap and poly(A) tail. AAUAAA is the polyadenylation signal (PAS).

1.5 Approaches for imaging translation in live cells

Fluorescence microscopy is a powerful tool to *in vivo* investigate gene expression, subcellular protein localization, protein–protein interactions, as well as protein dynamics in real-time. Fluorescent labeling of the target protein is a precondition for protein imaging in live cells.

Fluorescent protein (FP) tagging provided the initial instrument for protein visualization in live cells. Since the gene encoding green fluorescent protein (GFP) was identified and cloned from jellyfish in 1992 (Prasher et al., 1992), an increasing number of FPs have been developed and used to image proteins of interest. By directly tagging an FP (e.g., GFP) to the protein of interest at the N- or C-terminus, the target protein fused to a FP can be imaged by fluorescence microscopy. However, protein labeling by FP fusion is not applicable for proteins with a low abundance due to limited brightness. In addition, it is basically impossible to visualize a single protein molecule by FP fusion. To overcome this issue, some elegant strategies have been developed for amplification of signals from a single protein molecule in live cells by loading multiple FPs to the target protein.

1.5.1 Live imaging of proteins with the tandem split-FP systems

The split-FP system splits the FP into two parts (one small fragment and one large fragment). Expressing either of the two does not show fluorescence unless they are complemented into a complete FP molecule upon co-expression (**Fig. 1.10A**). As an example, the split-GFP system breaks the GFP polypeptide between the 10th and the 11th β-strand into two segments, namely, GFP_{1-10} and GFP_{11}, respectively. The GFP_{11} fragment is a short, 16 amino acid (aa) peptide (the tag), and is not fluorescent by itself. The larger fragment GFP_{1-10} (the detector) is not fluorescent by itself as well because the maturation and function of chromophore requires the E222 residue present in the GFP_{11} fragment (Barondeau et al., 2003). The fluorescence can be detected only when the two parts are complemented to be a reconstituted GFP (Cabantous et al., 2005).

Tandemly arranged spit-FP tags allow amplification of fluorescence signal (**Fig. 1.10B**). He et al., (2019) utilized the tandem split-GFP system in *C. elegans* and engineered a native and tissue-specific fluorescence (NATF) strategy. In this work, a tandem array of seven copies of the GFP_{11} fragment (7× *gfp*$_{11}$) is inserted at the genomic locus of the target gene and the target protein can be visualized by co-expressing the complementing GFP_{1-10} fragment (*gfp*$_{1-10}$). 7× GFP_{11} tandem increased the signal by ~3 fold (not 7-fold as expected). Similarly, Goudeau et al., (2021) developed the Split-wrmScarlet system and showed that 3× split-wrmScarlet$_{11}$ tandem increased the signal by 2.3-fold. It could be reasonable that tandem arrangement of split-FPs could cause steric hindrance, and the complete labeling (saturation) could not be achieved. On the other hand, considering the limited affinity between the two parts of the split-FP, the complete labeling may require a very high concentration ratio between FP_{1-10} and FP_{11} fragments.

1.5.2 Live imaging of proteins with the epitope-scFv-FP systems

Antibodies can recognize and bind to short peptide sequences with high affinity and specificity. The epitope peptide sequence can be designed to differ from the endogenous protein sequence to avoid cross-reactivity. Whereas exogenously expressed antibodies generally do not fold properly, several scFv (a fusion protein of the variable region of the heavy and light chains of the antibody) antibodies have been successfully expressed in cells in a soluble form (Colby et al., 2004; Lecerf et al., 2001). By co-expressing the scFv antibody fused to a fluorescent protein, the scFv::FP fusion protein can bind to its epitopes tagged to the target protein (**Fig. 1.10C**). This allows visualization of the target protein. The magnitude of signal amplification can be modified by different numbers of repeating epitopes. Several such imaging systems have already been developed, such as the SunTag (SUperNova) (Tanenbaum et al., 2014), MoonTag (Boersma et al., 2019), FLAG SM (Morisaki et al., 2016), as well as HA SM systems (Morisaki et al., 2016; Zhao et al., 2019).

The SunTag system is composed of two parts: the tandem repeats of GCN4 v4 epitope (the tag, 19 aa, referred to as SunTag) and its scFv antibody fused to an FP (the detector) (Tanenbaum et al., 2014). This GCN4 v4 peptide tag is modified from a part

of the transcription factor GCN4. This protein imaging approach has been deployed for imaging translation in mammalian cells (Boersma et al., 2019; Tanenbaum et al., 2014; Yan et al., 2016) and fly embryos (Dufourt et al., 2021). Through tagging a peptide array containing 24xSunTag, with each epitope separated by a five amino acids spacer, to a target protein, the fluorescence intensity of the tagged protein was found to increase 24-fold. This indicates that the linker sufficiently eliminates steric hindrance and allows binding of scFv antibodies to neighboring epitopes, and therefore full antibody occupancy (saturation) can be achieved (Tanenbaum et al., 2014). Recently, this system has been applied to image protein translation dynamics in fly embryos. By introducing 32xSunTag to the Twist protein, the fluorescence signal of the tagged protein is dramatically amplified (Dufourt et al., 2021). Although the coding sequence for both the SunTag and the scFv antibody may need to be optimized to allow successful expression in different organisms, this system is versatile.

The MoonTag system is a sister version of the SunTag system, which consists of tandem repeats of gp41 epitope (the tag, 15 aa, referred to as the MoonTag) and its scFv antibody fused to an FP (the detector) (Boersma et al., 2019). The gp41 peptide tag is modified from the HIV coat protein complex subunit gp41 (Lutje Hulsik et al., 2013). A analysis of the binding stoichiometry of the MoonTag epitope repeats and its scFv antibodies demonstrated that a 24xMoonTag array can recruit up to 12 copies of scFv::GFP (50% occupancy), which is slightly less than what was observed for the 24xSunTag (Tanenbaum et al., 2014). The MoonTag protein imaging system has been used in cultured human cells (Boersma et al., 2019), but not yet in other organisms. The tandem FALG tag system (also called the FALG spaghetti monster, FALG SM) and tandem HA tag system (also called the HA SM) are both very similar in composition to the SunTag system (Morisaki et al., 2016; Zhao et al., 2019). The FLAG tag (7 aa) and HA tag (9 aa) are much shorter than the SunTag and MoonTag. They have also been used for live imaging proteins in cultured human cells, but the copy number of the tag used in these studies is ten, which is half of the repeats used for the SunTag and MoonTag. Of note, all these systems have only been applied in mammalian cells cultured *in vitro*, except for the SunTag system, which has recently been adapted to flies. It is important to note that the optimization of the mRNA coding sequence for the epitope repeats is a key point.

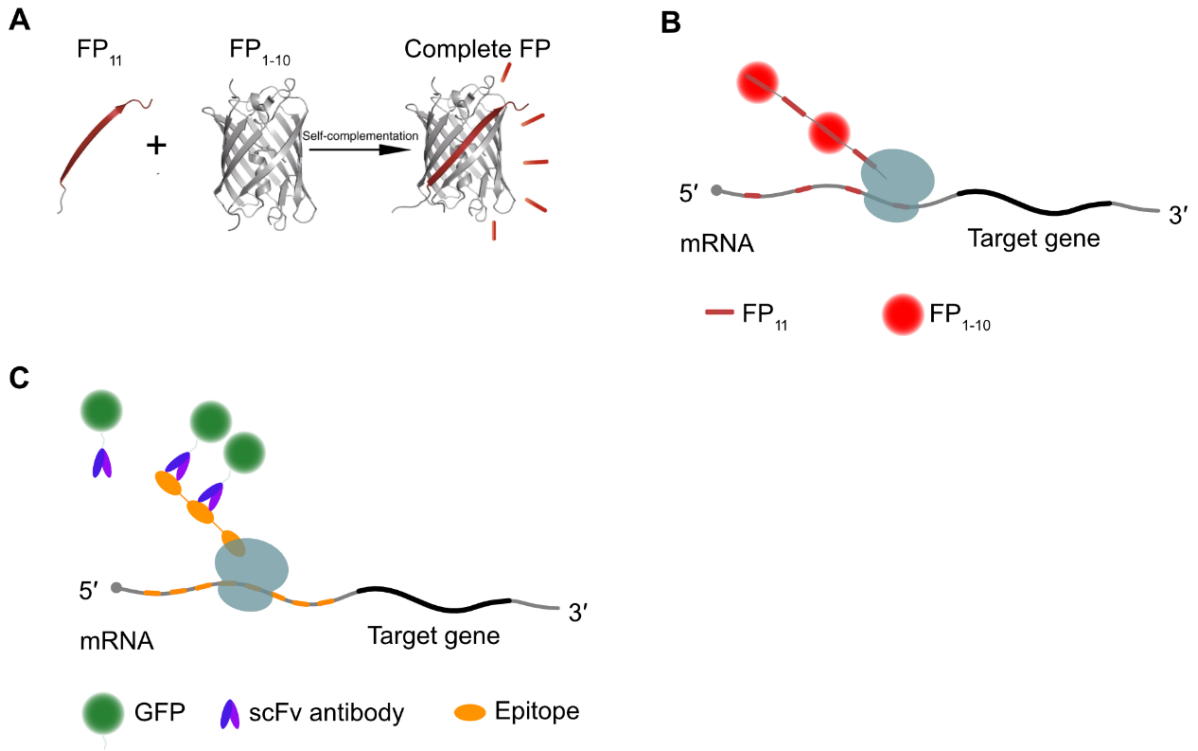

Figure 1.10 Two major strategies for signal amplification for imaging single protein molecules in live cells. (A) Schematic diagram of the split-fluorescent protein (FP). The split-FP technique is based on the self-complementation of two parts of FP: FP_{1-10} (the detector) and FP_{11} (the tag). Both parts are non-fluorescent by themselves; but when co-expressed, they can assemble spontaneously to form a complete fluorescent protein molecule. The images of the FP structure were modified from (Feng et al., 2017). (B) Schematic diagram for tandem split-FP system for signal amplification. The tandem repeats of the FP_{11} fragment can be genetically tagged to the protein of interest. Upon the translation of the tagged protein, the co-expressed FP_{1-10} fragment will spontaneously associate with FP_{11} repeats tagged to the target protein, through which the target protein can be visualized with the signal amplified by the multimerization of FP. (C) Schematic diagram for tandem epitope tag-scFv-FP system for signal amplification. The tandem-arranged epitope can be genetically tagged to the protein of interest. Upon the translation of the tagged protein, the co-expressed scFv antibody FP fusion will bind to the epitope repeats tagged to the target protein with high affinity and specificity, through which the target protein can be visualized with the signal amplified by the multimerization of FP.

1.6 Aims of the Project

Although the central apoptotic cell death pathway has been elucidated in the past four decades, the mechanism through which the cell death fate is specified remains not completely understood. Particularly, how the level of the key cell death activator EGL-1 BH3-only protein is kept below the threshold triggering cell death in non-dying cells and how it is increased above this threshold in cells programmed to die is not completely understood. It is meaningful and imperative to develop new targeted drugs that can kill cancer cells in targeted tissues with fewer side effects. Small molecules called 'BH3 mimetics' have proven to be a promising solution. The full understanding of the mechanism governing *egl-1* BH3-only expression in specific tissues may also promote the development of more specific and effective drugs. For example, with the delivery of exogenous mRNA drugs encoding BH3-only proteins, BH3-only protein synthesis could be manipulated to let them be activated only in cancer cells but not in healthy cells, through which side effects of anti-cancer drugs will be largely decreased. This study is aimed to identify new regulatory factors that contribute to the control of *egl-1* BH3-only expression at the post-transcriptional level.

To achieve this goal, I set out to address the following questions:

(1) What *cis*-acting elements within the *egl-1* 3′ UTR contribute to the control of *egl-1* expression? The conserved sequence elements are identified in the *egl-1* 3′ UTR, and their potential functions in the control of *egl-1* expression are determined.

(2) What trans-acting factors (i.e., RBPs) are involved in repressing or activating *egl-1* expression? By individually knocking down 660 RBP-encoding genes by RNAi, a genetic screen is performed to identify RBP repressors and activators of *egl-1* expression.

(3) How does *egl-1* mRNA translation occur in time and space in lineages where a cell death occurs? A live imaging approach is established to investigate spatiotemporal synthesis of the EGL-1 protein.

Materials and Methods

Chapter 2 Materials and Methods

2.1 Strains and alleles

The strains were maintained at 20°C on nematode growth medium (NGM) plates with *E. coli* OP50 bacterial lawns (Brenner, 1974), unless stated otherwise. The strain N2 (Bristol) was used as the wild-type reference in this study. The alleles, balancers, and transgenes used in this study are summarized in **Table 2.1** and **Table 2.2**.

Table 2.1 List of alleles and balancers used in this study. The allele name, gene affected, linkage group (LG), and origin are listed in the table.

Allele name	Gene affected	LG	Reference/Origin
ok1278	*hrpr-1 (hrp-2)*	I	Generated by the *C. elegans* Gene Knockout Consortium
ok1353	*eif-3.H*	I	Generated by the *C. elegans* Gene Knockout Consortium
hT2	(balancer)	I;III	-
mIn1	(balancer)	II	(Edgley and Riddle, 2001)
nDf50	*mir-35-41*	II	(Miska et al., 2007)
nDf49	*mir-42-44*	II	(Miska et al., 2007)
tm4263	*swsn-7*	II	Generated by the National Bioresource Project, Tokyo
lq133	*etr-1*	II	(Ochs et al., 2020)
ok91	*fbf-1*	II	(Crittenden et al., 2002)
q704	*fbf-2*	II	(Crittenden et al., 2002)
ed3	*unc-119*	III	(Maduro and Pilgrim, 1995)
n1653	*ced-9*	III	(Dreze et al., 2009)
n717	*ced-3*	IV	(Shaham et al., 1999)
n2427	*ced-3*	IV	(Reddien et al., 2007)
tm2262	*rack-1*	IV	(Demarco and Lundquist, 2010)
n3330	*egl-1*	V	(Sherrard et al., 2017)
on24	*egl-1*	V	Brent Derry lab
syb5181	*egl-1*	V	This study, made by SunyBiotech
syb5451	*egl-1*	V	This study, made by SunyBiotech
mjs2	*egl-1*	V	Made by Michael J. Smanski
bc449	*egl-1*	V	This study
hd20	*nre-1*	X	(Schmitz et al., 2007)
hd126	*lin-15b*	X	(Schmitz et al., 2007)
ma327	*stau-1*	X	(Ren et al., 2016)

Table 2.2 List of transgenes used in this study. The transgene name, linkage group (LG), transgene information, plasmid used, and origin are listed in the table.

Transgene	LG	Transgene detail	Plasmid	Reference/Origin
bcSi25	I	P_{mai-2}*gfp::h2b::mai-2 3′ UTR + unc-119(+)*	pBC1483	(Sherrard et al., 2017)
bcSi26	I	P_{mai-2}*gfp::h2b::egl-1 3′ UTR + unc-119(+)*	pBC1484	(Sherrard et al., 2017)
bcSi105	I	P_{mai-2}*gfp::h2b::egl-1 3′ UTR* $^{FBE\ mut}$ *+ unc-119(+)*	pBC1867	This study
bcSi106	I	P_{mai-2}*gfp::h2b::egl-1 3′ UTR* $^{FBE\ mut}$ *+ unc-119(+)*	pBC1868	This study
bcSi121	I	P_{mai-2}*gfp::h2b::egl-1 3′ UTR*$^{TPTE\ mut}$ *+ unc-119(+)*	pBC1947	This study
bcSi122	I	P_{mai-2}*gfp::h2b::egl-1 3′ UTR*$^{TPTE\ replaced\ by\ mai-2\ TPTE}$ *+ unc-119(+)*	pBC1948	This study
bcSi123	I	P_{mai-2}*gfp::h2b::mai-2 3′ UTR*$^{TPTE\ replaced\ by\ egl-1\ TPTE}$ *+ unc-119(+)*	pBC1949	This study
bcSi125	I	P_{tph-1}*his-24::gfp::his-24 3′ UTR + unc-119(+)*	pBC1968	This study
bcSi127	I	P_{mai-2}*gfp::h2b::egl-1 3′ UTR*$^{TPTE\ A/G,\ T/C\ substitution}$ *+ unc-119(+)*	pBC1970	This study
bcSi128	I	P_{mai-2}*gfp::h2b::egl-1 3′ UTR*$^{TPTE\ reversed}$ *+ unc-119(+)*	pBC1971	This study
bcSi132	I	P_{egl-1}*33xSunTag::egl-1::egl-1 3′ UTR + unc-119(+)*	pBC1989	This study
bcSi57	III	P_{egl-1}*egl-1(n3082)::mNeonGreen::egl-1 3′ UTR*	pBC1712	Made by Ryan Sherrard
bcIs66	III	P_{tph-1}*his-24::gfp + lin-15(+)*	pBC458	(Yan et al., 2013)
bcSi126	III	P_{tph-1}*his-24::gfp::tbb-2 3′ UTR + unc-119(+)*	pBC1969	This study
bcSi129	III	P_{hlh-34}*gfp::his-24 + unc-119(+)*	pBC1972	This study
bcSi133	III	$P_{hsp-16.41}$*scFv(GCN4)::sfGFP::GB1::NLS + unc-119(+)*	pBC1990	This study
bcSi134	III	$P_{hsp-16.41}$*scFv(GCN4)::sfGFP::GB1::NLS + unc-119(+)*	pBC2000	This study
juSi164	III	P_{mex-5}*his-72::miniSOG-39 + unc-119(+)*	-	(Noma and Jin, 2016)
bcSi135	V	$P_{hsp-16.41}$*scFv(GCN4)::sfGFP::GB1::NLS + unc-119(+)*	pBC2000	This study
ltIs44	V	P_{pie-1}*mCherry::PH(PLC1*^{delta1}*) + unc-119(+)*	-	(Audhya et al., 2005)
bcIs161	V	P_{unc-3}*unc-3::mScarlet + rol-6(su1006)*	pRF4 and PCR fragments	Made by Eric Lambie and Jimei Xu
bcIs65	X	P_{tph-1}*his-24::gfp + lin-15(+)*	pBC458	(Yan et al., 2013)
wgIs512	-	P_{swsn-7}*swsn-7::TY1::EGFP::3xFLAG + unc-119(+)*	-	(Audhya et al., 2005)

wgIs675		P_{atfs-1}*atfs-1::TY1::EGFP::3xFLAG + unc-119(+)*	-	(Audhya et al., 2005)
xdEx1091	-	P_{unc-3}*unc-3::gfp* + P_{sur-5}*rfp*	-	(Wang et al., 2015)
bcEx1394	-	$P_{hsp-16.41}$*24xSunTag::egl-1::egl-1 3′ UTR + rol-6(su1006)*	pBC2006 + pRF4	This study

2.2 Cloning and plasmid construction

The plasmids constructed in this study are summarized in **Table 2.3**. The primers used for plasmid constructions are listed in **Table 2.4**. All primers were ordered from Sigma-Alrich.

Plasmids pBC1867 and pBC1868 were modified from pBC1651 (generated by Kyoko Ikegami) using PCR site-directed mutagenesis. Primers were designed to introduce point mutations in the four predicted FBF binding elements (FBEs) in the *egl-1* 3′UTR. In the plasmid pBC1867, the first nucleotide in each of the four predicted FBEs was changed from T to A. The primers used for pBC1867 construction were YJ9 and YJ10 (**Table 2.4**). In the plasmid pBC1868, the first three nucleotides in each of the four predicted FBEs were changed from TGT to ACA. The primers used for pBC1867 construction were primers YW7, YW8, YJ11, YJ12, YJ13, and YJ14 (**Table 2.4**). PCRs were carried out with the Phusion High-Fidelity DNA polymerase (NEB, #M0530L) under following reaction conditions: 98°C for 3 min, 30 cycles of 98°C for 10 sec, 57°C for 10 sec and 72°C for 5 min 30 sec, then 72°C for 5 min.

Plasmids pBC1947, pBC1948, pBC1949, pBC1970, and pBC1971 were modified from pBC1484 (generated by Nadin Memar). Firstly, the plasmid pBC1484 was cut with restriction enzymes *NotI* and *AflII*, and the 10 kb fragment was recovered using the Monarch DNA Gel Extraction Kit (NEB, #T1020L). This fragment was used as the backbone. To generate the plasmid pBC1947, the 567 bp DNA fragment between *NotI* and *AflII* sites was synthesized using the Geneart service (Sigma), in which the 33 bp *egl-1* 3′ terminal element (TPTE) sequence CATATTTATCTAATAATAAATATGGTTTTTTTT was mutated (randomized) to ATTTTCTAATAACTAATAAATTGTTTATTTTGT. Then, the synthesized fragment was cut with *NotI* and *AflII*, purified using the Monarch PCR & DNA Cleanup Kit (NEB, #T1030L), and ligated to the 10 kb backbone by the Hi-T4 DNA ligase (NEB, # M2622S). To generate the plasmid pBC1948, the 567 bp DNA fragment between *NotI* and *AflII* sites was synthesized, in which the 33 bp *egl-1* TPTE was substituted by the *mai-2* TPTE TTCGTTTTCCTGTAATAAATTATAGTTTTTAGC. Then, the synthesized fragment was cut with restriction enzymes *NotI* and *AflII*, purified using the Monarch PCR & DNA Cleanup Kit (NEB, #T1030L), and ligated to the 10 kb backbone by the Hi-T4 DNA ligase (NEB, # M2622S). To generate the plasmid pBC1949, the 534 bp

DNA fragment between the *NotI* and *AflII* sites was synthesized using the Geneart service (Sigma), in which the TPTE in the *mai-2* 3′ UTR was replaced by the *egl-1* TPTE. Then, the synthesized fragment was cut with restriction enzymes *NotI* and *AflII*, purified using the Monarch PCR & DNA Cleanup Kit (NEB, #T1030L), and ligated to the 10 kb backbone by Hi-T4 DNA ligase (NEB, # M2622S). To generate the plasmid pBC1970, a 606 bp fragment was amplified by PCR from pBC1484 using primers YW2 and oYJ51 (**Table 2.4**). Primer oYJ51 was designed to mutate the 33 bp *egl-1* TPTE to CGCGCCCGCCTAATAGCGGGCGCGGTTTTTTTT. The obtained 606 bp DNA fragment was assembled in the 10 kb backbone using the NEBuilder HiFi DNA Assembly Master Mix (NEB, #E2621L). To generate the plasmid pBC1971, a 606 bp fragment was amplified by PCR from pBC1484 using primers YW2 and oYJ72 (**Table 2.4**). Primer oYJ72 was designed to mutate the 33 bp *egl-1* TPTE to CATAAAATACTAATATATTTTATGGTTTTTTTT. The obtained 606 bp DNA fragment was assembled in the 10 kb backbone using the NEBuilder HiFi DNA Assembly Master Mix (NEB, #E2621L). PCRs were carried out with the Q5 High-Fidelity DNA polymerase (NEB, #M0492L) under following reaction conditions: 98°C for 30 sec, 30 cycles of 98°C for 10 sec, 60°C for 15 sec and 72°C for 15 sec, then 72°C for 2 min. The nucleotide sequence of all constructed plasmids was confirmed using Sanger Sequencing (Azenta).

To generate the plasmid pBC1967, a 1.7 kb *tph-1* fragment including promoter region and the first exon was amplified by PCR from the genomic DNA of the N2 strain using primers oYJ42 and oYJ43 (**Table 2.4**), a 958 bp *GFP(S65C)* fragment was amplified by PCR from pBC1484 using primers oYJ44 and oYJ45 (**Table 2.4**), and a 1 kb *his-24* fragment was amplified by PCR from the genomic DNA using primers oYJ46 and oYJ47 (**Table 2.4**). The primers were designed to carry overlapping sequences between fragments. Then, the three fragments were assembled into the backbone pCFJ350 between *BsiWI* and *AvrII* sites using the NEBuilder HiFi DNA Assembly Master Mix (NEB, #E2621L). To generate the plasmid pBC1968, a 3 kb $P_{tph\text{-}1}$*gfp::his-24* fragment was amplified by PCR from pBC1967 using primers oYJ42 and oYJ48 (**Table 2.4**) and inserted into the backbone pCFJ350 between *BsiWI* and *AvrII* sites using the NEBuilder HiFi DNA Assembly Master Mix (NEB, #E2621L). To generate the plasmid pBC1969, a 371 bp *tbb-2* 3′ UTR fragment was amplified by PCR from the plasmid pCFJ601 using primers oYJ49 and oYJ50 (**Table 2.4**). Then, an overlap PCR

was performed to get a 3.7 kb fragment P_{tph-1}*gfp::his-24::tbb-2* 3′ UTR using pBC1967 along with the 371 bp *tbb-2* 3′ UTR fragment as the templates and using primers oYJ42 and oYJ50 (**Table 2.4**). This 3.7 kb fragment was assembled into the backbone plasmid pCFJ350 between *BsiWI* and *AvrII* sites using the NEBuilder HiFi DNA Assembly Master Mix (NEB, #E2621L). PCRs were carried out with the Phusion High-Fidelity DNA polymerase (NEB, #M0530L) under following reaction conditions: 98°C for 3 min, 30 cycles of 98°C for 10 sec, 57°C for 10 sec and 72°C for 1 min, then 72°C for 5 min. The nucleotide sequence of all constructed plasmids was confirmed using Sanger Sequencing (Azenta).

To generate the plasmid pBC1988, a 1.8 kb scFv::sfGFP::NLS fragment was amplified by PCR from the plasmid PL234 (provided by the Mounia Lagha lab) (Dufourt et al., 2021) using primers oYJ86 and oYJ87 (**Table 2.4**) and inserted in the backbone pPD49.83 at the *SmaI* site. PCR was carried out with the Q5 High-Fidelity DNA polymerase (NEB, #M0492L) under following reaction conditions: 98°C for 30 sec, 35 cycles of 98°C for 10 sec, 66°C for 30 sec and 72°C for 1 min, then 72°C for 2 min. To generate the plasmid pBC1990, a 3 kb $P_{hsp-16.41}$*scFv(GCN4)::sfGFP::GB1::NLS::unc-54* fragment was amplified by PCR from pBC1988 using the primers oYJ105 and oYJ106 (**Table 2.4**). PCR was carried out with the Q5 High-Fidelity DNA polymerase (NEB, #M0492L) under following reaction conditions: 98°C for 30 sec, 35 cycles of 98°C for 10 sec, 65°C for 30 sec and 72°C for 2 min, then 72°C for 2 min. Then this fragment was assembled into the backbone pCFJ350 between *BsiWI* and *AvrII* sites using the Hi-T4 DNA ligase (NEB, # M2622S). To generate the plasmid pBC2000, the 1.8 kb scFv::sfGFP::NLS fragment was modified by codon optimization using the *C. elegans* codon adaptor (worm.mpi-cbg.de/codons/cgi-bin/optimize.py) and synthesized using the Geneart service (Sigma). This codon-optimized scFv::sfGFP::NLS fragment was assembled into pBC1990 between *PspOMI* and *NheI* sites using the NEBuilder HiFi DNA Assembly Master Mix (NEB, #E2621L), through which the old version of scFv::sfGFP::NLS fragment was replaced the new one. The nucleotide sequence of all constructed plasmids was confirmed using Sanger Sequencing (Azenta).

To generate the plasmid pBC1989, a 2.4 kb 33xSunTag fragment was first amplified by PCR from the plasmid PL216 (provided by the Mounia Lagha lab) (Dufourt et al.,

2021) using primers oYJ90 and oYJ91 (**Table 2.4**). PCR was carried out with the Q5 High-Fidelity DNA polymerase (NEB, #M0492L) under following reaction conditions: 98°C for 30 sec, 35 cycles of 98°C for 10 sec, 67°C for 30 sec and 72°C for 2 min, then 72°C for 2 min. Next, a 7.8 kb *egl-1* upstream fragment was amplified from pBC1712 (generated by Ryan Sherrard) using primers oYJ88 and oYJ89 (**Table 2.4**), and a 6.5 kb *egl-1* downstream fragment was amplified by PCR from pBC08A (Generated by Barbara Conradt) using primers oYJ91 and oYJ92 (**Table 2.4**). PCRs were carried out with the Q5 High-Fidelity DNA polymerase (NEB, #M0492L) under following reaction conditions: 98°C for 30 sec, 35 cycles of 98°C for 10 sec, 55°C for 30 sec and 72°C for 3 min 30 sec, then 72°C for 2 min. The three fragments were assembled into the backbone plasmid pCFJ909 at the *StuI* site using the NEBuilder HiFi DNA Assembly Master Mix (NEB, #E2621L). To generate the plasmid pBC2001, a 503 bp *mai-2* promoter fragment was amplified by PCR from pBC1484 (generated by Nadin Memar) using primers oYJ115 and oYJ116 (**Table 2.4**), and a 1.7 bp mCherry fragment was amplified by PCR from pCFJ90 using primers oYJ117 and oYJ118 (**Table 2.4**). PCRs were carried out with the Q5 High-Fidelity DNA polymerase (NEB, #M0492L) under following reaction conditions: 98°C for 30 sec, 30 cycles of 98°C for 10 sec, 57°C for 30 sec and 72°C for 1 min, then 72°C for 2 min. These two fragments were assembled along with the 2.4 kb 33xSunTag fragment (used before) into pBC1484 between *AflII* and *AfeI* sites using the NEBuilder HiFi DNA Assembly Master Mix (NEB, #E2621L). The nucleotide sequence of all constructed plasmids was confirmed using Sanger Sequencing (Azenta).

The plasmid pBC2005 was generated by Minjia Pan (an undergraduate student mentored by me). To construct it, the 1.3 kb *egl-1* transcription unit including the 3′ UTR was amplified by PCR from pBC08A (generated by Barbara Conradt) using primers oYJ149 and oYJ150 (**Table 2.4**). PCR was carried out with the Q5 High-Fidelity DNA polymerase (NEB, #M0492L) under following reaction conditions: 98°C for 30 sec, 35 cycles of 98°C for 10 sec, 59°C for 30 sec and 72°C for 1 min, then 72°C for 1 min. and the pPD49.83 backbone was linearized by PCR using primers oYJ151 and oYJ152 (**Table 2.4**). PCR was carried out with the Q5 High-Fidelity DNA polymerase (NEB, #M0492L) under following reaction conditions: 98°C for 30 sec, 35 cycles of 98°C for 10 sec, 66°C for 30 sec and 72°C for 1 min, then 72°C for 1 min. The two fragments were assembled using the NEBuilder HiFi DNA Assembly Master

Mix (NEB, #E2621L). To generate the plasmid pBC2006, a 1.8 kb 24xSunTag fragment was amplified by PCR from the SunTag plasmid (plasmid name unknown, provided by the Suzan Ruijtenberg lab) (Tanenbaum et al., 2014) using primers oYJ159 and oYJ160 (**Table 2.4**), and the pBC2005 was linearized by PCR using primers oYJ165 and oYJ166 (**Table 2.4**). PCRs were carried out with the Q5 High-Fidelity DNA polymerase (NEB, #M0492L) under following reaction conditions: 98°C for 30 sec, 30 cycles of 98°C for 10 sec, 63°C for 30 sec and 72°C for 2 min, then 72°C for 2 min. The two fragments were assembled using the NEBuilder HiFi DNA Assembly Master Mix (NEB, #E2621L). The nucleotide sequence of all constructed plasmids was confirmed using Sanger Sequencing (Azenta).

Table 2.3 List of plasmids constructed in this study.

Plasmid	Backbone	Insert	Reference/Origin
pBC1867	pCFJ350	P_{mai-2}*gfp::h2b::egl-1 3′ UTR* $^{FBE\ mut}$	This study
pBC1868	pCFJ350	P_{mai-2}*gfp::h2b::egl-1 3′ UTR* $^{FBE\ mut}$	This study
pBC1947	pCFJ350	P_{mai-2}*gfp::h2b::egl-1 3′ UTR*$^{TPTE\ mut}$	This study
pBC1948	pCFJ350	P_{mai-2}*gfp::h2b::egl-1 3′ UTR*$^{TPTE\ replaced\ by\ mai-2\ TPTE}$	This study
pBC1949	pCFJ350	P_{mai-2}*gfp::h2b::mai-2 3′ UTR*$^{TPTE\ replaced\ by\ egl-1\ TPTE}$	This study
pBC1967	pCFJ350	P_{tph-1}*his-24::gfp::his-24 3′ UTR*	This study
pBC1968	pCFJ350	P_{tph-1}*his-24::gfp::his-24 3′ UTR*	This study
pBC1969	pCFJ350	P_{tph-1}*his-24::gfp::tbb-2 3′ UTR*	This study
pBC1970	pCFJ350	P_{mai-2}*gfp::h2b::egl-1 3′ UTR*$^{TPTE\ A/G,\ T/C\ substitution}$	This study
pBC1971	pCFJ350	P_{mai-2}*gfp::h2b::egl-1 3′ UTR*$^{TPTE\ reversed}$	This study
pBC1988	pPD49.83	$P_{hsp-16.41}$*scFv(GCN4)::sfGFP::GB1::NLS*	This study
pBC1989	pCFJ909	P_{egl-1}*33xSunTag::egl-1::egl-1 3′ UTR*	This study
pBC1990	pCFJ350	$P_{hsp-16.41}$*scFv(GCN4)::sfGFP::GB1::NLS*	This study
pBC2000	pCFJ350	$P_{hsp-16.41}$*scFv(GCN4)::sfGFP::GB1::NLS* (codon optimized)	This study
pBC2001	pCFJ350	P_{mai-2}*33xSunTag::mCherry::unc-54 3′ UTR*	This study
pBC2005	pPD49.83	$P_{hsp-16.41}$*egl-1::egl-1 3′ UTR*	This study, generated by Minjia Pan
pBC2006	pPD49.83	$P_{hsp-16.41}$*24xSunTag::egl-1::egl-1 3′ UTR*	This study

Table 2.4 List of primers used for plasmid construction. The primer name and its sequence are listed in the table below.

Name	Sequence (5′–3′)
oYJ2 (YW2)	GGTGGAGCTCCACCGGTGGC
oYJ7 (YW7)	CCCGGACATTTTTCTTCATTACAGATTATTTTTCG
oYJ8 (YW8)	TGTAATGAAGAAAAATGTCCGGGTATTATGAGAAAT
oYJ9 (YJ9)	CCCGGAGTTTTTTCTTCATTAGTGATTATTTTTCG
oYJ10 (YJ10)	TAATGAAGAAAAAACTCCGGGTATTATGAGAAATC
oYJ11 (YJ11)	CCAACTTTTCTCCAATTACAACCATGATTTC
oYJ12 (YJ12)	GAAATCATGGTTGTAATTGGAGAAAAGTTGG
oYJ13 (YJ13)	CCCCTCAATATTACAACCATAGTCC
oYJ14 (YJ14)	GGACTATGGTTGTAATATTGAGGGG
oYJ42	TGCATCGCGCGCACCGTACGTTCTCGCGAATTGCGGCCGAC
oYJ43	GGAGCTGAAAGTACAGAAATTAC
oYJ44	ATTTCTGTACTTTCAGCTCCATGAGTAAAGGAGAAGAACTTTTC
oYJ45	ACAACAGCGGAATCAGACATACTAGTTCTAGAGCGGCCGCCAC
oYJ46	ATGTCTGATTCCGCTGTTGTTG
oYJ47	GGTACCAGAGCTCACCTAGGACAGTTTTAAATTTTACAATGTTTATTGAAGACGTTGAACGTCAAATTATC
oYJ48	GGTACCAGAGCTCACCTAGGGAAGACGTTGAACGTCAAATTATC
oYJ49	AGCCAGCCGCCAAGGCCTAAATGCAAGATCCTTTCAAGCATTC
oYJ50	AGAGGGTACCAGAGCTCACCTAGGTGAGACTTTTTTCTTGGCGGCAC
oYJ51	GCCAGTCCGTAATACGACTCACTTAAGAAAAAAAACCGCGCCCGCTATTAGGCGGGCGCGAGCAATAAAGGACTATGGTACAAATATTG
oYJ72	GCCAGTCCGTAATACGACTCACTTAAGAAAAAAAACCATAAAATATATTAGTATTTTATGAGCAATAAAGGACTATGGTACAAATATTG
oYJ86	AAAATCCTCATCGGGATCCCCGGGATGGGCCCCGACATCGTGATGAC
oYJ87	TGGGTCCTTTGGCCAATCCCGGGTTACACCTTGCGCTTCTTCTTG
oYJ88	GCTCTGGTACCCTCTAGTCAAGGCCTAACTAGAACAAAAACATTAGATCAAG
oYJ89	GCCGCTGCCGCTAAGCTTGGTACCCATATCAACTGAATTGAAAAGAG
oYJ90	ATGGGTACCAAGCTTAGCGGCAG
oYJ91	ACCGGTGATATCGCTGCCC
oYJ92	AGGGCAGCGATATCACCGGTCTGGTAAGTCTAGAAATTATTTA
oYJ93	CCGTAATACGACTCACTTAAGGCCTCCCTAACATATTTCTCAAAGATAC
oYJ105	TCTTCGAATGCATCGCGCGCACCGTACGCCAAAAACGGAACGTTGAGCTG
oYJ106	TGACTAGAGGGTACCAGAGCTCACCTAGGAAACAGTTATGTTTGGTATATTG

oYJ115	TCTTGGGTTTCGAGCCCGCAAAC
oYJ116	CTGCCGCTAAGCTTGGTACCCATTCTGAAAATTGAGTGAATTAGAG
oYJ117	AGATTAAAAAAGGGCAGCGATATCACCGGTATGGTCTCAAAGGGTGAAGAAG
oYJ118	ACGGCCAGTCCGTAATACGACTCACAAACAGTTATGTTTGGTATATTG
oYJ149	AAAAAACTTCGAAAATCCTCATCGGGATCCAGCTGTGCACGCACACCATTC
oYJ150	TAAAAATAGGCGTATCACGAGGCCCTTAAGAGTATACAATCGTAGGCATAC
oYJ151	CTTAAGGGCCTCGTGATACG
oYJ152	GGATCCCGATGAGGATTTTCGAAG
oYJ159	ACCTTACTAATTTCCAGATGCTCACCTTTGCCTCAACCTCTTCGGATCTTCTACCAATGGAAGAACTTTTGAGCAAG
oYJ160	GTTCTTTTCGTTGTAGAAAACGGAAGATTGAACGTCAAAAACGTTGGACATTGGTAGAAGCTTTTTAAGTCGGGCTACTTCATTCTCG
oYJ163	ACCTTACTAATTTCCAGATGC
oYJ165	CATTGGTAGAAGATCCGAAGAG
oYJ166	TCCAACGTTTTTGACGTTCAATC

2.3 Microinjection and generation of transgenic animals

The procedures for DNA transformation by microinjection into the germline of *C. elegans* are detailed in the previous protocol (Rieckher and Tavernarakis, 2017). First, 1 µl of the DNA solution was loaded by a microloader pipette tip (Eppendorf, #5242956.003) into a microinjection capillary (World Precision Instrument, #GQF100-70-7.5), the microinjection capillary was then installed into the needle holder of the micromanipulator (NARISHIGE, Model MMO-203), and the micromanipulator was connected to the microinjector unit for pressure appliance (Eppendorf FemtoJet 4i). Next, a drop of about 20 µl halocarbon oil (Sigma, #MKCL4315) was placed on a dry 2% agarose pad, animals were transferred into the halocarbon oil and attached to the agarose surface under a stereoscope, and the agarose pad was placed onto the gliding table of a light microscope equipped with DIC optics for microinjection (Zeiss AxioVert.A1). Then, the gonad of the animal immobilized in the halocarbon oil on the agarose pad was focused and the tip of the injection capillary was adjusted along the x, y, and z axis in proximity of the gonad and in focus. The injection capillary was then inserted in the syncytium (cytoplasmic core) of the distal gonad of the animal. Finally, a small amount of the DNA solution was released into the gonad by pressing the 'Inject' button on the Microinjector unit.

To generate Mos1 transposon-mediated Single-Copy Insertion (MosSCI) (Frokjaer-Jensen et al., 2012; Frokjaer-Jensen et al., 2008) transgenes, including *bcSi105, bcSi106, bcSi121, bcSi122, bcSi123, bcSi125, bcSi126, bcSi127, bcSi128, bcSi129, bcSi133, bcSi134, bcSi135* (**Table 2.2**), the universal MosSCI strain EG8078 [*oxTi185* I; *unc-119(ed3)* III], EG8080 [*oxTi444* III *unc-119(ed3)* III], or [*unc-119(ed3)* III; *oxTi365* V] was used for germline microinjection and targeted insertion of the transgene onto chromosome I, III, and V, respectively. The plasmids used for the insertion of transgenes via MosSCI were those that contain pCFJ350 as the backbone (listed in **Table 2.3**). Each MosSCI plasmid was injected at a concentration of 20–40 ng/µl with co-injection plasmids 50 ng/µl pCFJ601 ($P_{eft\text{-}3}$*Mos1 transposase*), 10 ng/µl pGH8 ($P_{rab\text{-}3}$*mCherry::unc-54 3′ UTR*), 2.5 ng/µl pCFJ90 ($P_{myo\text{-}2}$*mCherry::unc-54 3′ UTR*), and 5 ng/µl pCFJ104 ($P_{myo\text{-}3}$*mCherry::unc-54 3′ UTR*). The genotype was verified by analyzing the phenotype and via PCR.

To generate minimal Mos1 transposon (miniMos)-mediated single-copy insertion (Frokjaer-Jensen et al., 2012; Frokjaer-Jensen et al., 2008) transgene *bcSi132*, the universal miniMos strain HT1593 [*unc-119(ed3)* III] was used for germline microinjection and random insertion of the transgenes into the genome. The plasmids used for the insertion of transgenes via miniMOS were those that contain pCFJ909 as the backbone (listed in **Table 2.3**). The miniMos plasmid pBC1989 was injected at a concentration of 20–40 ng/µl with co-injection plasmids 50 ng/µl pCFJ601 (P_{eft-3}*Mos1 transposase*), 10 ng/µl pGH8 (P_{rab-3}*mCherry::unc-54 3′ UTR*), 2.5 ng/µl pCFJ90 (P_{myo-2}*mCherry::unc-54 3′ UTR*), and 5 ng/µl pCFJ104 (P_{myo-3}*mCherry::unc-54 3′ UTR*). The genotype was verified by analyzing the phenotype and via PCR and Sanger sequencing.

To generate the multi-copy extra-chromosomal array *bcEx1394*, 5 ng/µl plasmid pBC2006 was injected together with 50 ng/µl injection marker plasmid pRF4 [*rol-6(su1006)*] together with 50 ng/µl 1 kb DNA Ladder (NEB, #N3232L).

The multi-copy integration transgene *bcIs161* was generated by mini-Singlet Oxygen Generator (miniSOG)-mediated integration as described previously (Noma and Jin, 2016, 2018). To generate *bcIs161*, the *unc-3* fosmid WRM0618c was digested with *AflII*. The mScarlet fragment was amplified from plasmid 2020AAF2PD (ThermoFisher) with primers 5′-CCTCCAGTCGTCGTCCCGTCTGTCTATGGTCTCCAAGGGAGAGG-3′ and 5′-CTCGGCGAGTTTCCAAATTGCT-3′. PCR was carried out with the Q5 High-Fidelity DNA polymerase (NEB, #M0492L) under following reaction conditions: 98°C for 30 sec, 35 cycles of 98°C for 10 sec, 65°C for 10 sec and 72°C for 1 min, then 72°C for 5 min. The purified *unc-3* fragments and mScarlet fragment (30 ng/µl) were injected with 10 ng/µl pRF4 [*rol-6(su1006)*] into the germline of the miniSOG strain CZ20310 [*juSi164* III *unc-119(ed3)* III]. Six hours after microinjection, animals were exposed with blue light at 2 mW/mm2 and 4 Hz for 30 min. These P0 worms were distributed on OP50-seeded plates with five animals on each plate. Four days later, all transgenic F1 rollers were transferred to individual plates (F1 plates). Among these F1 plates, the plates with more than 50% F2 rollers were selected, and 12 single roller F2s from each selected F1 plate were transferred onto individual plates. Four days later, lines

showing 100% transmission were screened. The obtained integrant line was backcrossed six times with the N2 strain.

2.4 RNA *in vitro* transcription and dsRNA microinjection

For RNA-mediated interference (RNAi) experiments using microinjection as the method of delivering dsRNA, bacterial strains in the Ahringer RNAi feeding library (Kamath and Ahringer, 2003; Kamath et al., 2003) distributed by Source BioScience Ltd (https://sourcebioscience.com) were used to amplify the DNA fragment flanked by the T7 promoter via PCR. The *T7* promoter oligodeoxynucleotide (5′-TAATACGACTCACTATAGGG-3′) was used as the primer. Purified PCR product was used as the DNA template for *in vitro* transcription of dsRNAs using the MEGAscript RNAi Kit (Ambion, #AM1626). About 200 ng of DNA was added in each *in vitro* transcription reaction. dsRNA product was 1:5 diluted with the RNase-free water and delivered to young adults via microinjection. For genes that are not covered by the Ahringer RNAi feeding library, the genomic DNA of the N2 strain was used to amplify DNA fragments flanked by the *T7* promoter using primers listed in **Table 2.5**. PCRs were carried out with the OneTaq DNA polymerase (NEB, #M0480L) under following reaction conditions: 94°C for 3 min, 30 cycles of 94°C for 30 sec, 50°C for 30 sec and 68°C for 2 min, then 68°C for 5 min.

Table 2.5 Primers used for dsRNA preparation. The T7 promoter sequence at the 5′ end is underlined.

Name	Sequence (5′–3′)
oYJ52_tiar-1 F	TAATACGACTCACTATAGGGCGAGGTCGACGGTATCGCTGTTGTCCAGGTCCTCCAT
oYJ53_tiar-1 R	TAATACGACTCACTATAGGGTCCCAAGCTCTTCAGACGAT
oYJ54_exc-7 F	TAATACGACTCACTATAGGGCGAGGTCGACGGTATCGAAAGGCGTTGGATTTGTACG
oYJ55_exc-7 R	TAATACGACTCACTATAGGGACAGTTGCTCATGAAAGGGG
oYJ56_puf-12 F	TAATACGACTCACTATAGGGCGAGGTCGACGGTATCGCTCGTGACTCTTTGTGCTCG
oYJ57_puf-12 R	TAATACGACTCACTATAGGGGCTCCAATAACCTCGTCCA
oYJ58_nhl-2 F	TAATACGACTCACTATAGGGCGAGGTCGACGGTATCGCCAATTGGATATGGGGTCTG
oYJ59_nhl-2 R	TAATACGACTCACTATAGGGTTTGGCAGCACTTACGAATG
oYJ60_nex-2 F	TAATACGACTCACTATAGGGCGAGGTCGACGGTATCGATCAGTTGAAAAGTCTGCGTCTC
oYJ61_nex-2 R	TAATACGACTCACTATAGGGACCGAACACTAATTCCCAAAAAT
oYJ62_puf-13 F	TAATACGACTCACTATAGGGCGAGGTCGACGGTATCGAACCGAAAGGAACACACCAG
oYJ63_puf-13 R	TAATACGACTCACTATAGGGGACAACCGGATAGCTACGG
oYJ64_pab-2 F	TAATACGACTCACTATAGGGCGAGGTCGACGGTATCGTCAGAGAATATTACGACCTTGGC
oYJ65_pab-2 R	TAATACGACTCACTATAGGGACTTTTCTTCCTTCGGAACAATC
oYJ66_puf-11 F	TAATACGACTCACTATAGGGCGAGGTCGACGGTATCGACGGAGGCTCGCAATGTGTC
oYJ67_puf-11 R	TAATACGACTCACTATAGGGAGGCATTGCTCAATGATAAC
oYJ68_sqd-1 F	TAATACGACTCACTATAGGGCGAGGTCGACGGTATCGACGCCTCTGAGACTATCAAG
oYJ69_sqd-1 R	TAATACGACTCACTATAGGGTTAGAACTGTTGGGCTTGAGCAG

2.5 *egl-1* transcriptional or translational reporter assays

2.5.1 Analysis of P_{mai-2}*gfp::h2b::egl-1 3′ UTR* (*bcSi26*) reporter expression

In the P_{mai-2}*gfp::h2b::egl-1 3′ UTR* (*bcSi26*) transgene (Sherrard et al., 2017), the *egl-1* 3′ UTR is appended to a *gfp::h2b* fusion gene which is driven by the ubiquitously active *mai-2* promoter (Fernandez-Cardenas et al., 2017). A single copy of this transgene is integrated into the genome of *C. elegans*. The expression of this reporter can be regulated by the *egl-1* 3′ UTR, and it hereby can be used to identify factors or elements that repress *egl-1* expression (Sherrard et al., 2017). The expression of this reporter in four-cell embryos was analyzed using a Zeiss Axio Imager.M2 microscope with a 100x objective (oil). For each embryo, a Z-stack of 25 z-slices from the top to the bottom of the embryo with an interval of 1 µm was captured. Images were analyzed using Fiji (Image J) software (Schindelin et al., 2012), and a three-dimensional (3D) region of interest (ROI) was defined for each nucleus of four-cell embryos. The GFP signal intensity was summed from z-projection summing all slices of the defined ROI.

2.5.2 Analysis of *egl-1(mjs2)* reporter expression

egl-1(mjs2) is a loss of function allele of *egl-1*, in which the endogenous *egl-1* CDS region is replaced by mNeonGreen through the CRISPR/Cas9 genome editing technology (Dickinson et al., 2015). This reporter was generated by Michael J. Smanski lab (not published yet). The expression of this reporter in live embryos was analyzed using a Leica TCS SP8 confocal microscope with a 63x objective (oil, 1.4 NA). The Leica LAS AF software was used with the following setting: pinhole 95.53 µm (Airy 1), zoom factor 3, bidirectional scanning, line average 1, 512 x 512 pixels, Z-stack interval 1 µm. For representative images, the brightness and contrast were adjusted using Fiji (Image J) software (Schindelin et al., 2012).

2.6 Determining NSM sister cell survival percentage

The serotonergic neuron reporter P_{tph-1}*his-24::gfp* (*bcSi126* III, *bcIs66* III, or *bcIs65* X) is expressed in the left and right pharyngeal NSM neurons after the two-fold embryo stage and expression persists throughout life (Sze et al., 2000). This reporter hereby labels serotonergic neurons including the NSM neurons. In mutants where the apoptotic NSM sister cells (NSMsc) survive, this reporter is also expressed in these inappropriately surviving cells (Yan et al., 2013). For example, inactivation of *egl-1* leads to the inappropriate survival of the NSMsc, and thus the presence of three/four instead of two GFP-positive cells in the anterior pharynx, which can be detected in L3/L4 larvae using a fluorescence microscope (Yan et al., 2013).

2.7 Determining the percentage of embryonic lethality

To determine embryonic lethality, embryos were collected by dissecting gravid adults using a scalpel in a glass bowl containing distilled water. All the mixed-stage embryos were transferred to an empty NGM plate (not seeded with OP50) and the total number of embryos was counted. Following this, the plates were incubated at 20°C for 24 hours. Next, the number of dead eggs and hatched animals was counted. The percentage of lethality was calculated by dividing the total number of dead eggs from the total number of eggs placed on the NGM plate.

2.8 Determining the number of large cell corpses in embryos

The presence of large cell corpse phenotype was examined using differential interference contrast (DIC) microscopy with a 100x (oil) objective (Sherrard et al., 2017). To count the total number of large cell corpses during embryogenesis, two- or four-cell stage embryos were collected by dissecting gravid adults using a scalpel in a glass bowl containing distilled water and mounted on a 2% agarose pad on a glass slide. The slide was covered with a cover slip, and the cover slip was sealed with white Vaseline. 4D recordings were made throughout embryonic development at 25°C, unless stated otherwise, using a Zeiss Axio Imager.M2 microscope and the ‘Time to

Live' software (Version 2017, Caenotec) as described previously (Schnabel et al., 2006; Schnabel et al., 1997). The recording captures 25 z-slices from the top to the bottom of the embryo with an interval of 1 µm, every 35 seconds for each frame. The entire recording time is ~7 hours. Lineaging analysis was performed using 'Simi BioCell' software (Simi Reality Motion Systems). The number of large cell corpses (> 2.6 µm in diameter) per embryo was scored until the end of ventral enclosure.

2.9 Genetic screen by RNA-mediated interference

Genetic screen by RNA-mediated interference (RNAi) was performed using the updated Ahringer RNAi feeding library (Kamath and Ahringer, 2003; Kamath et al., 2003) distributed by Source BioScience Ltd (https://sourcebioscience.com). This library covers around ~87% of the currently annotated *C. elegans* protein-coding genes. Bacterial RNAi clones carrying the constructs that express desired dsRNAs were cultured overnight in 100 µL of LB medium containing 100 µg/mL carbenicillin in a 96-well plate at 37°C. 10 µL of each bacteria culture was seeded into individual well of a 12-well NGM plate containing 6 mM IPTG and 100 µg/mL carbenicillin as described previously (Rolland et al., 2019). The seeded plates were incubated at 20°C overnight in the dark to induce dsRNA expression before use.

In the primary screen, the *egl-1* 3′ UTR reporter transgene $P_{mai\text{-}2}$*gfp::h2b::egl-1 3′ UTR* (*bcSi26*) was used to screen for an up-regulation or down-regulation of *gfp::h2b* expression. Ten L3 larvae carrying the *bcSi26* transgene were transferred into each well of the 12-well NGM plate seeded with bacterial RNAi clones. After the animals were fed with bacterial RNAi clones for 48 hours on the plate, the expression of *gfp::h2b* in nuclei of 4-cell stage embryos and oocytes was scored. In wild-type animals, this reporter is repressed in embryos but moderately expressed in oocytes and germ cells. If *gfp::h2b* expression was up-regulated in 4-cell stage embryos after knocking down of a RBP gene, this RBP was considered as a repressor candidate of *egl-1*. If *gfp::h2b* expression was down-regulated in oocytes after knocking down of an RBP gene, this RBP was considered as an activator candidate of *egl-1*.

In the re-screen for *egl-1* repressor candidates, L3 larvae animals were transferred into NGM plates seeded with bacterial RNAi clones as before. After the animals were

fed with bacterial RNAi clones carrying the dsRNA for 48 hours, the embryonic lethality and large cell corpses, which are indicative of precocious/ectopic cell death, were determined. The identity of bacterial RNAi clones was confirmed by Sanger sequencing of the insert in RNAi construct.

In the rescreen for *egl-1* activator candidates, I first performed a negative screen for a down-regulation of the *mai-2* 3′ UTR reporter $P_{mai\text{-}2}$*gfp::h2b::mai-2 3′ UTR* (*bcSi25*) in 4-cell stage embryos to excluded some non-specific regulators. Those candidates were excluded if the expression of this reporter was downregulated after they were knocked down. Then, I screened for the down-regulation of reporter $P_{mai\text{-}2}$*gfp::h2b::egl-1 3′ UTR* (*bcSi26*) in the *mir-35* family loss-of-function mutant background, in which this reporter transgene is moderately expressed in embryos. Finally, I determined the NSMsc survival after RNAi-mediated knockdown of RBP genes. In this assay, three L3 stage animals carrying NSM neuron marker $P_{tph\text{-}1}$*his-24::gfp* (*bcSi126*) were transferred in the NGM plate seeded with bacterial RNAi clones. After three days, L3/L4 stage F1 progenies were scored for extra NSM-like cells, which are in the anterior pharynx and labelled by GFP. If knocking down of certain RBP genes caused larval arrest, earlier stage F1 animals were scored. The identity of bacterial RNAi clones was confirmed by Sanger sequencing of the RNAi construct.

2.10 CRISPR/Cas mediated genome editing

The TPTE in the endogenous *egl-1* 3′ UTR was manipulated via CRISPR/Cas9 technology (Ran et al., 2013), generating the *egl-1* alleles *syb5181* and *syb5451*. The guide sequence of two sgRNAs used are 5′-CGAAAAAGTCCAGAAGACGA-3′ and 5′-TATTTATCTAATAATAAATA-3′, respectively. The DNA repair templates flanked with the homology sequence were prepared by PCR with mutations in the TPTE. For allele *syb5181*, ATATTTATCTAATAATAAATAT was mutated to GCGCCCGCctaataGCGGGCGC; for allele *syb5451*, CATATTTATCTAATAATAAATATGGTTTTTTT was mutated to ATTTTCTAATAACTAATAAATTGTTTATTTTG. Cas9 nuclease, two sgRNAs, the DNA repair template, and the plasmid $P_{myo\text{-}2}$*mCherry* (as co-injection marker) were microinjected into the germline of N2 young adults. The candidate lines were screened

by PCR genotyping and confirmed by sequencing. These two alleles were made by SunyBiotech Ltd.

The 18xSunTag repeats were inserted into the endogenous *egl-1* gene at the N-terminus after the 3rd start codon via CRISPR/Cas12(Cpf1) technology (Zetsche et al., 2015), generating the allele *bc449*. The guide sequence of the sgRNA used was 5′-CCTCAACCTCTTCGGATCTTCTA-3′. A 1.8 kb single-strand DNA repair template, which carries 24xSunTag repeats flanked with 48 nt *egl-1* homology sequence, was prepared by the asymmetric PCR using a single primer oYJ163 (**Table 2.4**). The dsDNA template used for the asymmetric PCR was amplified from the plasmid PBC2006 using primers oYJ159 and oYJ160 (**Table 2.4**). PCRs were carried out with the Q5 High-Fidelity DNA polymerase (NEB, #M0492L) under following reaction conditions: 98°C for 30 sec, 35 cycles of 98°C for 10 sec, 64°C for 10 sec and 72°C for 1 min, then 72°C for 2 min. The microinjection of Cas12a(Cpf1)-sgRNA ribonucleoproteins together with the ssDNA repair template and screening for genome editing were performed as previously described (Ghanta et al., 2021). The generated knock-in lines were confirmed via Sanger sequencing. Among four knock-in lines obtained, only one line did not have a frameshift mutation and could be used. Of note, 18xSunTag repeats were inserted but 6x SunTag repeats were missing. The other three lines all have frameshift mutations and hence could not be used.

2.11 Live imaging *egl-1* mRNA translation

For fluorescent images in **Fig. 5.1,** embryos of genotype [*bcSi134* III; *egl-1(bc449)* V *ltIs44* V; *bcIs161*] were isolated from gravid adults, mounted on 2% agarose pads, and incubated at 25°C for 2 hours. Embryos were subjected to a heat shock for 30 minutes at 30°C and incubated at 25°C for a further 30 minutes before imaging to allow $P_{hsp\text{-}16.41}$*scFv::sfGFP::NLS* (*bcIs134*) expression. Next, embryos were imaged using a Leica TCS SP8 confocal microscope with a 63x objective (oil, 1.4 NA). The Leica LAS AF software was used with the following setting: pinhole 95.53 µm (Airy 1), zoom factor 3, bidirectional scanning, line average 1, 1024 x 1024 pixels, Z-stack interval 1 µm, GFP excitation using a 488 nm laser at 10% intensity, and mCherry excitation using a

561 nm laser at 10% intensity. Then, the brightness of representative images was adjusted using Fiji (Image J) software (Schindelin et al., 2012).

For fluorescent images in **Fig. 5.2,** embryos of genotype [*bcSi134* III; *egl-1(bc449)* V *ltIs44* V; *bcIs161*] were prepared as described above. A Zeiss LSM980 microscope equipped with an AiryScan 2 detector and a 63x /1.40 Plan-Apochromat oil objective lens was used to acquire super resolution images of the RIDnb and its two daughter cells, RID and RIDsc. RIDnb and its two daughters were identified in embryos using a transgene $P_{unc\text{-}3}$*unc-3::mScarlet* (*bcIs161*). Images were acquired as Z-stacks spanning the whole embryo. A GaAsP detector was used to detect fluorescence with the following settings: GFP excitation using a 488 nm laser at 0.5% intensity, mScarlet and mCherry excitation using a 561 nm laser at 0.5% intensity, frame size 1024 x 1024 pixels, Z-stack interval 1 µm, 8-bit, line average none, and zoom 2.5. The images were submitted for AiryScan image processing by ZEN software. Then, the brightness of representative images was adjusted using Fiji (Image J) software (Schindelin et al., 2012).

Results

Chapter 3 Study of the *cis*-acting elements in the *egl-1* 3′ UTR

Genetic information is stored in DNA and transmitted via mRNA to proteins, which are the workhorses of cells and form the basis of living tissues. For a long time, it was thought that the information transfer from DNA to proteins happens exclusively via the coding region (CDS) of mRNAs, while it was well-known that mRNAs also contain untranslated regions (UTRs) at their 5′ and 3′ ends. In the past few decades, the concept has been established that the UTRs, especially the 3′ UTR, extensively regulate gene expression by affecting the stability, localization, and translation of the mRNA (Mayr, 2017). 3′ UTRs of mRNAs determine mRNA stability and spatiotemporal protein synthesis through sequence motifs and structural elements, which interact with trans-acting factors, such as miRNAs and RBPs (Barreau et al., 2005; Bartel, 2009; Martin and Ephrussi, 2009). New findings indicate that 3′ UTRs are also able to mediate protein-protein interactions, involved in protein complex formation and protein localization (Berkovits and Mayr, 2015; Chartron et al., 2016; Duncan and Mata, 2011). In this chapter, I describe my work on the function of conserved sequence and structural elements identified in the *egl-1* 3′ UTR in *C. elegans*.

3.1 Analysis of *C. elegans egl-1* 3′ UTR sequence and structure

The *C. elegans* 3′ UTRome has been profiled, and only one form of the *egl-1* 3′ UTR was identified (Steber et al., 2019). The 3′ UTR of *C. elegans egl-1* is 172 nt in length and contains several features, and some of them are evolutionarily conserved (**Fig. 3.1**, **Table 3.1**). There are binding sites for the miR-35 and miR-58 family miRNAs (Sherrard et al., 2017) and four predicted binding elements for the PUF family proteins FBF-1 and FBF-2 (FBE, two canonical FBEs and two alternative FBEs) (Porter et al., 2019; Prasad et al., 2016). In addition, an interaction site for ALG-1 Argonaut was identified in the *egl-1* 3′ UTR (Broughton and Pasquinelli, 2013; Grosswendt et al., 2014; Zisoulis et al., 2010).

The last 33 nt of the *egl-1* 3′ UTR are highly conserved with other *Caenorhabditis* species including *C. briggsae*, *C. brenneri*, and *C. remanei*. This element is referred to as the 3′ terminal element (TPTE). This region is predicted to form a stem-loop structure by base-pairing between two 9 nt segments of stem 1 and stem 2 (**Fig. 3.2**). This stem-loop represents a potential binding site for the *C. elegans* Staufen protein STAU-1. Staufen protein preferentially binds to stable stem-loops of mRNA (dsRNA structure) (LeGendre et al., 2013). The *egl-1* TPTE also contains the canonical AU-rich element (ARE), AUUUA, and could potentially interact with hnRNP proteins (encoded by *msi-1*, *hrpa-1*, *sqd-1*), HuR (*exc-7*) and/or TIA1/TIAL1 (cytotoxic granule-associated RNA binding and–like protein) (encoded by *tiar-1*, *2*, *3*). Likewise, the poly(U) segment could potentially interact with multiple members of the hnRNP family and TIAR-1, 2 or 3 (**Table 3.2**). These proteins might be involved in the control of *egl-1* mRNA stability, localization, and translation by interacting with the *egl-1* 3′ UTR. These RBP candidates were subjected to a genetic screen for *egl-1* regulators (described in the following **Chapter 4**).

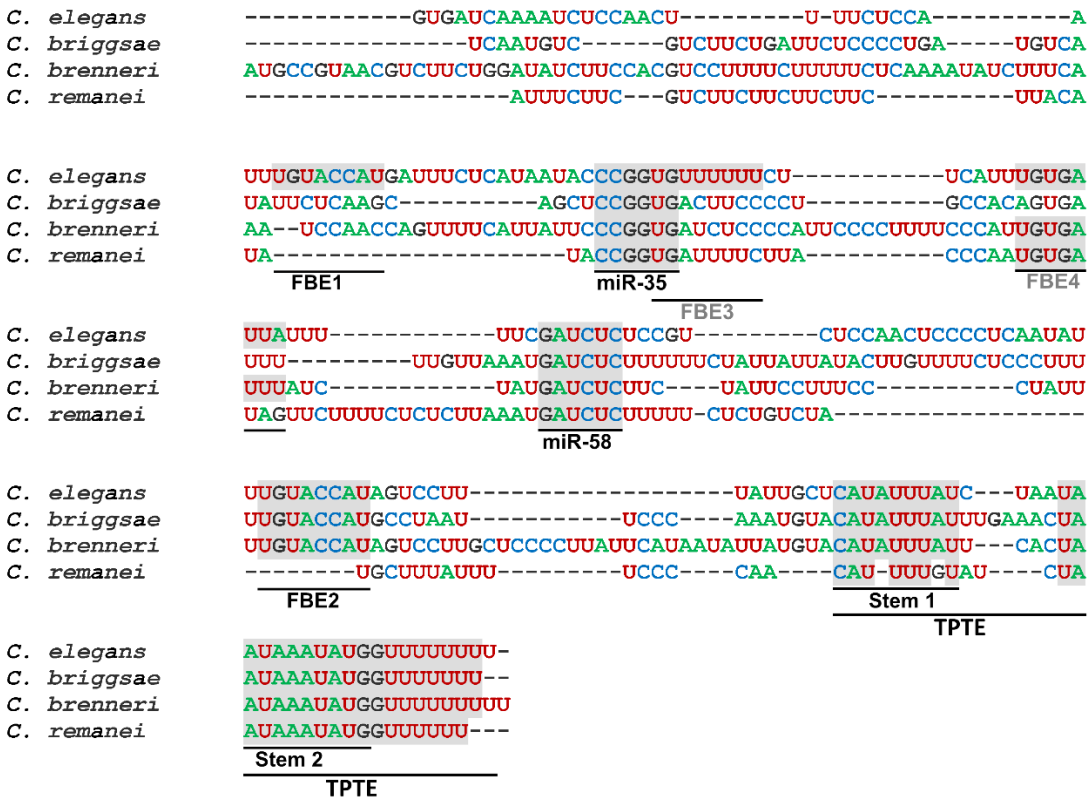

Figure 3.1 Clustal Omega alignment of the *egl-1* 3′ UTR sequence. The *C. elegans egl-1* 3′ UTR contains conserved elements in comparison to those of three other *Caenorhabditis* species. (www.ebi.ac.uk/Tools/msa/clustalo/). The conserved features, such as binding sites for miR-35 and miR-58 family miRNAs, PUF family protein FBF1/2 binding elements (FBE), and the 3′ terminal element (TPTE), are indicated. The FBEs in black color indicate canonical FBF-binding elements, and those in grey color indicate alternative FBF-binding elements. The stem 1 in the TPTE contains an AU-rich element (ARE, AUUUA).

Table 3.1 Predicted *cis*-acting elements in the *egl-1* 3′ UTR.

Element	Start	Stop	Sequence	Conservation
FBE1	31	38	UGUACCAU	-
ALG-1 binding site	62	118	UUUUCUUCAUUUGUGAUUAUUUUUCGAUCUCUCCGUCUCCAACUCCCCUCAAUAUUU	-
miR-35 biding site	54	59	CCGGUG	*Cele*, *Cbri*, *Cbre*, *Crem*
FBE3	58	65	UGUUUUUU	
FBE4	73	80	UGUGAUUA	*Cele*, *Cbre*
miR-58 binding site	87	92	GAUCUC	*Cele*, *Cbri*, *Cbre*, *Crem*
FBE2	118	125	UGUACCAU	*Cele*, *Cbri*, *Cbre*
TPTE	140	172	CAUAUUUAUCUAAUAAUAAAUAUGGUUUUUUUU	*Cele*, *Cbri*, *Cbre*, *Crem*

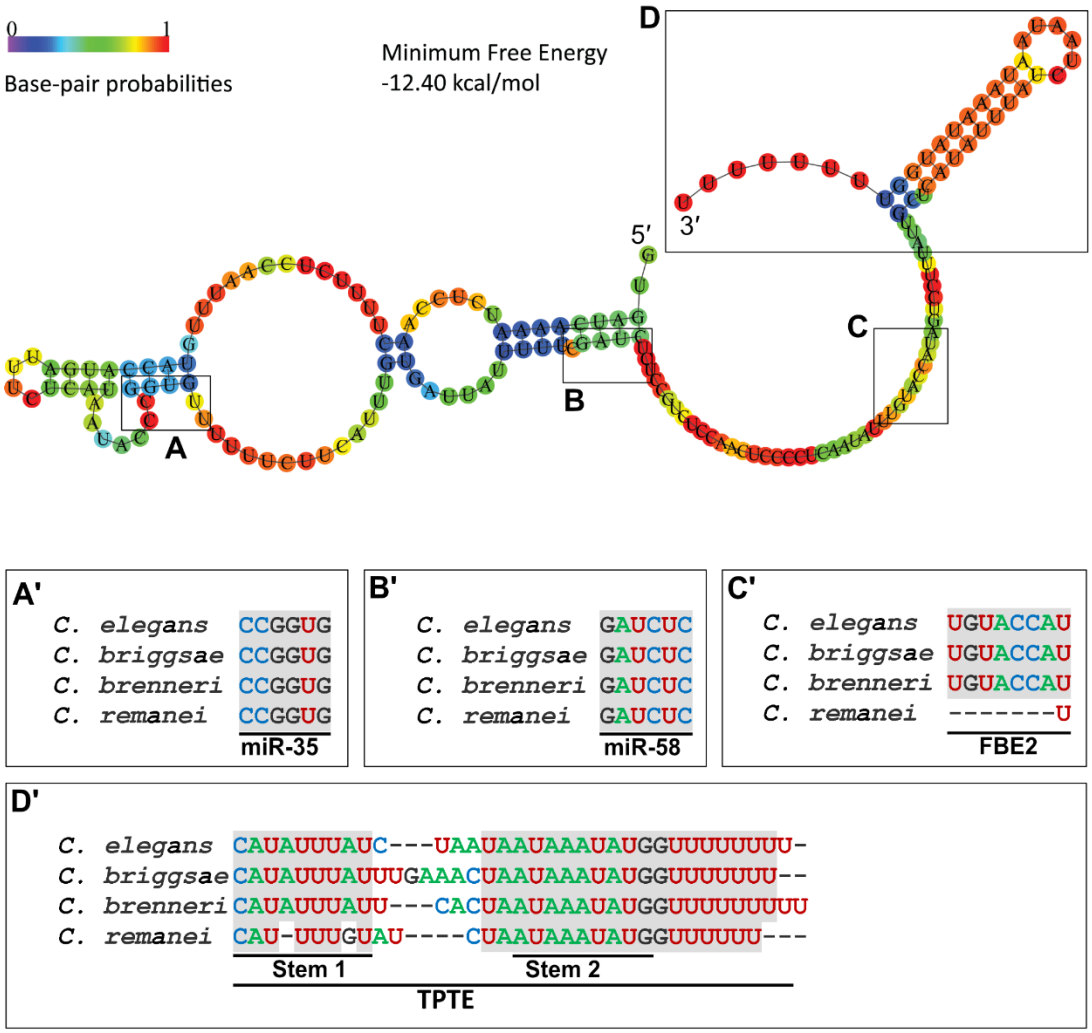

Figure 3.2 The predicted secondary structure of the *egl-1* 3' UTR. The predicted minimum free energy structure of the entire 3′ UTR of the *egl-1* mRNA is shown and colored according to base-pair probabilities. The minimum free energy is indicated. Several conserved features such as binding sites for miR-35 and miR-58 miRNAs, FBF binding element FBE2, as well as the 3′ terminal element (TPTE) are detailed in the box, including the sequence alignment with other *Caenorhabditis* species. The secondary structure of the *egl-1* 3′ UTR is predicted using the RNAfold web server (http://rna.tbi.univie.ac.at; Lorenz et al., 2011).

Table 3.2 RBP candidates predicted to interact with the *egl-1* 3′ UTR. Based on published literature and bioinformatics prediction, 32 RBPs from several families are predicted to interact with elements that are found in the *egl-1* 3′ UTR. The human protein and corresponding *C. elegans* ortholog(s) as well as gene knockout phenotypes in *C. elegans* are indicated. *puf-4* and *puf-10* are pseudogenes and not included.

Protein name in humans	***C. elegans* ortholog genes**	**Knockout allele phenotype**	**Potential binding element**
Annexin 2	*nex-2*	viable	Stem 1 ARE?
hnRNP A/B	*msi-1, hrpa-1 (hrp-1), sqd-1*	viable, sterile, sterile	Stem 1 ARE, Poly(A) tail?
CELF1	*etr-1*	sterile	Stem 1 ARE
HuR	*exc-7*	viable	Stem 1 ARE
miRISC	*alg-1, alg-2, cgh-1, ain-1, nhl-2*	viable, viable, sterile, viable, viable	miRNA binding sites
PABP	*pab-1, pab-2*	lethal, lethal	Poly(A) tail
PUF	*fbf-1, fbf-2, puf-3–13* (nine in total)	wild-type – sterile	FBEs
PUF-Ago	*alg-1, alg-2*	viable, viable	ALG-1 binding site
Staufen	*stau-1*	viable	TPTE stem-loop
Syncrip	*hrpr-1 (hrp-2)*	lethal	Poly(A) tail?
TIA1 and TIAL1	*tiar-1, tiar-2, tiar-3*	viable, viable, viable	Stem 1 ARE
TRIM2 and TRIM3	*ncl-1*	viable	FBEs?
GYF-domain protein	*sao-1*	viable	miRNA binding sites
GIGYF1 and GIGYF2	*gyf-1*	partially lethal	miRNA binding sites

3.2 TPTE contributes to the repression of *egl-1* expression

To determine the functionality of the TPTE in the regulation of *egl-1* expression, I assessed the effect of the TPTE on the expression of reporter genes. Firstly, the *egl-1* 3′ UTR is appended to the *gfp::h2b* fusion gene, which is driven by the promoter of a widely expressed gene *mai-2*. Use of the *mai-2* promoter thereby ensures constitutive transcription of the reporter gene in all cells (Ichikawa et al., 2006). A single copy of this reporter gene is inserted into the *C. elegans* genome, generating a transgene $P_{mai\text{-}2}$*gfp::h2b::egl-1* 3′ UTR (*bcSi26*) (**Fig. 3.3A**, 1st row). The expression of this reporter gene is expected to be controlled by the 3′ UTR at the post-transcriptional level. As a control, the 3′ UTR in this reporter gene is replaced by the *mai-2* 3′ UTR, generating a single-copy transgene $P_{mai\text{-}2}$*gfp::h2b::mai-2 3′ UTR* (*bcSi25*) (**Fig. 3.3A**, 4th row). GFP intensity in the nuclear area of 4-cell embryos from these two transgenic strains was analyzed using fluorescence microcopy. Surprisingly, the expression of the transgene $P_{mai\text{-}2}$*gfp::h2b::egl-1 3′ UTR* (*bcSi26*) is largely repressed in embryos (**Fig. 3.3A and B**). By contrast, the transgene $P_{mai\text{-}2}$*gfp::h2b::mai-2 3′ UTR* (*bcSi25*) is highly expressed in embryos. These two reporters only differ in their 3′ UTRs. This suggests that the *egl-1* 3′ UTR largely represses gene expression.

Next, to ask whether the TPTE is necessary for the *egl-1* 3′ UTR-mediated gene repression, I scrambled the *egl-1* TPTE and generated a variant reporter transgene $P_{mai\text{-}2}$*gfp::h2b::egl-1 3′ UTR*$^{TPTE\ mut}$ (*bcSi121*) (**Fig. 3.3A**, 2nd row). With this mutation, I expect that the function of the *egl-1* TPTE will be disrupted. Not surprisingly, *egl-1* TPTE disruption up-regulates *gfp::h2b* expression (**Fig. 3.3A and B**). In addition, I replaced the *egl-1* TPTE in the reporter with the *mai-2* TPTE and generated another variant reporter transgene $P_{mai\text{-}2}$*gfp::h2b::egl-1 3′ UTR*$^{mai\text{-}2\ TPTE}$ (*bcSi122*) (**Fig. 3.3A**, 3rd row). Consistently, the replacement of the *egl-1* TPTE by the *mai-2* TPTE also up-regulates *gfp::h2b* expression (**Fig. 3.3A and B**). These results suggest that the *egl-1* TPTE is necessary for the *egl-1* 3′ UTR-mediated gene repression.

Finally, to determine whether the *egl-1* TPTE is sufficient to repress gene expression, I put the *egl-1* TPTE into the reporter $P_{mai\text{-}2}$*gfp::h2b::mai-2 3′ UTR* (*bcSi25*) to replace the *mai-2* TPTE and generated a variant reporter transgene $P_{mai\text{-}2}$*gfp::h2b::mai-2 3′ UTR*$^{egl\text{-}1\ TPTE}$ (*bcSi123*) (**Fig. 3.3A**, 5th row). Compared to $P_{mai\text{-}2}$*gfp::h2b::mai-2 3′ UTR* (*bcSi25*), the expression of $P_{mai\text{-}2}$*gfp::h2b::mai-2 3′ UTR*$^{egl\text{-}1\ TPTE}$ (*bcSi123*) is

significantly down-regulated (**Fig. 3.3A and B**). This suggests that the *egl-1* TPTE is partially sufficient to repress gene expression.

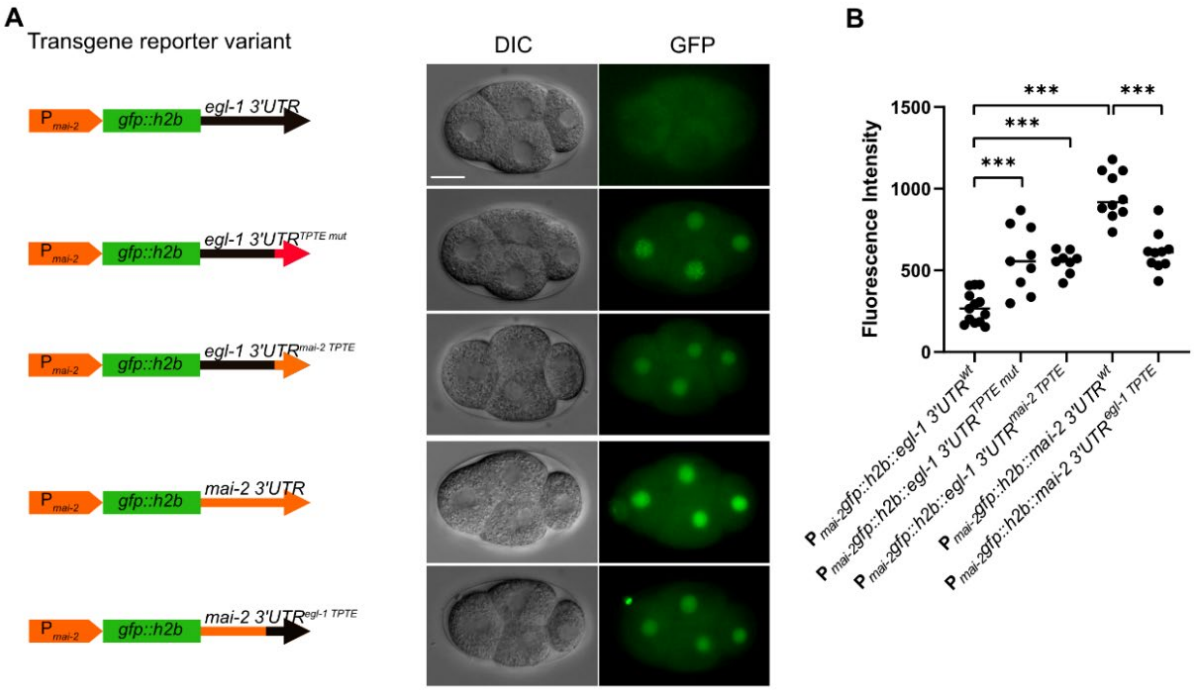

Figure 3.3 The *egl-1* 3′ UTR TPTE represses the reporter gene expression. (A) Expression of *egl-1* 3′ UTR reporter gene variants. The schematics of the 3′ UTR reporter transgenes are shown on the left. The representative DIC and GFP images of 4-cell stage embryos from each reporter transgenic strain are shown on the right. Scale bar, 10 μm. (B) Quantitative analyses of GFP intensity (mean value) in nuclear area in the sum of Z-stacks. The number of embryos analyzed (n) is 13 for $P_{mai\text{-}2}$*gfp::h2b::egl-1* 3′ UTR (*bcSi26*), 9 for $P_{mai\text{-}2}$*gfp::h2b::egl-1 3′ UTR*$^{TPTE\ mut}$ (*bcSi121*), 8 for $P_{mai\text{-}2}$*gfp::h2b::egl-1 3′ UTR*$^{mai\text{-}2\ TPTE}$ (*bcSi122*), 10 for $P_{mai\text{-}2}$*gfp::h2b::mai-2 3′ UTR* (*bcSi25*), and 10 for $P_{mai\text{-}2}$*gfp::h2b::mai-2 3′ UTR*$^{egl\text{-}1\ TPTE}$ (*bcSi123*). *** $p < 0.001$ via one-way ANOVA with the Tukey post hoc test.

The TPTE in the *egl-1* 3′ UTR is predicted to form a stem-loop structure by the complementary base pairing between nucleotides (the minimum free energy is -4.6 kcal/mol) (**Fig. 3.4A**). Stem-loop structures within an mRNA have been proposed to regulate mRNA with respect to its stability, localization, and translation (Bao et al., 2022; Heinrich et al., 2017; Marzluff et al., 2008; Sanchez and Marzluff, 2002). To explore the functionality of the structure of the TPTE in the *egl-1* 3′ UTR, I switched the A and U to G and C, respectively, in the TPTE stem 1 and stem 2 region, generating a variant reporter transgene $P_{mai\text{-}2}$*gfp::h2b::egl-1 3'UTR*$^{TPTE\ A->G,U->C}$ (*bcSi127*). Through this change, the structure of the *egl-1* TPTE presumably becomes more stable (the minimum free energy is changed from -4.6 kcal/mol to -19.6 kcal/mol after nucleotide substitution) (**Fig. 3.4A**). While the expression of the reporter transgene $P_{mai\text{-}2}$*gfp::h2b::egl-1* 3′ UTR (*bcSi26*) is largely repressed in early embryos, it is moderately expressed in germ cells and oocytes (**Fig. 3.4B and C**). By contrast, the expression of the variant reporter transgene $P_{mai\text{-}2}$*gfp::h2b::egl-1 3'UTR*$^{TPTE\ A->G,U->C}$ (*bcSi127*) is largely repressed not only in embryos but also in germ cells and oocytes (**Fig. 3.4B and C**). This suggests that the transgene is further repressed by this mutation. This down-regulation could result from the stabilized stem-loop structure.

Most eukaryotic mRNAs (except for histone mRNAs) are polyadenylated at their 3′ end under the regulation of the poly(A) signal (PAS) and cleavage and polyadenylation specificity factor (CPSF) complex. The poly(A) tail is thought to protect mRNAs from degradation and required for translation initiation (Eckner et al., 1991; Hilleren et al., 2001). Nucleotide substitution in the variant reporter transgene $P_{mai\text{-}2}$*gfp::h2b::egl-1 3'UTR*$^{TPTE\ A->G,U->C}$ (*bcSi127*) leads to disruption of the PAS, which could result in the loss of poly(A) tail and thereby destabilize the mRNA molecule. To determine whether the loss of the PAS in the *egl-1* 3′ UTR causes a down-regulation of the reporter gene expression, I reversed the sequence in stem1 and stem 2 region of the *egl-1* TPTE and generated a variant reporter transgene $P_{mai\text{-}2}$*gfp::h2b::egl-1 3'UTR*$^{PAS\ reversed}$ (*bcSi128*). Through this, the PAS in the 3′ UTR is disrupted, without affecting the stability of the TPTE structure (**Fig. 3.5A**). Unexpectedly, this reporter $P_{mai\text{-}2}$*gfp::h2b::egl-1 3'UTR*$^{PAS\ reversed}$ (*bcSi128*) is highly expressed rather than repressed (**Fig. 3.5B**). This suggests that the PAS in the *egl-1* 3′ UTR seems dispensable for the reporter gene expression. Although it is technically impossible to completely uncouple

the effects of the sequence and structure in the *egl-1* TPTE, it seems plausible that both are involved in the *egl-1* 3′ UTR-mediated gene repression.

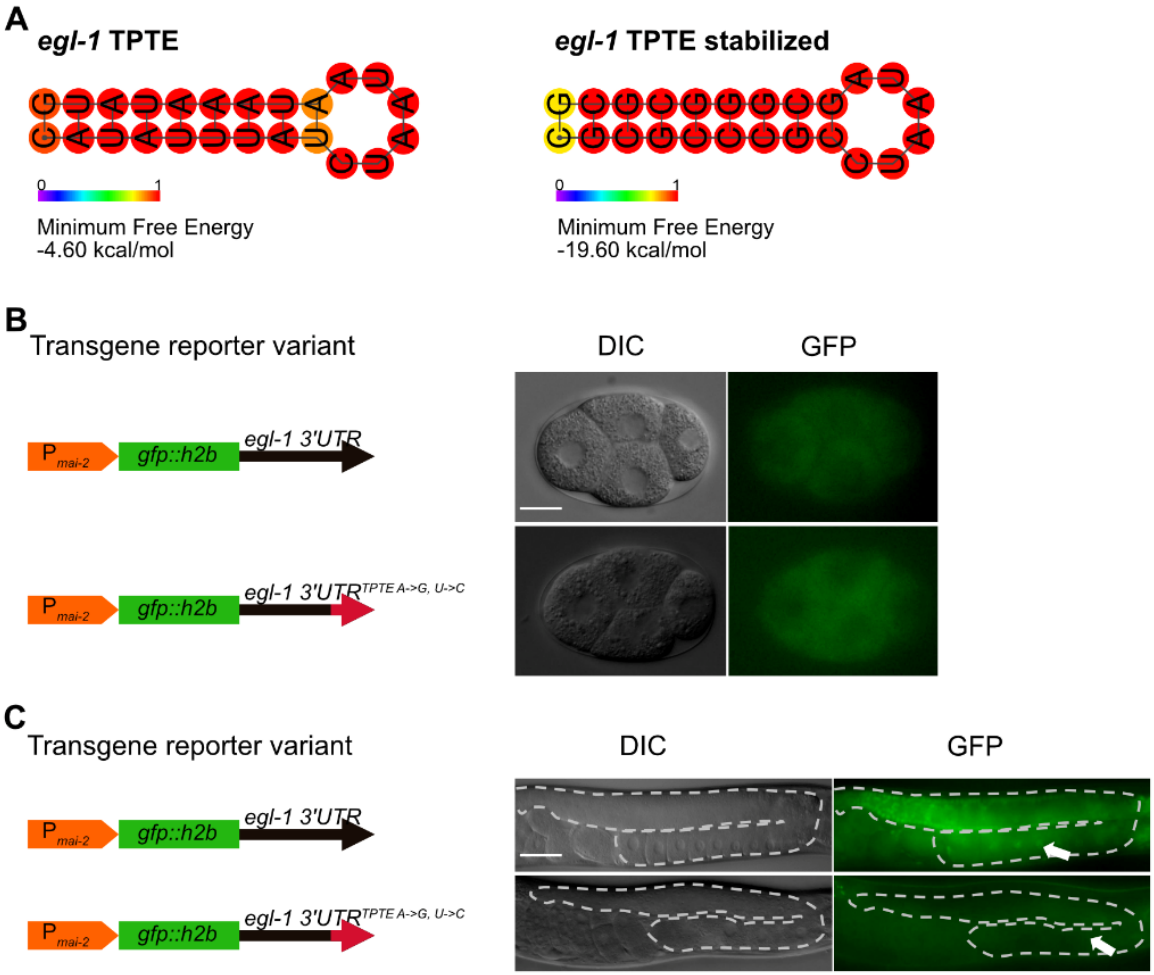

Figure 3.4 Effect of the structural stabilization of the TPTE on the expression of the *egl-1* 3′ UTR reporter. (A) The predicted minimum free energy structure for wild-type *egl-1* TPTE and structurally stabilized *eg-1* TPTE through A->G and U->C substitution, colored according to base-pair probabilities. The minimum free energy is indicated. Secondary structure prediction is performed using the RNAfold web server (http://rna.tbi.univie.ac.at; Lorenz et al., 2011). (B) The 3′ UTR reporter expression in embryos. The schematics of the 3′ UTR reporter transgenes are shown on the left. The representative DIC and GFP images of 4-cell stage embryos from each reporter transgenic strain are shown on the right. The number of embryos analyzed (n) is 13 for $P_{mai\text{-}2}$*gfp::h2b::egl-1* 3′ UTR (*bcSi26*), and 7 for $P_{mai\text{-}2}$*gfp::h2b::egl-1 3'UTR*$^{TPTE\ A\text{->}G,U\text{->}C}$ (*bcSi127*). Scale bar, 10 µm. (C) The 3′ UTR reporter expression in the germline. The H2B::GFP signal in oocyte nucleus is indicated by white arrows. The number of animals analyzed (n) is 6 for $P_{mai\text{-}2}$*gfp::h2b::egl-1* 3′ UTR (*bcSi26*), and 3 for $P_{mai\text{-}2}$*gfp::h2b::egl-1 3'UTR*$^{TPTE\ A\text{->}G,U\text{->}C}$ (*bcSi127*). Scale bar, 50 µm.

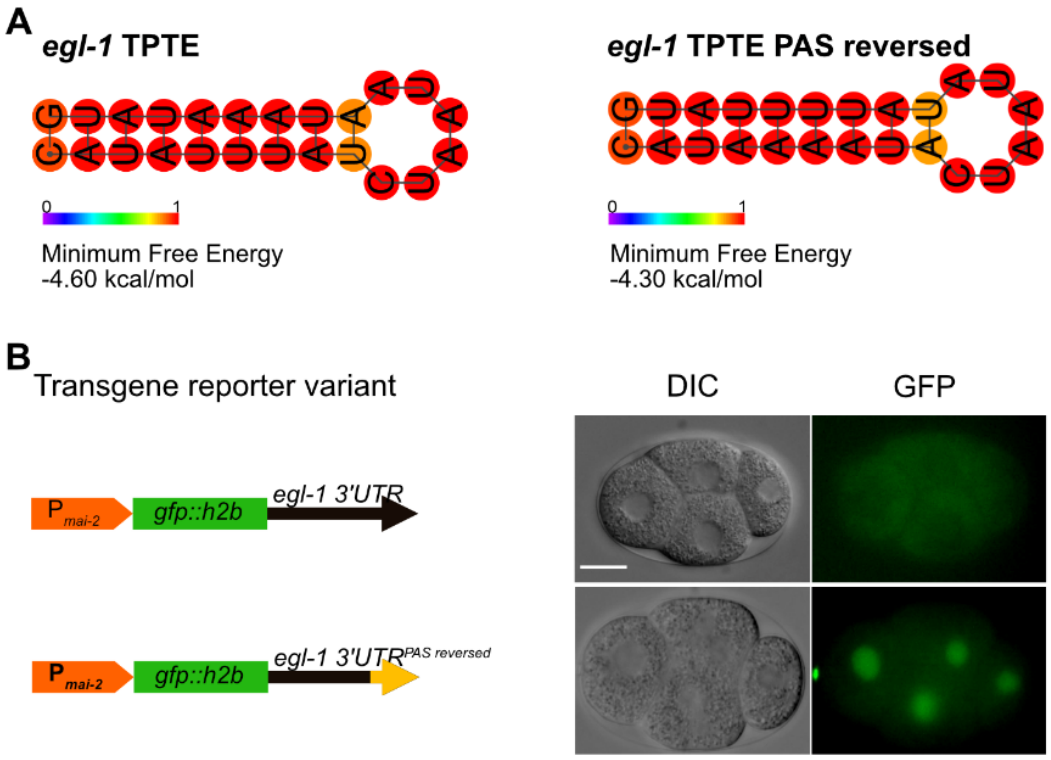

Figure 3.5 Poly(A) signal is not required for the *egl-1* 3′ UTR reporter expression. (A) The predicted minimum free energy structure for wild-type *egl-1* TPTE and the poly(A) signal (PAS, AAUAAA) reversed *eg-1* TPTE, colored according to base-pair probabilities. The minimum free energy is indicated. Secondary structure prediction is performed using the RNAfold web server (http://rna.tbi.univie.ac.at; Lorenz et al., 2011). (B) The 3′ UTR reporter expression in embryos. The schematics of the 3′ UTR reporter transgenes are shown on the left. The representative DIC and GFP images of 4-cell stage embryos from each reporter transgenic strain are shown on the right. The number of embryos analyzed (n) is 3 for $P_{mai\text{-}2}$*gfp::h2b::egl-1* 3′ UTR (*bcSi26*), and 3 for $P_{mai\text{-}2}$*gfp::h2b::egl-1 3′UTR*$^{PAS\ reversed}$ (*bcSi128*). Scale bar, 10 μm.

To determine whether the *egl-1* 3′ UTR TPTE contributes to the repression of endogenous *egl-1* expression and regulates apoptosis, I randomized the *egl-1* TPTE sequence using Random DNA Sequence Generator (www.faculty.ucr.edu/~mmaduro/random) and then replaced the endogenous *egl-1* TPTE sequence through the CRISPR/Cas genome editing technology, generating the allele *egl-1(syb5451)* (**Fig. 3.6A**). Through this mutation, I expect that both the sequence and structure as well as the function of the *egl-1* 3′ UTR TPTE will be disrupted. Most cells that die during *C. elegans* development form refractile 'cell corpses' with a size of 2 ± 0.3 µm (maximum 2.6 µm, measured from cell corpses formed during the first wave cell deaths) in diameter (**Fig. 3.6B**; +/+, black arrowhead), after being generated through asymmetric cell divisions. Apart from these 'normal' cell corpses, in *egl-1(syb5451)* mutant embryos, I also observed cell corpses larger than 2.6 µm in diameter (**Fig. 3.6B**; white arrowhead), which are possibly generated from precocious death of mothers of cells programmed to die or ectopic cell death due to *egl-1* dysregulation. I quantified the number of these large cell corpses until the end of ventral closure (~400 minutes or ~280 after the first cleavage of the zygote at 15°C or 25°C, respectively) and observed on average 0.1 large corpses per embryo in the *egl-1(syb5451)* mutant at 25°C, which is a very weak phenotype and not significant when compared to the wild-type embryos (**Fig. 3.6C**). Then, I assessed this phenotype in a weak *ced-9* BCL-2 loss of function mutant background *ced-9(n1653ts)*, in which the apoptotic pathway is already partially activated, and which therefore provides a sensitized background. As expected, a weak but significant enhancement of the 'large cell corpse' phenotype was observed (on average 2.3 large cell corpse in *ced-9(n1653ts)* and 3.8 in *ced-9(n1653ts)*; *egl-1(syb5451)* double) mutant at 15°C (**Fig. 3.6C**). The enhancement was also observed at 25°C; however, this was not statistically significant. These data suggest that the *egl-1* 3′ UTR TPTE may contribute to the repression of *egl-1* expression and the prevention of precocious or ectopic cell death.

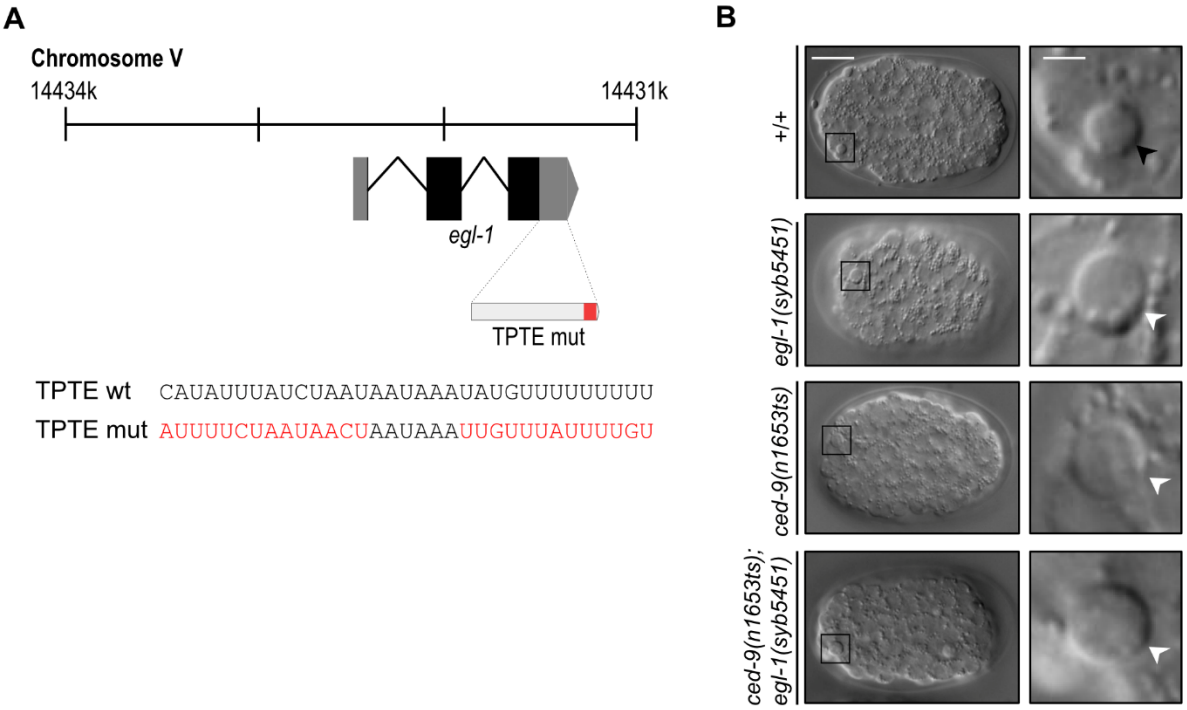

C

Genotypes	Large cell corpse per embryo		n	Temperature
+/+	0		10	15°C
egl-1(syb5451)	0		10	15°C
ced-9(n1653ts)	2.3 ± 0.3	***	10	15°C
ced-9(n1653ts); egl-1(syb5451)	3.8 ± 0.3		10	15°C
+/+	0	ns	10	25°C
egl-1(syb5451)	0.1 ± 0.1		10	25°C
ced-9(n1653ts)	3.6 ± 0.6	ns	10	25°C
ced-9(n1653ts); egl-1(syb5451)	4.5 ± 0.5		10	25°C

Figure 3.6 Mutation of the TPTE in the endogenous *egl-1* causes abnormal cell deaths in embryos. (A) Schematics for the mutation of the TPTE in the endogenous *egl-1*. The wild-type TPTE sequence and sequence after mutation are indicated. (B) The differential interference contrast (DIC, Nomarski) images for the normal size cell corpse (black arrowheads) and the large cell corpse (white arrowheads) in embryos. Representative cell corpses are shown enlarged (5x) on the right. Scale bars: 10 μm for the embryo image and 2 μm for the enlarged cell corpse image. (C) The total number of large cell corpses observed throughout embryogenesis until the end of the ventral enclosure. The assays were performed at two temperature conditions, namely at 15°C and 25°C, respectively. The data are shown as mean ± SEM. *** $p < 0.001$ via one-way ANOVA with the Tukey post hoc test. ns indicates no significance.

Staufen is a double-stranded-RNA- and tubulin-binding protein, which forms ribonucleoprotein complexes (RNPs) that play critical roles in the localization, translational repression, and turnover of mRNAs (LeGendre et al., 2013; Wickham et al., 1999). I was expecting that *C. elegans* Staufen protein STAU-1 could bind to the *egl-1* TPTE stem-loop to regulate the *egl-1* mRNA. To determine whether STAU-1 functions as a repressor for *egl-1*, I assessed the expression of the reporter gene $P_{mai\text{-}2}$*gfp::h2b::egl-1* 3′ UTR (*bcSi26*) (**Fig. 3.7A**) in a *stau-1(ma327)* mutant background. *stau-1(ma327)* is an full loss of function mutation (Ren et al., 2016). Unexpectedly, the expression of the *egl-1* 3′ UTR reporter is not up-regulated in *stau-1(ma327)* mutant embryos (**Fig. 3.7B**). In addition, large cell corpses were not observed in *stau-1(ma327)* mutant embryos (10 embryos analyzed). These results suggest that STAU-1 might not contribute to the repression of *egl-1* expression.

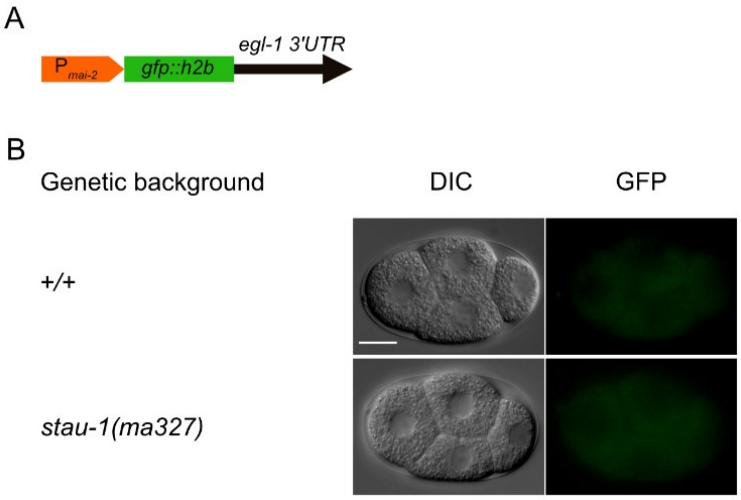

Figure 3.7 Effect of *stau-1* on the *egl-1* 3′ UTR reporter expression. (A) The schematics of the *egl-1* 3′ UTR reporter P_{mai-2}*gfp::h2b::egl-1* 3′ UTR (*bcSi26*). (B) The *egl-1* 3′ UTR reporter expression in wild-type and *stau-1(ma327)* mutant embryos. The number of embryos analyzed (n) is 13 for wild-type embryos and 6 for *stau-1(ma327)* mutant embryos. Scale bar, 10 μm.

Overall, the *egl-1* TPTE is likely necessary and partially sufficient to repress *egl-1* expression. Both the stem-loop structure and sequence in this region appear to contribute to the *egl-1* 3′ UTR mediated repression of *egl-1* expression. However, the *trans*-acting factors that interact with this element and repress *egl-1* expression remain to be uncovered.

3.3 FBEs contribute to the repression of the *egl-1* 3′ UTR reporter

The *C. elegans* FBF-1 and FBF-2 proteins (collectively referred as FBF) belong to the PUF (Pumilio/FBF) family of RNA-binding proteins, which are crucial for the sperm-to-oocyte switch during germ cell development (Bachorik and Kimble, 2005; Lamont et al., 2004). Through immunoprecipitating FBF-1::GFP protein-RNA complexes from animal extracts using an anti-GFP antibody, the *egl-1* mRNA was detected in the purified FBF complexes by probed microarray analysis (Kershner and Kimble, 2010). The canonical as well as alternate binding elements for FBF proteins have been precisely mapped using the iCLIP (individual-nucleotide resolution UV crosslinking and immunoprecipitation) technology (Prasad et al., 2016). In the *egl-1 3′ UTR*, two canonical FBEs (FBE1/2, UGUNNNAU) and two additional non-canonical alternate elements (FBE3/4) are found. To determine whether the four FBEs are involved in the repression of *egl-1* expression, the first three nucleotides in each of the four FBEs in the *egl-1* 3′ UTR reporter were changed from UGU to ACA, generating the reporter transgene $P_{mai\text{-}2}$*gfp::h2b::egl-1 3′ UTR*$^{FBE\ mut}$ (*bcSi106*). With these mutations, I expect that binding of FBF proteins to the *egl-1 3′ UTR* in the reporter mRNA is disrupted (**Fig. 3.8A**). As expected, mutation in these four FBEs de-repressed the reporter expression in embryos (**Fig. 3.8B**), indicating that these FBEs contribute to the repression of the *egl-1* 3′ UTR reporter expression.

To determine whether the de-repression of the *egl-1* 3′ UTR reporter caused by the FBE mutations is due to the loss of FBF-1 and FBF-2 binding to these sites, I determined the expression of the reporter transgene $P_{mai\text{-}2}$*gfp::h2b::egl-1 3′ UTR* (*bcSi26*) in a *fbf-1(ok91) fbf-2(q704)* double mutant background. Animals lacking *fbf-1* and *fbf-2* cannot be maintained due to defects in germline development and sterility; therefore, the *mIn1 [dpy-10(e128); mIs14]* chromosome II balancer is used (i.e. *fbf-1(ok91) fbf-2(q704)/mIn1*) and the strain is maintained as heterozygotes. The homozygous *fbf-1(ok91) fbf-2(q704)* F1 animals were used for experiments. Unexpectedly, the expression of the reporter transgene $P_{mai\text{-}2}$*gfp::h2b::egl-1 3′ UTR* (*bcSi26*) doesn't change in *fbf-1(ok91) fbf-2(q704)* embryos (**Fig. 3.8B**). To rule out that the lack of phenotype in *fbf-1(ok91) fbf-2(q704)* is caused by maternal *fbf-1* and/or *fbf-2* mRNAs that are inherited from the heterozygous mother's germline, where *fbf-1* and *fbf-2* are highly expressed, I injected the *fbf-1* dsRNA into animals carrying the

reporter transgene P_{mai-2}*gfp::h2b::egl-1 3' UTR* (*bcSi26*) to knock down both *fbf-1* and *fbf-2* (sequence is highly homologous). This *fbf-1* dsRNA has been shown to cause degradation of both *fbf-1* and *fbf-2* mRNAs (Zhang et al., 1997). The efficient knockdown of *fbf-1 and fbf-2* was confirmed by the phenotype of F1 animals, which exhibit improper germline development and sterility. The expression of the reporter P_{mai-2}*gfp::h2b::egl-1 3' UTR* (*bcSi26*) was determined in embryos from the *fbf-1* dsRNA injected animals. However, no obvious change in the expression of this reporter was observed (**Fig. 3.8B**). Furthermore, large cell corpses were not observed in *fbf-1(ok91) fbf-2(q704)* mutant embryos (10 embryos were analyzed) and embryos from the *fbf-1* dsRNA injected animals (10 embryos were analyzed). These results indicate that FBF proteins either don't repress *egl-1* expression or that they have functionally redundant factors. The promotive effect of FBF proteins on *egl-1* expression should be determined in the future. This suggests that the up-regulation of P_{mai-2}*gfp::h2b::egl-1 3' UTR*$^{FBE\ mut}$ is because of changes in the binding of regulators other than FBF proteins to the *egl-1* 3' UTR.

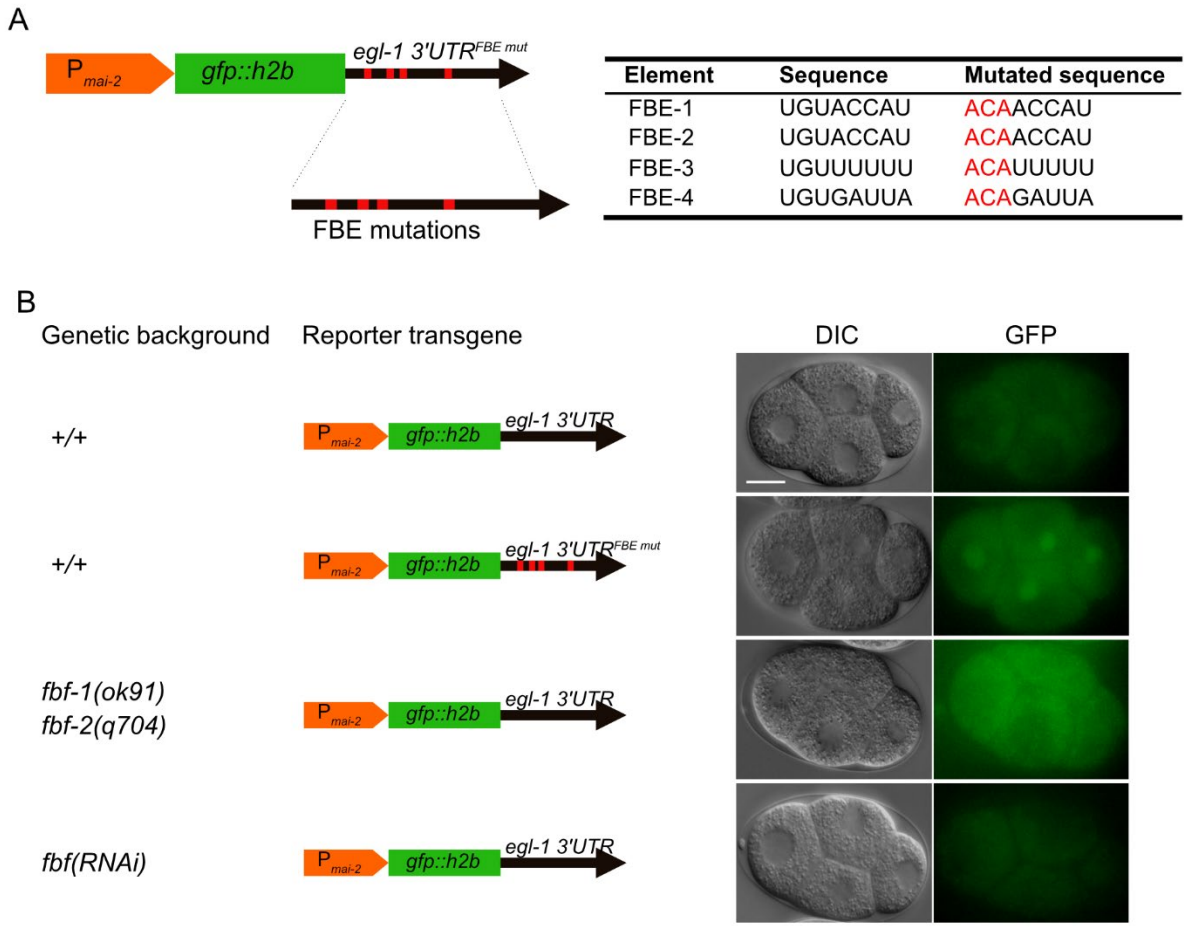

Element	Sequence	Mutated sequence
FBE-1	UGUACCAU	ACAACCAU
FBE-2	UGUACCAU	ACAACCAU
FBE-3	UGUUUUUU	ACAUUUUU
FBE-4	UGUGAUUA	ACAGAUUA

Figure 3.8 Effects of FBF and FBEs on the repression of reporter gene expression. (A) Schematics for the mutation of FBEs in the reporter transgene $P_{mai\text{-}2}$*gfp::h2b::egl-1 3′ UTR*$^{FBE\ mut}$ (*bcSi106*). The wild-type FBE sequence and mutant sequence are provided on the right. (B) The expression of reporter genes in wild-type, *fbf-1(ok91) fbf-2(q704)* mutant, or *fbf(RNAi)* embryos. The genetic background is indicated on the left. The schematics of the *egl-1* 3′ UTR reporter transgenes are shown in the middle. The representative DIC and GFP images of 4-cell stage embryos are shown on the right. The number of embryos analyzed (n) is 4 for wild-type embryos carrying $P_{mai\text{-}2}$*gfp::h2b::egl-1 3′ UTR* (*bcSi26*), 4 for wild-type embryos carrying $P_{mai\text{-}2}$*gfp::h2b::egl-1 3′ UTR*$^{FBE\ mut}$ (*bcSi106*), 3 for *fbf-1(ok91) fbf-2(q704)* mutant embryos carrying $P_{mai\text{-}2}$*gfp::h2b::egl-1 3′ UTR* (*bcSi26*), and 3 for *fbf(RNAi)* embryos carrying $P_{mai\text{-}2}$*gfp::h2b::egl-1 3′ UTR* (*bcSi26*). Scale bar, 10 μm.

In the study described in this chapter, I analyzed *egl-1* 3' UTR features and investigated the function of evolutionarily conserved elements in the *egl-1* 3' UTR, such as the TPTE and FBEs, on the regulation of *egl-1* expression and apoptosis. I also determined the effects of the RBPs that are presumed to bind these elements, namely, Staufen protein STAU-1 and FBF proteins, respectively. Interestingly, I found that the TPTE in the *egl-1* 3' UTR contributes to the repression of *egl-1* expression and modulates the invariant pattern of apoptotic cell death during *C. elegans* development. Staufen protein is known as a dsRNA region-binding protein and it regulates mRNA transport and translation (Wickham et al., 1999). I expected the *C. elegans* Staufen protein STAU-1 to repress *egl-1* expression by interacting with the stem-loop structure of the TPTE; however, a loss of function mutation of the *stau-1* gene did not show an up-regulation of *egl-1* 3' UTR reporter expression and apoptosis. The disruption of FBF protein binding elements (FBEs) in the *egl-1* 3' UTR up-regulates *egl-1* 3' UTR reporter expression, but the loss of FBF proteins did not show an up-regulation of *egl-1* 3' UTR reporter expression or apoptosis. Overall, the TPTE and FBEs in the *egl-1* 3' UTR are likely involved in the repression of *egl-1* expression, but their binding partners and the underlining molecular mechanisms remain unclear.

Most functions of 3′ UTRs are mediated by miRNAs and RBPs. miRNAs base-pair with miRNA binding sites within their target mRNAs, usually in the 3′ UTR, through a critical region called the 'seed region' which includes nucleotides 2-8 from the 5′ end of the miRNA (Chen et al., 2008b). Binding sites for miR-35 and miR-58 families of miRNAs have been found in the *egl-1* 3' UTR. These miRNAs have been shown to repress *egl-1* expression by binding to their binding sites (Sherrard et al., 2017). In contrast to miRNA binding sites, the binding elements for many RBPs are still not clear. As multiple elements can work redundantly, functional binding sites cannot easily be identified by element mutations (Mayr, 2017). Nevertheless, through searching for known binding sites for common RBPs in the *egl-1* 3′ UTR, some RBPs were presumed to bind *egl-1* 3′ UTR (**Table 3.2**). I individually knocked down the gene encoding these candidate RBPs to look for those that could regulate *egl-1* expression. This is included in the following **Chapter 4**.

Chapter 4 Identification of RBPs that regulate *egl-1* expression

While transcription contributes to coordinated gene expression in time and space, studies have revealed that the level of a given mRNA and the amount of protein it encodes do not directly correlate (Becker et al., 2018; Komili and Silver, 2008; Schwanhausser et al., 2011). Protein synthesis can be controlled at the post-transcriptional level by RBPs and non-coding RNAs. Over the past years, studies based on high-throughput methods to detect RNA-protein interactions, such as RNA immunoprecipitation (IP) and crosslink IP (CLIP)-based techniques, allowed to identify over 2000 proteins that interact with RNA molecules (McHugh et al., 2014; Van Nostrand et al., 2016). Moreover, thanks to the development of RNA interactome capture technologies, the catalog of RBPs has been dramatically improved (Baltz et al., 2012; Beckmann et al., 2015; Castello et al., 2016; Conrad et al., 2016; Matia-Gonzalez et al., 2015). Interestingly, many of these experimentally identified RBPs lack known RNA-binding domains (RBDs) (Beckmann et al., 2015; Matia-Gonzalez et al., 2015). However, many known RBPs are omitted from some of these RBP repertoires revealed by biochemical works. In this context, large-scale computational prediction of protein-RNA interactions, for example by genome-wide searching for RBDs, can provide a better coverage of the protein-RNA interactions.

C. elegans is an excellent model system for studying apoptosis and performing systematic genetic screening. With the availability of the RNAi feeding libraries, namely the Ahringer RNAi library (Kamath and Ahringer, 2003; Kamath et al., 2003) and Vidal RNAi library (Rual et al., 2004), the expression of endogenous genes can be specifically knocked down by feeding bacterial clones expressing double-stranded RNA (dsRNA) of corresponding genes. The Ahringer RNAi feeding library covers about 85% of the protein-coding genes in *C. elegans* and the Vidal RNAi feeding library covers about half of the *C. elegans* protein-coding genes. These two RNAi feeding libraries provide a powerful way for genetic screens.

In this chapter, I first describe my work on the characterization of *C. elegans* RBPs and the construction of an mRNA-binding protein (mRBP) compendium. Then, I introduce my work on a genetic screen by RNAi for identifying RBPs that might be involved in the control of *egl-1* expression and, hence, apoptotic cell death during *C. elegans* development.

4.1 Construction and characterization of *C. elegans* RBP repertoire

To perform the systematic RNAi screen for RBPs that might regulate *egl-1* expression and apoptosis, I first constructed and characterized the RBP repertoire in *C. elegans*. The initial list of RBPs in *C. elegans* identified by Wang et al., (2009) only contains 319 genes (Wang et al., 2009). They excluded genes that encode proteins that are unlikely to have RNA binding function, such as those that are predicted to also bind DNA, and genes encoding ribosomal proteins. Among 319 RBP genes, 190 of them are expressed in the germline and 131 are expressed in the soma. Tamburino et al., (2013) expanded the list to 887, including 94% of the genes in the initial one (**Figure 4.1A**), by searching for the sequence signatures of known RBDs (Tamburino et al., 2013). They included additional RBDs and protein classes (i.e., dsRBDs, ribosomal proteins, C2H2 zinc fingers, SAM domains). Besides, systematic approaches have been employed to experimentally map mRNA-binding proteins (mRBPs) in yeast and mammalian cells by capturing *in vivo* cross-linked mRNA–protein complexes combined with subsequent mass spectrometry analysis. These studies have suggested that many mRBPs lacking canonical RNA-binding domains (RBDs) can bind RNAs (Scherrer et al., 2010; Tsvetanova et al., 2010). In a poly(A)-containing mRNAs capturing study, 594 proteins were experimentally identified to interact with polyadenylated mRNAs in *C. elegans*. These mRNA-binding proteins are defined as the mRBPome of *C. elegans*, encoded by 591 genes (Matia-Gonzalez et al., 2015). However, only a small proportion of RBP genes in this list overlapped with the other two lists of RBP genes (**Figure 4.1B and 4.1C**). In addition, many previously reported mRBPs are missing from this list, suggesting that the RBPs presented by Matia-Gonzalez et al., (2015) do not represent all mRBPs in *C. elegans*.

Thus, I incorporated all these lists and conducted Gene Ontology (GO) enrichment, phenotype enrichment, and tissue enrichment analysis using WormBase Enrichment Analysis (**Figure 4.1D**). The GO enrichment analysis shows that most RBP genes are enriched in processes such as metabolism, nucleotide binding, and organelle composition (**Figure 4.1E**). Those genes that are proposed to have very general functions, such as genes encoding tRNA binding proteins, ribosomal subunits, and ribonucleases, were excluded. The phenotype enrichment analysis shows that most RBP genes are enriched in phenotypes such as developmental timing variant, growth

rate variant, and fertility decrease (**Figure 4.1F**), suggesting that the majority of RBPs are essential for development and fertility. Interestingly, some RBP genes are also enriched in phenotypes such as apoptosis increase and cell death variant. These genes were retained in the final list for the RNAi screen, despite the fact that some of them are components of ribosomes. I also looked at the tissue enrichment of the RBPs. Not surprisingly, most RBPs are enriched in the reproductive system and the germline as well as neurons (**Figure 4.1G**). After these processes, a final RBP compendium containing 800 genes was generated (**Figure 4.1D**). Among these genes, 660 genes are represented in the Ahringer RNAi library (Kamath and Ahringer, 2003; Kamath et al., 2003). These genes were subjected to the following RNAi screens for *egl-1* repressors and activators.

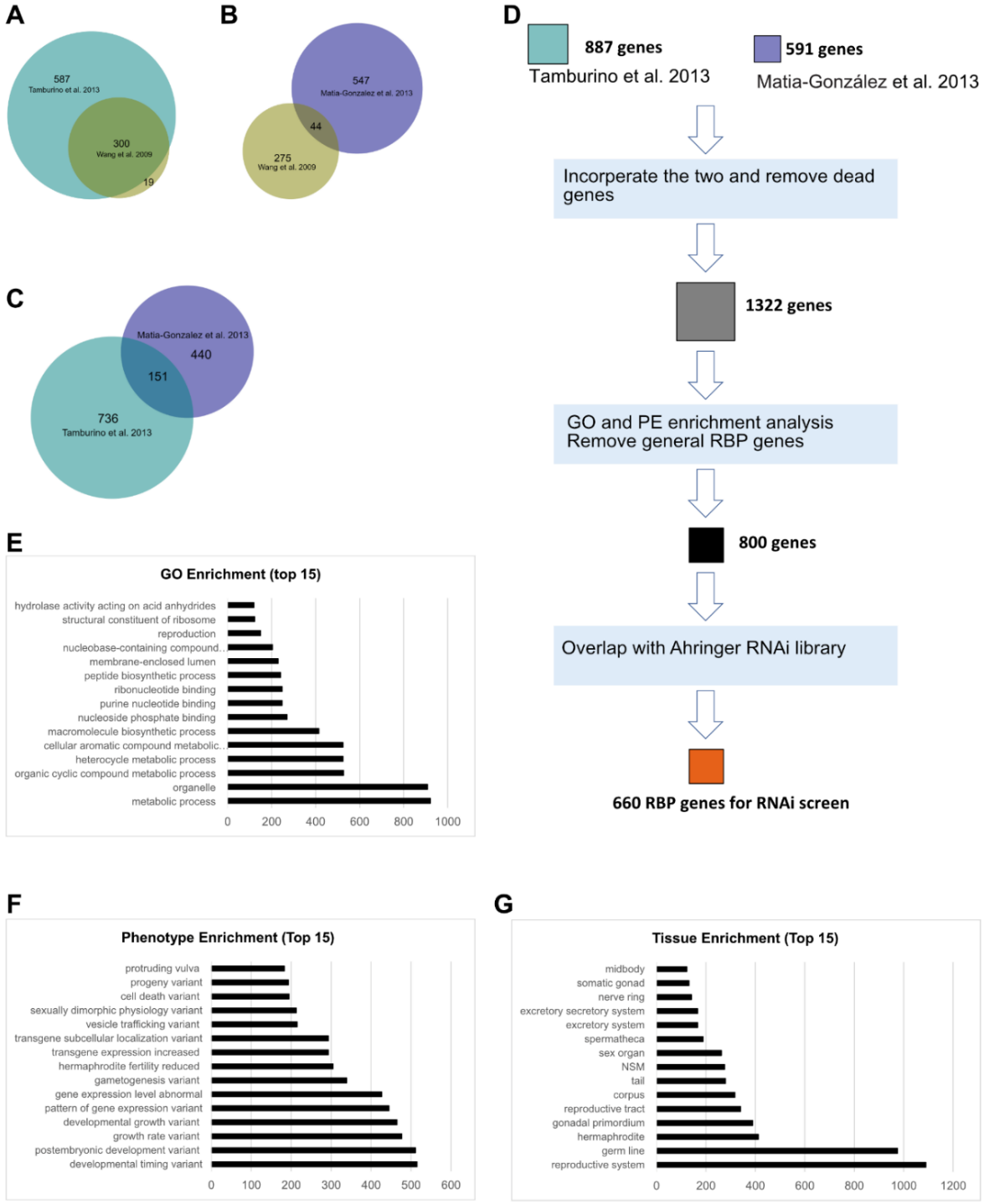

Figure 4.1 Analysis of *C. celegans* RNA-binding proteins. (A) Overlap analysis of RNA-binding protein (RBP) genes reported by Wang et al., (2009) and Tamburino et al., (2013). (B) Overlap analysis of RBP genes reported by Wang et al., (2009) and Matia-Gonzalez et al., (2015). (C) Overlap analysis of RBP genes reported by Tamburino et al., (2013) and Matia-Gonzalez et al., (2015). (D) Pipeline for RBP gene analysis, characterization, and selection. (E) Gene Ontology (GO) enrichment analysis of 1322 RBP genes (total). (F) Phenotype enrichment analysis of 1322 RBP genes. (G) Tissue enrichment analysis of 1322 RBP genes.

4.2 RNAi screen for *egl-1* repressor candidates

4.2.1 Primary screen via the reporter assay

Most of the RBP genes (about 80%) are present in the Ahringer RNAi library (Kamath and Ahringer, 2003; Kamath et al., 2003). I performed RNAi by feeding to knock down each of these genes individually and screened for *egl-1* repressors using the reporter $P_{mai\text{-}2}$*gfp::h2b::egl-1 3′ UTR* (*bcSi26*). The procedure for RNAi feeding is illustrated in **Figure 4.2A**. As shown in **Chapter 3**, the expression of this transgene reporter is controlled by the *egl-1* 3′ UTR and it is largely repressed in early-stage embryos. By screening for an increase in GFP::H2B signal in early-stage embryos, 37 repressor candidates were identified from the primary screen (**Fig. 4.2B, C, Table 4.1**). To verify the identity of the RNAi clones, I sequenced their inserts and found that 31 were correct. The other six clones were matched to genes that do not encode RBPs.

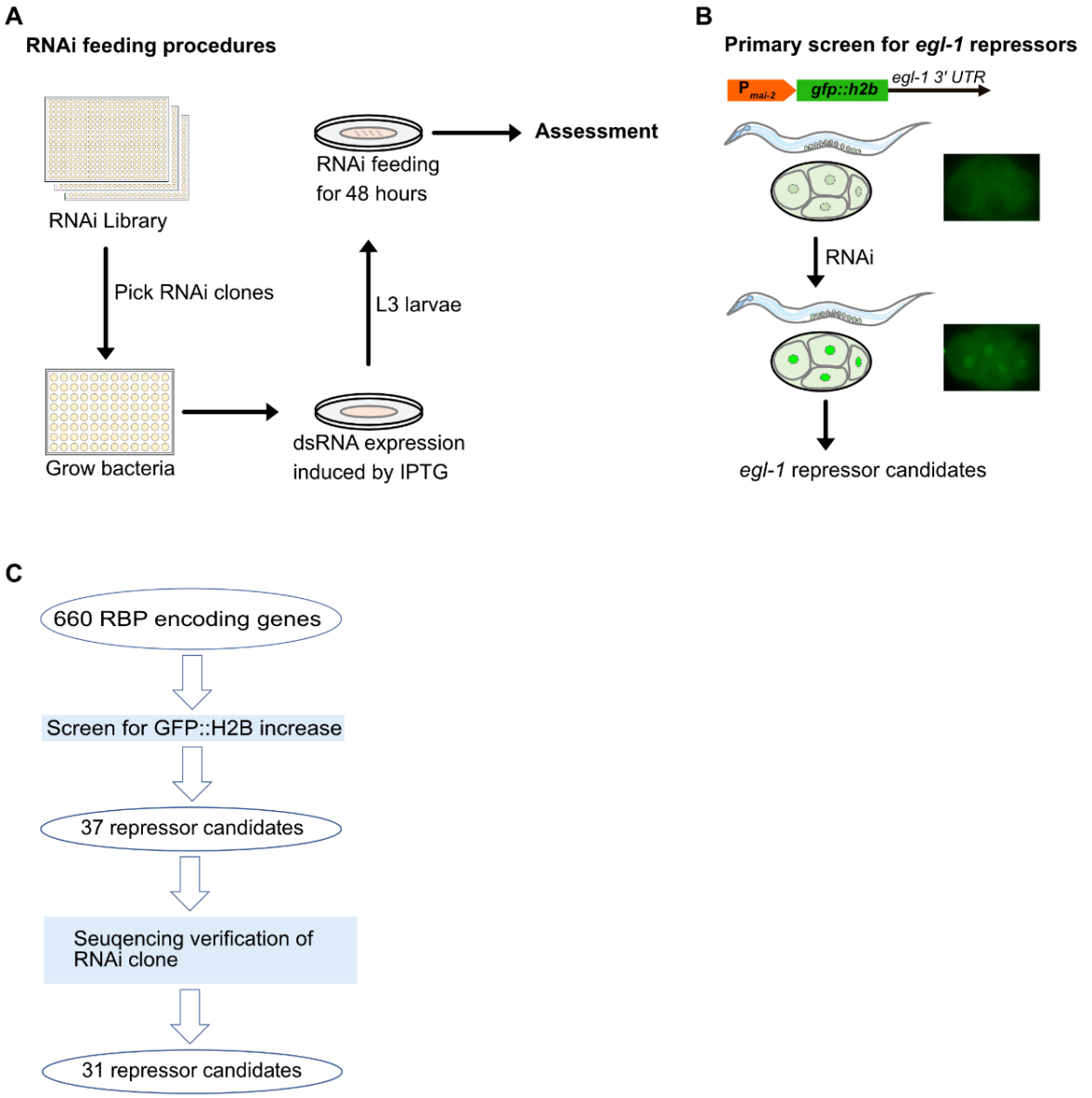

Figure 4.2 Primary screen for RBPs that might repress *egl-1* expression using RNAi feeding. (A) Procedures for RNAi screen by feeding. (B) The repressor candidates were screened by looking for the de-repression of the reporter P_{mai-2}*gfp::h2b::egl-1 3′ UTR (bcSi26)* in early-stage embryos. (C) The pipeline for the primary screen for *egl-1* repressors.

Table 4.1 31 *egl-1* repressor candidates screened by looking for the de-repression of the reporter P_{mai-2}*gfp::h2b::egl-1 3′ UTR* (*bcSi26*) in embryos. The identity of RNAi clones for these candidates was verified by Sanger sequencing and mismatched ones were excluded.

Gene name	Human ortholog	Gene name	Human ortholog
vha-10	ATPase H+ transporting V1 subunit G2	***rpn-3***	Proteasome 26S subunit, non-ATPase 3
pbs-4	Proteasome 20S subunit beta 2	***ubq-1***	ubiquitin C
ztf-2	Zinc finger putative Transcription Factor	***C50C3.1***	/
eef-2	Eukaryotic translation elongation factor 2	***let-754***	Adenylate kinase 2
puf-8	*Pumilio* RNA binding family member PUM1 and PUM2	***Y43F4A.3***	/
swsn-7	AT-rich interaction domain 2	***rde-4***	TARBP2 subunit of RISC loading complex
rha-1	DExH-box helicase 9	***ubq-2***	Ubiquitin A-52 residue ribosomal protein fusion product 1
ddx-19	DEAD-box helicase 19A/B	***ztf-29***	Zinc finger putative Transcription Factor
cdc-48.1	Valosin containing protein	***rack-1***	Receptor for activated C kinase 1
lir-3	/	***puf-3***	/
rsp-7	Splicing regulatory glutamic acid and lysine rich protein 1	***rho-1***	Ras homolog family member A
sop-2	/	***snr-1***	Small nuclear ribonucleoprotein D3 polypeptide
wago-5	/	***pas-6***	Proteasome 20S subunit alpha 1
arf-1.2	ADP ribosylation factor 1/3	***myo-3***	Myosin
B0336.7	/	***dyn-1***	Dynamin
rpn-2	Proteasome 26S subunit; non-ATPase 1		

4.2.2 Rescreen for cell death-related phenotypes

egl-1 repressors are expected to have anti-apoptotic activity. Upon the loss of repressors, the up-regulation of *egl-1* might cause precocious cell death or ectopic cell death, which means the cells that should survive die inappropriately. These precocious or ectopic cell deaths may cause embryonic lethality. *ced-9* is an anti-apoptotic gene, and a weak *ced-9* loss of function mutation partially activates the apoptotic pathway, thus, providing a sensitized background to screen for *egl-1* up-regulation. Up-regulation of pro-apoptotic *egl-1* through the loss of a of *egl-1* repressor during embryogenesis might cause an enhancement of embryonic lethality in a weak *ced-9* loss of function mutant. For this reason, the 31 repressor candidates of *egl-1* (listed in **Table 4.1)** were subjected to rescreening for embryonic lethality enhancement in the background of the weak *ced-9* loss of function allele *n1563ts*. Of note, most of the RBPs that are predicted to bind *egl-1* 3′ UTR (listed in **Table 3.2)** did not show an effect on *egl-1* 3′ UTR reporter expression in the primary RNAi screen. Some interesting candidates might be omitted in the primary screen due to the limitation of the *egl-1* 3′ UTR reporter. Therefore, I re-screened these candidates for embryonic lethality enhancement in the *ced-9(n1653ts)* background. After going through candidates listed in **Table 4.1** and **Table 3.2**, a total of 14 candidates showed embryonic lethality enhancement in the *ced-9(n165sts)* mutant background (**Table 4.2, Fig. 4.3A**).

Table 4.2 14 *egl-1* repressor candidates showing embryonic lethality enhancement in the *ced-9(n1653ts)* mutant background. The embryonic lethality is represented as the percentage of unhatched eggs. The data in the table are shown as the average of two replicates. The sample size is shown in parenthesis.

Genotype	**Embryonic lethality**		
	wt	***ced-9(n1653ts)***	**Fold change***
Control RNAi	0 (n = 899)	10.4% (n = 698)	1
vha-10(RNAi)	29.2% (n = 161)	80% (n = 85)	4.9
swsn-7(RNAi)	52.3% (n = 356)	93.9% (n = 241)	4
rack-1(RNAi)	5.5% (n = 520)	29.4% (n = 91)	2.3
etr-1(RNAi)	5% (n = 345)	21.3% (n = 208)	1.6
hrpa-1(RNAi)	0% (n = 464)	33.1% (n = 172)	3.2
eef-2(RNAi)	1% (n = 392)	30.6% (n = 408)	2.8
sop-2(RNAi)	0.8% (n = 418)	16.5% (n = 239)	1.5
C50C3.1(RNAi)	0.2% (n = 718)	19.7% (n = 260)	1.9
snr-1(RNAi)	15.5% (n = 71)	51.6% (n = 31)	3.6
pab-1(RNAi)	6.3% (n = 32)	20.6% (n = 34)	1.4
hrpr-1(RNAi)	13% (n = 462)	34.1% (n = 149)	2.1
alg-2(RNAi)	0 (n = 299)	30.6% (n = 177)	2.9
msi-1(RNAi)	0.2% (n = 573)	27.3% (n = 58)	2.6
sao-1(RNAi)	0% (n = 379)	30.7% (n = 213)	3

*Fold change = [*gene(RNAi); ced-9(n1653ts)* lethality - *gene(RNAi)* lethality] / [*ced-9(n1653ts)* lethality – *wt* lethality]

Most cells that die during *C. elegans* development are generated through asymmetric cell divisions and they are smaller than their sister cells that normally survive. These dying cells form refractile 'cell corpses' with a size of 2 ± 0.3 μm (maximum 2.6 μm, measured from cell corpses formed during first wave cell deaths) in diameter and that are eventually engulfed by neighboring cells. The expression of *egl-1* during *C. elegans* development should be activated in the right cell at the right time to induce programmed cell death in a highly reproducible manner. The loss of an *egl-1* repressor is expected to lead to inappropriate activation of *egl-1* expression, which could result in the precocious death of mothers of cells programmed to die or ectopic death of cells that should survive (Sherrard et al., 2017). Based on the previous study, cell corpses formed from precocious or ectopic cell deaths are larger in size (Sherrard et al., 2017). The 14 *egl-1* repressor candidates from the above screen were subjected to rescreening for large cell corpses (> 2.6 μm) (**Fig. 4.3A**). Most cells programmed to die during embryogenesis are generated during neuroblast divisions. Some neuron precursors and some neuroblasts show resistance to RNAi. The *nre-1(hd20) lin-15b(hd126)* background has been shown to enhance neuronal RNAi efficiency (Schmitz et al., 2007). For this reason, I performed RNAi in the *nre-1(hd20) lin-15b(hd126)* background to screen for a large cell corpse phenotype in developing embryos. During this screening, the normal cell corpses at the same embryonic stage were used as references. Surprisingly, five candidates caused large cell corpses upon RNAi knockdown (**Fig. 4.3B**). As a control, no large cell corpses were found in *nre-1(hd20) lin-15b(hd126)* embryos upon *gfp* RNAi. Among these candidates, the large cell corpse phenotype was more penetrant (≥ 25% embryos) in *vha-10(RNAi)*, *swsn-7(RNAi)* or *rack-1(RNAi)* embryos; by contrast, it was less penetrant (≤ 10% embryos) in *etr1(RNAi)*, or *hrpa-1(RNAi)* embryos (**Fig. 4.3C**).

A

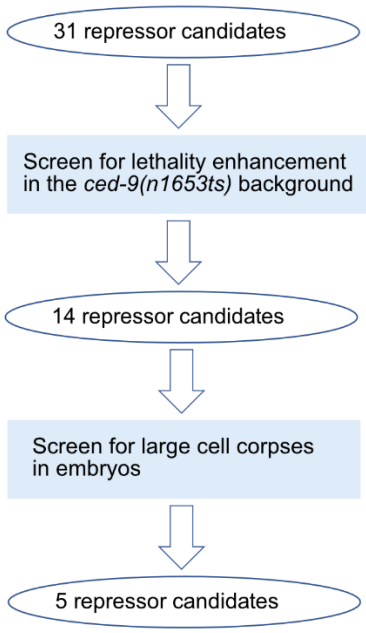

B

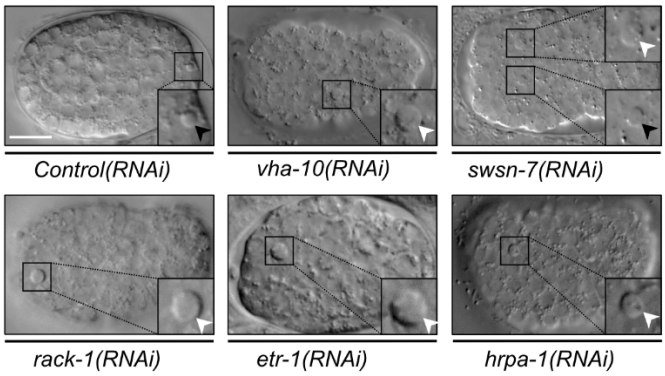

C

Genotypes	Frequency of large cell corpse phenotype	n
Control(RNAi)	0	20
vha-10(RNAi)	35%	20
swsn-7(RNAi)	40%	20
rack-1(RNAi)	25%	20
etr-1(RNAi)	10%	20
hrpa-1(RNAi)	5%	20

Figure 4.3 Rescreen for *egl-1* repressor candidates that show the large cell corpse phenotype in embryos upon RNAi knockdown. (A) Pipeline for the re-screen for the *egl-1* repressor candidates. (B) The differential interference contrast (DIC, Nomarski) images for the normal size cell corpse (black arrowheads) and the large cell corpses (white arrowheads) in embryos, with insets showing representative cell corpses that are enlarged 2x. Scale bar: 10 μm. (C) The frequency of the embryos that display the large cell corpse phenotype. This is calculated by dividing the number of embryos analyzed by the number of embryos that display the large cell corpse phenotype.

4.2.3 *rack-1(tm2262)* and *swsn-7(tm4263)* mutants show abnormal cell death

After obtaining these repressor candidates for *egl-1*, I attempted to confirm the apoptosis-relevant phenotype in their loss of function mutants. *C. elegans* RACK-1 is an ortholog of the human receptor for activated C kinase 1 (RACK1), which is involved in several cellular processes and can regulate translation through interacting with ribosomes (Angenstein et al., 2002; Gallo et al., 2018; Nilsson et al., 2004). *rack-1(tm2262)* is a 331 bp deletion in the *rack-1* coding region, which leads to the loss of *rack-1* function (Demarco and Lundquist, 2010). The *rack-1(tm2262)* mutant exhibits a low rate of embryonic lethality and a significant delay in embryogenesis, indicating *rack-1* is important for *C. elegans* development. I determined the number of large cell corpses during embryogenesis until the end of ventral closure (~360 minutes after the first cleavage of the zygote at 25°C) and observed 0.3 large corpses per embryo on average in *rack-1(tm2262)* mutant embryos, which is a very weak phenotype and not statistically significant when compared to wild-type embryos (**Fig. 4.4A, B**). Next, the number of large cell corpses is determined in a sensitized background, *egl-1(on24)*, in which the miR-35 miRNA binding site (CCGGUG) in the *egl-1* 3′ UTR is mutated, thereby slightly activating *egl-1* expression (Tran et al., 2019). Surprisingly, the number of large cell corpses is significantly increased from 1.3 in *egl-1(on24)* embryos to 2.9 in *rack-1(tm2262)*; *egl-1(on24)* embryos (**Fig. 4.4B**). The large cell corpse phenotype in *rack-1(tm2262)* embryos is blocked by the loss of *egl-1*, indicating that the formation of these larger cell corpses is dependent on the activity of the apoptosis pathway (**Fig. 4.4B**). These results indicate that RACK-1 could play an anti-apoptotic role through repressing *egl-1* expression, thereby preventing precocious and ectopic apoptosis.

SWSN-7 is an ortholog of human BAF200, which is a component of the SWI/SNF nucleosome remodeling complex. SWSN-7 protein carries an AT-rich interaction domain 2 (ARID2) at the N-terminus and C2H2 Zinc fingers at the C-terminus (Large and Mathies, 2014; Tamburino et al., 2013). These domains were originally identified as DNA-binding domains, but they were later proposed to interact also with mRNA (Korn and Schlundt, 2022; Tamburino et al., 2013). *swsn-7(tm4263)* is a 1307 bp deletion in the coding region, which results in complete loss of *swsn-7* function. The *swsn-7(tm4263)* homozygotes exhibit maternal effect lethality (MEL) and a significant

delay in embryogenesis. To maintain the strain, *swsn-7(tm4263)* is balanced by *mIn1[dpy-10(e128) mIs14]*, which carries an integrated pharyngeal GFP transgene. I counted the number of large cell corpses in *swsn-7(tm4263)* mutant embryos until the end of ventral enclosure (~380 minutes after the first cleavage of the zygote at 25°C). There were on average 2 large cell corpses found per embryo (**Fig. 4.4A, C**). This phenotype could be blocked by the loss of *egl-1*, indicating that the formation of these larger cell corpses is dependent on the activity of the apoptosis pathway (**Fig. 4.4C**). The effect of other components of the SWI/SNF complex on apoptosis needs to be determined in the future.

The loss of function mutants of the other three repressor candidates for *egl-1*, namely *vha-10*, *etr-1*, and *hrpa-1* are not viable. *vha-10* or *etr-1* loss of function mutant is early embryonic lethal. *hrpa-1* loss of function mutant is sterile. Because I could not collect homozygous embryos from these mutants, they were not further studied.

A

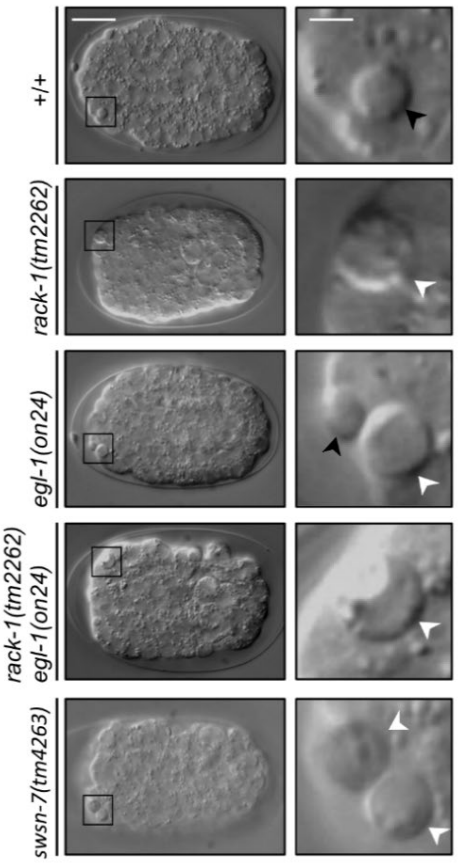

B

Genotype	Large cell corpse per embryo (#)		n
+/+	0	ns	10
rack-1(tm2262)	0.3 ± 0.2		10
egl-1(on24)	1.3 ± 0.2	**	11
rack-1(tm2262); egl-1(on24)	2.9 ± 0.3		11
egl-1(n3330)	0		10
rack-1(tm2262); egl-1(n3330)	0		10

C

Genotype	Large cell corpse per embryo (#)		n
+/+	0	****	10
swsn-7(tm4263)	2 ± 0.4		10
egl-1(mjs2)	0		10
swsn-7(tm4263); egl-1(mjs2)	0		10

Figure 4.4 The large cell corpse phenotype in *rack-1(tm2262)* and *swsn-7(tm4263)* mutants. (A) Differential interference contrast (DIC, Nomarski) images for normal cell corpses (black arrowheads) and large cell corpses (white arrowheads) in embryos of various genotypes. Representative cell corpses are shown enlarged (5x) on the right. Scale bars: 10 µm for embryo images and 2 µm for cell corpse images. (B, C) The total number of large cell corpses observed in *rack-1(tm2262)* and *swsn-7(tm4263)* mutant embryos until the end of ventral enclosure. The homozygous *swsn-7(tm4263)* mutants are from balanced heterozygous mothers. *mjs2* is a loss of function allele of *egl-1*. The assays were performed at 25°C. The data are shown as mean ± SEM. ns indicates no significance via two-tailed Mann-Whitney Test; ** $p < 0.01$ via unpaired two-tailed *Student's t-test*; **** $p < 0.0001$ via two-tailed Mann-Whitney Test.

4.2.4 Effect of *swsn-7* on *egl-1* reporter expression

Next, I asked whether the loss of the repressor candidates of *egl-1* could cause the up-regulation of *egl-1* expression. To test this, I used the *egl*-1allele *mjs2,* in which *egl-1* exons and introns are replaced by the GFP sequence but UTRs are not changed (**Fig. 4.5A**). Through this, 'EGL-1 protein' levels can be read out by GFP levels. Considering the *egl-1* mRNA are predominantly transcribed in cell death lineages, post-transcriptional effects on *egl-1* expression should be detectable in these lineages. As an example, I determined GFP levels in the neurosecretory motor neuron (NSM) neuroblasts (referred to as NSMnb) and its two daughter cells (**Fig. 4.5B**). The two NSMnb are born ~280 minutes after the first zygotic cleavage (at 20°C). Each of them divides at ~410 min, giving rise to the NSM cell, which is larger and programmed to survive, and the NSM sister cell (NSMsc), which is smaller and programmed to die ~20 minutes after its birth. The NSMnb can be identified based on its position, neighboring cells, and morphology (**Fig. 4.5C**) (Yan et al., 2013). The cell boundary is labeled by a transgene $P_{pie\text{-}1}$*mCherry::ph*$^{plc\delta}$ (*ltIs44*). Unexpectedly, GFP signal was not detected in the NSMnb not only in *egl-1(mjs2)* (control) embryos but also in *swsn-7(tm4263); egl-1(mjs2)* embryos (**Fig. 4.5C**). Similarly, no GFP signal was detected in the NSM and NSMsc 10 minutes after the NSMnb division. GFP was only seen in cells that should have died but have persisted for a long time due to lacking *egl-1*. Of note, the identification and tracking of the NSMsc in *swsn-7(tm4263); egl-1(mjs2)* embryos is extremely difficult due to the morphological abnormalities caused by *swsn-7(tm4263)*. Thus, I could not do imaging in NSMsc later than 10 minutes after NSMnb division. Overall, it seems that *egl-1(mjs2)* is not a good way to detect a change in EGL-1 protein levels due to the low abundance. Besides, the effect of *swsn-7(tm4263)* on *egl-1* expression could be very subtle and only affected a small number of cells.

In the case of another *egl-1* repressor candidate *rack-1*, *rack-1(tm2262); egl-1(mjs2)* turned out to exhibit a synthetic lethality. For this reason, this strain could not be successfully obtained. The large cell corpse phenotype in the *rack-1(tm2262)* mutant has a very low penetrance. I decided not to investigate it further.

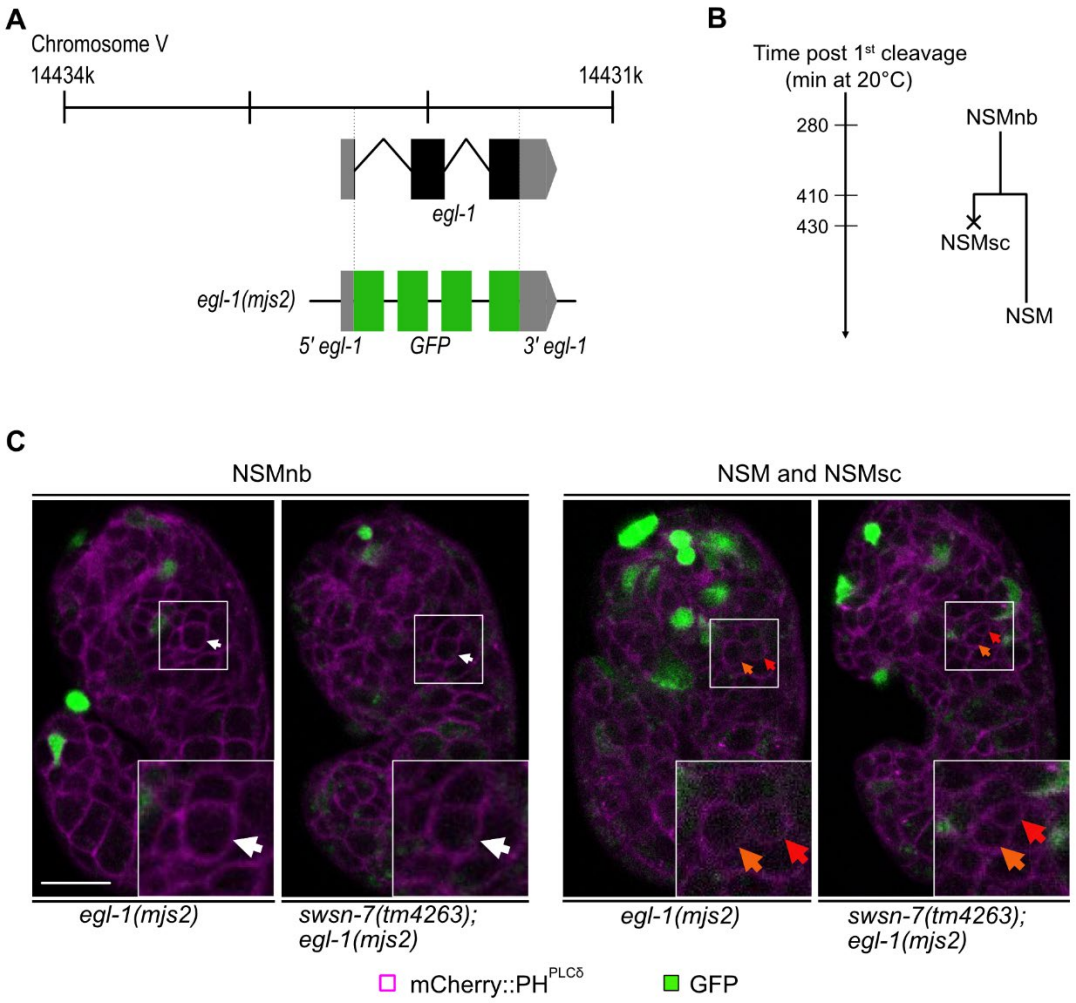

Figure 4.5 Effect of the loss of *swsn-7* on *egl-1* reporter expression in the NSM lineage. (A) Schematic of the substitution of *egl-1* exons and introns with GFP sequence through the CRISPR/Cas genome editing technology, generating the allele *egl-1(mjs2)*. (B) The NSM lineage depicting the NSM neuroblast (NSMnb), which is born ~280 minutes after the first zygotic cleavage (at 20°C). The NSMnb (ABaraapapaa or ABaraapppaa) divides at ~410 min, generating the NSM cell (ABaraapapaad or ABaraapppaad), which is larger and programmed to survive, and the NSM sister cell (NSMsc, ABaraapapaav or ABaraapppaav), which is smaller and programmed to die ~20 minutes after its birth. (C) The expression of *egl-1(mjs2)* in the NSM lineage in wild-type and *swsn-7(tm4263)* mutant embryos. Insets show 2x enlarged images for NSMnb (white arrows) or NSM (orange arrows) and NSMsc (red arrowheads). The NSMnb can be identified based on its position, neighboring cells, and morphology. The cell boundary is labeled by $P_{pie\text{-}1}$*mCherry::ph*$^{plc\delta}$ (*ltIs44*) and EGL-1 protein levels are reflected by GFP intensity. The number of embryos analyzed (n) is 10 for *egl-1(mjs2)* and 3 for *swsn-7(tm4263); egl-1(mjs2).* Scale bar: 10 µm.

4.3 RNAi screen for *egl-1* activator candidates

4.3.1 Primary screen via the reporter assay

I also performed a screen for *egl-1* activator candidates. First, I conducted a primary RNAi screen using the reporter $P_{mai\text{-}2}$*gfp::h2b::egl-1 3′ UTR* (*bcSi26*). The RNAi procedure used was the same as that used for the *egl-1* repressor screen (**Fig. 4.2A**). This transgene reporter is moderately expressed in oocytes. By screening for a decrease in GFP::H2B signal in oocytes, 66 activator candidates were identified (**Fig. 4.6A, B, Table 4.3**).

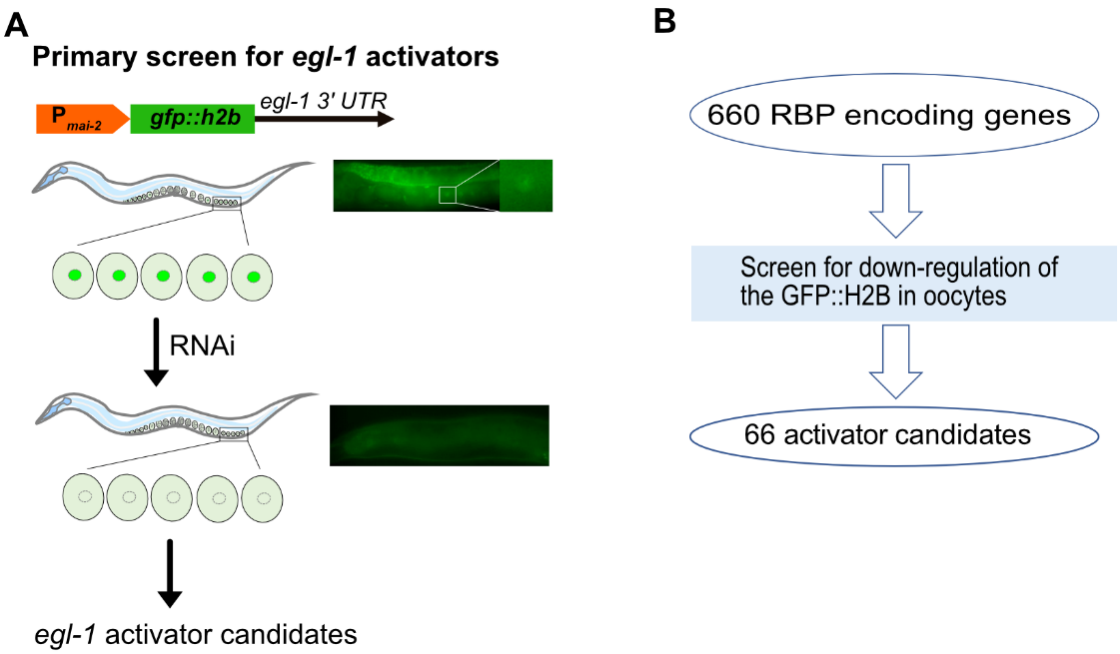

Figure 4.6 Primary screen for RBPs that might act as *egl-1* activators. (A) With the help of the transgene reporter P_{mai-2}*gfp::h2b::egl-1 3' UTR (bcSi26)*, *egl-1* activator candidates were screened by looking for a decrease in GFP::H2B signal in oocytes after RNAi. (B) Pipeline showing the primary screen for *egl-1* activator candidates.

Table 4.3 66 *egl-1* activator candidates identified by screening for a decrease in GFP::H2B signal in oocytes.

Gene name	Sequence Name	Gene name	Sequence Name	Gene name	Sequence Name
rpl-13	C32E8.2	*hel-1*	C26D10.2	*eif-3.D*	R08D7.3
rps-10	D1007.6	*cct-2*	T21B10.7	*prp-8*	C50C3.6
rps-17	T08B2.10	*rps-9*	F40F8.10	*snu-23*	ZK686.4
gld-2	ZC308.1	*eif-3.B*	Y54E2A.11	*egl-45*	C27D11.1
eif-3.H	C41D11.2	*atp-2*	C34E10.6	*rpl-35*	ZK652.4
rpl-19	C09D4.5	*rps-1*	F56F3.5	*dars-1*	B0464.1
nars-1	F22D6.3	*F26F4.8*	F26F4.8	*vha-14*	F55H2.2
eif-2beta	K04G2.1	*larp-1*	R144.7	*T26G10.1*	T26G10.1
rps-19	T05F1.3	*rpl-3*	F13B10.2	*rpl-20*	E04A4.8
exos-3	F59C6.4	*nifk-1*	T04A8.6	*rps-8*	F42C5.8
rla-0	F25H2.10	*rps-0*	B0393.1	*nog-1*	T07A9.9
tct-1	F25H2.11	*ucr-1*	F56D2.1	*rps-5*	T05E11.1
eif-3.E	B0511.10	*rps-3*	C23G10.3	*rps-23*	F28D1.7
atp-1	H28O16.1	*rpl-6*	R151.3	*rps-11*	F40F11.1
B0511.6	B0511.6	*pars-1*	T20H4.3	*ZK795.3*	ZK795.3
rps-26	F39B2.6	*let-716*	C16A3.3	*copg-1*	T14G10.5
toe-1	ZK430.1	*rpl-21*	C14B9.7	*rpl-12*	JC8.3
F44G4.1	F44G4.1	*ZK686.2*	ZK686.2	*rpl-18*	Y45F10D.12
mrpl-10	K01C8.6	*rha-2*	C06E1.10	*hsp-1*	F26D10.3
nst-1	K01C8.9	*C16A3.4*	C16A3.4	*rpl-39*	C26F1.9
eif-3.G	F22B5.2	*F57B9.3*	F57B9.3	*rps-16*	T01C3.6
ifg-1	M110.4	*inf-1*	F57B9.6	*nxf-1*	C15H11.3

4.3.2 Negative screen

Following the primary screen, I conducted a 'negative screen' for activators that are specific for the *egl-1* reporter using another transgene reporter P_{mai-2}*gfp::h2b::mai-2 3′ UTR* (*bcSi25*), which is ubiquitously expressed and and contains the 3'UTR of the gene *mai-2* (**Fig. 4.7A**). By screening for a decrease in GFP::H2B signal in embryos carrying P_{mai-2}*gfp::h2b::mai-2 3′ UTR* (*bcSi25*), 41 out of 66 candidates were considered general translation activators (nonspecific) and were therefore excluded from subsequent analyses. The remaining 25 candidates were considered more specific to the *egl-1* mRNA. I confirmed the identities of RNAi clones (from the Ahringer library) for these 25 genes by Sanger sequencing and found that 20 candidates showed the correct sequence (**Fig. 4.7B**, **Table 4.4**).

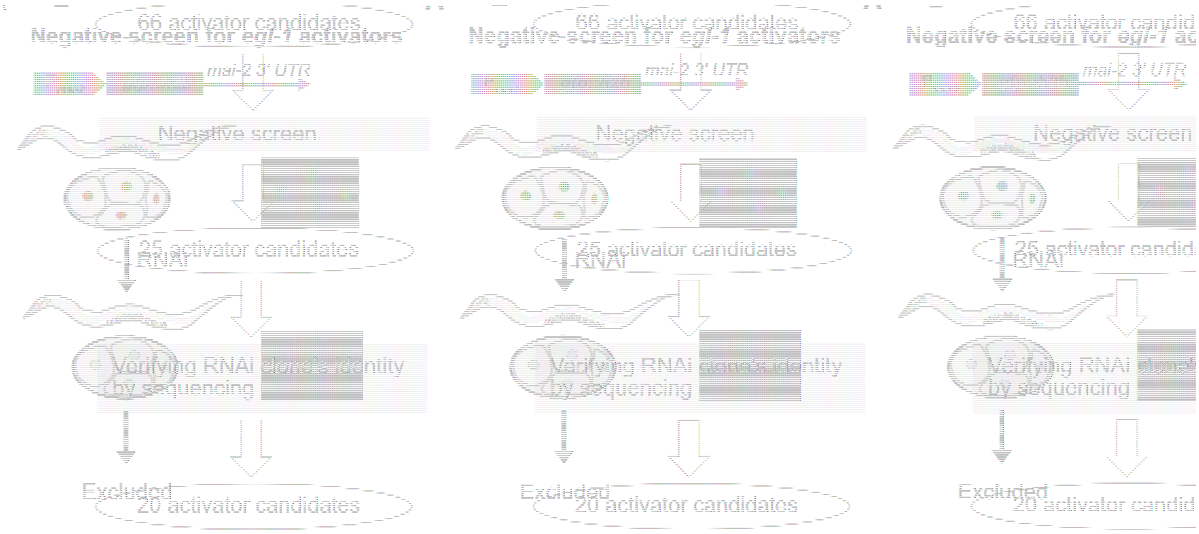

Figure 4.7 Negative screen for *egl-1* activator candidates. (A) Using the reporter P_{mai-2}*gfp::h2b::mai-2 3′ UTR (bcSi25)*, nonspecific candidates were eliminated by screening for a decrease in GFP::H2B signal in embryos. (B) Pipeline showing the negative screen for *egl-1* activator candidates.

Table 4.4 *egl-1* activator candidates from the negative screen. Nonspecific candidates are eliminated by screening for a decrease in GFP::H2B signal in embryos carrying P_{mai-2}*gfp::h2b::mai-2 3′ UTR (bcSi25)*. The identities of RNAi clones for these candidates were verified by Sanger sequencing. 20 candidates that showed the correct sequence are listed in the table and their human orthologs are provided.

Gene name	Human ortholog	Gene name	Human ortholog
gld-2	Terminal nucleotidyltransferase 2	***nifk-1***	Nucleolar protein interacting with the FHA domain of MKI67
eif-3.H	Eukaryotic translation initiation factor 3 subunit H	***ucr-1***	Ubiquinol-cytochrome c reductase core protein 1
exos-3	Exosome component 3	***let-716***	Programmed cell death 11
B0511.6	DEAD-box helicase 18	***ZK686.2***	DEAD-box helicase 51
toe-1	HEAT repeat containing 1	***rha-2***	DEAH-box helicase 37
F44G4.1	Ribosome production factor 1 homolog	***eif-3.D***	Eukaryotic translation initiation factor 3 subunit D
mrpl-10	Mitochondrial ribosomal protein L10	***prp-8***	pre-mRNA processing factor 8
nst-1	G protein nucleolar 3 like	***vha-14***	ATPase H+ transporting V1 subunit D
atp-2	ATP synthase F1 subunit beta	***T26G10.1***	DEAD-box helicase 47
larp-1	La ribonucleoprotein 1	***ZK795.3***	IMP U3 small nucleolar ribonucleoprotein 4

4.3.3 Re-screen in *mir-35* mutant embryos

To further confirm the effect of the 20 activator candidates (**Table 4.4**) on the expression of the *egl-1* 3′ UTR reporter *P*$_{mai-2}$*gfp::h2b::egl-1 3′ UTR* (*bcSi26*) in embryos, they were subjected to a further re-screening in a *mir-35* mutant background, in which the expression of the reporter P$_{mai-2}$*gfp::h2b::egl-1 3′ UTR* (*bcSi26*) is slightly de-repressed (Sherrard et al., 2017). Finally, five out of 20 *egl-1* activator candidates showed a decrease in GFP:H2B signal upon RNAi in *mir-35* mutant embryos carrying *P*$_{mai-2}$*gfp::h2b::egl-1 3′ UTR* (*bcSi26*) (**Fig. 4.8A, B**). These five candidates are eukaryotic translation initiation factor 3 subunit H (EIF-3.H), DEAD-box helicase 18 (B0511.6), HEAT repeat containing 1 (TOE-1), ATP synthase F1 subunit beta (ATP-2), and La ribonucleoprotein 1 (LARP-1).

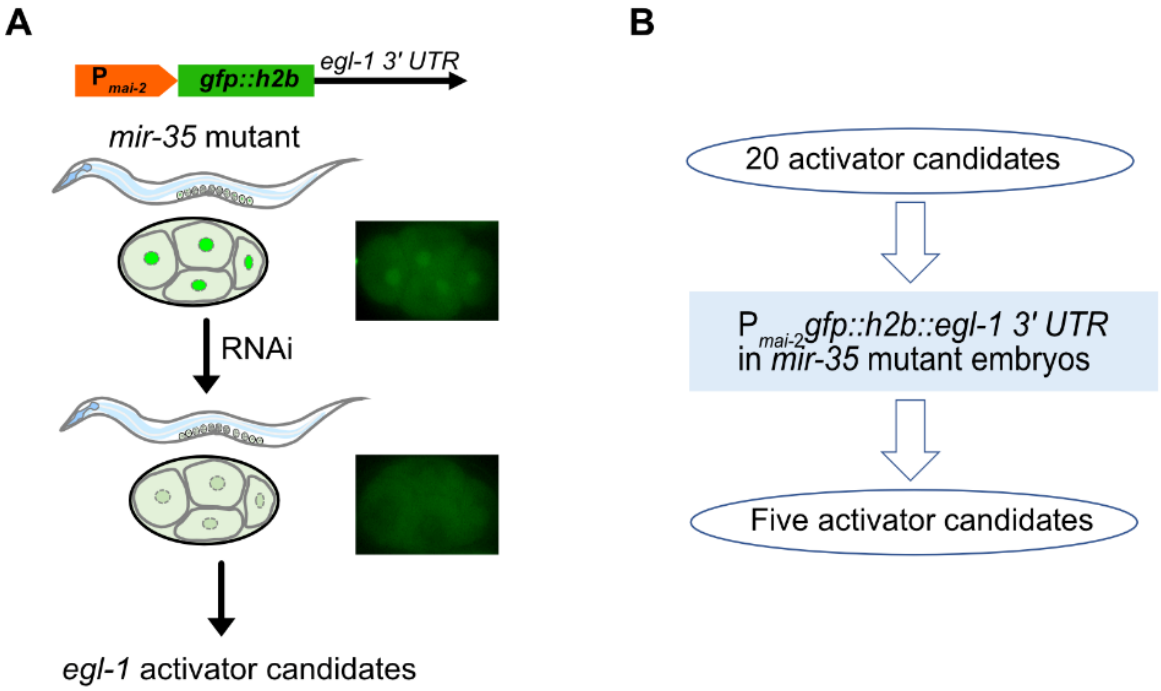

Figure 4.8 Re-screen of *egl-1* activator candidates in *mir-35* mutant embryos carrying P_{mai-2}*gfp::h2b::egl-1 3' UTR (bcSi26)*. (A) The activator candidates were identified by looking for a decrease in GFP::H2B signal in embryos upon RNAi. (B) Five *egl-1* activator candidates remained after this screening.

4.3.4 *egl-1* activator candidates promote apoptosis during *C. elegans* development

The five *egl-1* activator candidates were then analyzed with respect to apoptosis-related phenotypes. To that end, I screened for the inappropriate survival of cells that are normally eliminated through apoptosis during *C. elegans* development. In wild-type embryos, the NSMsc dies soon after the NSMnb division (**Fig. 4.9A**). The loss of activators of *egl-1* is expected to down-regulate *egl-1* expression and result in a cell-death defective phenotype, namely, the inappropriate survival of cells that should die. The surviving NSMsc has been shown to form NSM-like cells (Yan et al., 2013). The NSM and undead NSMsc can be visualized by the expression of the transgene $P_{tph\text{-}1}$*gfp::his-24* (*bcIs65* X, *bcIs66* III, or *bcSi126* III) (**Fig. 4.9A**). Some neuron precursors and some neuroblasts show resistance to RNAi. The *nre-1(hd20) lin-15b(hd126)* background has been shown to enhance neuronal RNAi efficiency (Schmitz et al., 2007). For this reason, I performed RNAi in a *nre-1(hd20) lin-15b(hd126)* background to enhance the RNAi efficiency in the NSM lineage. Among the five activator candidates of *egl-1*, only *eif-3.H* RNAi caused a low rate of survival (1.7%) of NSMsc (**Fig. 4.9B**).

Of note, most of the predicted *egl-1*-binding RBPs in **Table 3.2** did not show an effect on the reporter $P_{mai\text{-}2}$*gfp::h2b::egl-1 3' UTR* (*bcSi26*) expression in the primary RNAi screen. To rule out possible false negative effects, I determined NSMsc survival for those candidates in **Table 3.2**. Among these 32 candidates, only *RNAi of hrpr-1 (*also known as *hrp-2*) showed NSMsc survival (2.83%) (**Fig. 4.9B**). Because *hrpr-1 RNAi* cause larval arrest, NSMsc survival was scored in L1/L2-stage larvae instead of L3/L4-stage animals.

Then, I determined the NSMsc survival in the background of a weak *ced-3* loss function mutation *n2427*. In the *ced-3(n2427)* background, the apoptosis pathway is partially inactivated and NSMsc shows a low rate of survival (13.7%) (**Fig. 4.9B**). This *ced-3* mutation provides a sensitized background for determining NSMsc survival. I expected to observe enhancement of NSMsc survival upon the knockdown of *egl-1* activator candidates. *eif-3.H(RNAi)* and *hrpr-1(RNAi)* showed a significant enhancement of NSMsc survival in *ced-3(n2427)* animals (44.12% for *eif-3.H(RNAi)* and 59.13% for *hrpr-1(RNAi)*, respectively) (**Fig. 4.9B**).

To determine if NSMsc survival observed in *eif-3.H(RNAi)* and *hrpr-1(RNAi)* animals is caused by the loss of *eif-3.H* and *hrpr-1*, I scored NSMsc survival in their null mutants. The *eif-3.H* loss of function mutation *ok1353* causes sterility and, thus, the *eif-3.H(ok1353)* mutation is balanced by the translocation balancer *hT2* (I;III), which carries an integrated transgene expressing pharyngeal GFP. The homozygous *eif-3.H(ok1353)* F1 animals were picked to score NSMsc survival. However, the *eif-3.H(ok1353)* homozygotes did not show NSMsc survival. To rule out the possibility that the absence of a phenotype was caused by maternal *eif-3.H* mRNAs from the germline of the heterozygous mother, I injected dsRNA for *eif-3.H* into the heterozygous mother at the L4 stage. Then, NSMsc survival was scored in the *eif-3.H(ok1353)* homozygous F1 animals at the L3/L4 stage. There were no extra NSM-like cells observed. This could be because of the low penetrance of the phenotype. It would be interesting to determine NSMsc survival in the sensitized *ced-3(n2427)* background.

The *hrpr-1* loss of function mutation *ok1278* causes lethality and it is balanced by *hT2* (I;III). Some homozygous *hrpr-1*(*ok1278)* embryos could escape from embryonic arrest and develop to the L1 larval stage. I scored NSMsc survival in these escapers and found 1.02% NSMsc survived. To remove the maternal effect, I injected dsRNA for *hrpr-1* into the heterozygous mother and aimed to score NSMsc survival in *hrpr-1*(*ok1278)* homozygous F1 animals. However, all embryos from the dsRNA injected *ok1278* heterozygotes were arrested at the early embryonic stage and for this reason, NSMsc survival could not be scored.

Overall, knocking down either *eif-3.H* or *hrpr-1* causes a very low rate of NSMsc survival, and this phenotype is significantly enhanced in a *ced-3(n2427)* background. These data suggest that *eif-3.H* and *hrpr-1* might contribute to the promotion of apoptosis, possibly through activating *egl-1* expression.

A

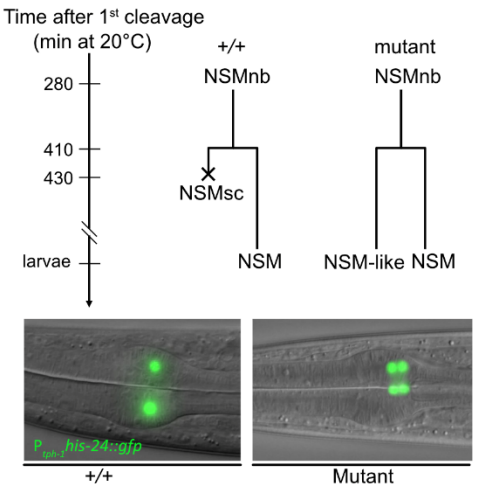

B

Genotypes	NSMsc survival	n
+/+	0	100
ced-3(n2427)	13.7%	696
eif-3.H(RNAi feeding)	1.7%	120
eif-3.H(RNAi feeding); ced-3(n2427)	44.12%	170
eif-3.H(ok1353) [a]	0	90
eif-3.H(dsRNA); eif-3.H(ok1353) [a]	0	54
hrpr-1(RNAi feeding)	2.83%	106
hrpr-1(RNAi feeding); ced-3(n2427)	59.13%	230
hrpr-1(ok1278) [a]	1.02%	488
hrpr-1(dsRNA); hrpr-1(ok1278) [a, b]	/	0

Figure 4.9 *egl-1* activator candidates promote apoptosis in the NSM lineage. (A) Schematics showing the NSM lineage and NSMsc survival assay. The NSMnbs (ABaraapapaa and ABaraapppaa) divide ~410 minutes after the first zygotic cleavage (at 20°C), generating the NSM cells (ABaraapapaad and ABaraapppaad), which are larger and programmed to survive, and the NSM sister cells (NSMsc, ABaraapapaav and ABaraapppaav), which are smaller and programmed to die. In wild-type (+/+) animals, the NSMsc undergoes apoptotic cell death, resulting in one NSM neuron from each NSM neuroblast, and there are totally two NSM neurons. If apoptosis is partially blocked, the NSMsc may survive, resulting in extra 'NSM-like' cells from each NSM neuroblast, and there would be three/four 'NSM-like' cells. NSM-like cells can be identified in the anterior pharynx of L3/L4 larvae using the transgene $P_{tph\text{-}1}$*his-24::gfp*. (B) RNAi knockdown or loss of function mutation of *egl-1* activator candidates causes NSMsc survival. [a]Homozygous *eif-3.H(ok1353) or hrpr-1*(*ok1278)* mutants are from balanced heterozygous mothers. [b] embryo arrested. The sample size (n) is shown in the table.

In the work presented in this chapter, I first analyzed the RBPomes reported in *C. elegans* and constructed an mRBP compendium containing 800 genes for screening for repressors and activators of *egl-1*. Following this, I performed RNAi screens for RBP regulators that may repress or activate *egl-1* expression, including screens using reporters and screens for apoptosis-related phenotypes. Through this work, several repressor candidates and activator candidates of *egl-1* were identified.

Chapter 5 Live Imaging *egl-1* mRNA translation in developing *C. elegans*

Through single-molecule RNA fluorescence *in situ* hybridization (smRNA FISH), the *egl-1* mRNA was found predominantly in cell lineages where apoptotic cell death occurs in developing *C. elegans* embryos (Sherrard et al., 2017). Interestingly, the *egl-1* mRNA is found not only in cells programmed to die but also in their mother cells with various copy numbers in different lineages. However, no studies have ever been able to detect *egl-1* mRNA translation in the mother cells. *egl-1* expression level is extremely low and the signal from a single EGL-1 protein is too dim to visualize by the traditional GFP fusion. Besides, immunostaining of *C. elegans* EGL-1 using antibodies is not feasible due to lacking a good anti-EGL-1 antibody. Moreover, the physical interaction between EGL-1 and CED-9 has been well documented *in vitro* (Conradt and Horvitz, 1998). CED-9 has been found to reside in the outer mitochondrial membrane (OMM) (Chen et al., 2000; Pourkarimi et al., 2012; Tan et al., 2007). It has been assumed that the localization of BH3-only proteins to the OMM is a common and necessary step for the efficient activation of apoptosis (Shamas-Din et al., 2011). However, it remains unclear whether and when the EGL-1 protein localizes to the OMM where it exerts its pro-apoptotic function. Besides, an intriguing question is whether the *egl-1* mRNA is translated locally in the proximity of mitochondria. To answer these questions, live imaging of *egl-1* mRNA translation at the single protein molecule level will be necessary. To this end, amplifying the signal from a single EGL-1 protein molecule is indispensable.

As described in the introduction (**Chapter 1.5**), the SunTag system has emerged as a promising strategy for the live imaging of single-molecule protein. It allows a dramatic enhancement of fluorescence signal by bringing as many as 32 GFPs to a single-molecule target protein (Dufourt et al., 2021; Tanenbaum et al., 2014; Yan et al., 2016). However, this system has only been tested in human cells cultured *in vitro* and in *Drosophila* embryos. It has not yet been established for use in *C. elegans*. In this study, I attempted to establish this system for imaging *egl-1* mRNA translation in *C. elegans* and to investigate EGL-1 protein synthesis with high sensitivity in live cells during *C. elegans* development.

5.1 Establishment of the SunTag system for imaging *egl-1* mRNA translation

The SunTag system is comprised of two components, namely, the SunTag (GCN4 v4 peptide) repeats (the tag) that is fused to the protein of interest and the scFv antibodies fused to a fluorescent protein (FP) (the detector) (Tanenbaum et al., 2014). By loading the multi-copy of scFv::FP onto the SunTag repeats fused to the target protein, the target protein can be visualized in live cells (**Figure 1.10C**). To test whether the scFv antibody for the SunTag can be expressed in *C. elegans*, I constructed a single-copy transgene, *bcSi133* ($P_{hsp\text{-}16.41}$*scFv::sfGFP::NLS,* this sequence is from *Drosophila* and has been used by Dufourt et al.. 2021) (**Fig. 5.1A.*a***), In *bcSi133,* the expression of *scFv::sfGFP::NLS* is under the control of the promoter of the heat-shock responsive gene *hsp-16.41*. A nuclear localization signal (NLS) is included to localize unbound *s*cFv::sfGFP to the nucleus and to make it easier to distinguish labelled target proteins from unbound *s*cFv::sfGFP. Upon heat-shock, I expected to see bright GFP signal in the nucleus. However, the GFP signal from this transgene was very dim. This suggests that this version of *scFv::sfGFP::NLS* cannot be properly expressed in *C. elegans*. To optimize the sequence for *C. elegans*, I utilized an online tool called '*C. celegans* Codon Adapter' (Redemann et al., 2011) to modify the codon sequence and introduced three introns to enhance its expression. Following this, the sequence-optimized *scFv::sfGFP::NLS* DNA fragment was synthesized and a new single-copy transgene *bcSi134* ($P_{hsp\text{-}16.41}$*scFv::sfGFP::NLS*) was constructed. *scFv::sfGFP::NLS* expression from this transgene was high enough for use.

I then tested whether the SunTag peptide can be expressed in *C. elegans*. To do so, I constructed a single-copy transgene *bcSi132* ($P_{egl\text{-}1}$*33xSunTag::egl-1::egl-1 3′ UTR*, this SunTag sequence is from *Drosophila* and has been used by Dufourt et al., 2021). In *bcSi132,* the 33 repeats of SunTag were inserted into a 17 kb *egl-1* fragment (including coding regions and all regulatory regions) at the N-terminus of the *egl-1* coding sequence immediately after the start codon. This transgene was introduced in an *egl-1* null mutant background *egl-1*(*n3330*). I would have expected it to rescue the cell death defect (Ced) phenotype exhibited in *egl-1*(*n3330*) mutants. Unfortunately, the Ced phenotype of this mutant was not rescued by the transgene, indicating that

the 33xSunTag::EGL-1 fusion protein is not synthesized or not functional. To figure out what is the problem, I fused the *33xSunTag* fragment to sequence coding *mCherry*, used the promoter of the widely expressed gene *mai-2* to drive expression of *33xSunTag::mCherry,* and constructed a multi-copy extra-chromosomal array of P_{mai-2}*33xSunTag::mCherry*. However, I could not detect any mCherry signal from this multi-copy extra-chromosomal array. These results suggest that the *33xSunTag* fragment could not be expressed in *C. elegans*, possibly because of unoptimized codon sequences. Thus, I tested the 24xSunTag used in mammalian cells (Tanenbaum et al., 2014) (provided by Ruijtenberg lab) by constructing a muti-copy extra-chromosomal array *bcEx1394* ($P_{hsp-16.41}$*24x SunTag::egl-1::egl-1 3' UTR*). Surprisingly, the overexpression of $P_{hsp-16.41}$*24xSunTag::egl-1* upon heat-shock resulted in ectopic cell death in developing embryos of *C. elegans*. This suggests this version of *24xSunTag* can be successfully expressed in *C. elegans*.

Next, I attempted to insert the *24xSunTag* sequences into the endogenous *egl-1* loci using CRISPR/cas12a mediated genome editing technology. Among four knock-in lines obtained, one line did not have an associated frameshift mutation. In this line, 18xSunTag repeats were inserted into the *egl-1* gene but 6xSunTag repeats were missing due to unknown reasons (**Fig. 5.1A.*b***). I used this line (named *bc449*) in the following studies. With the co-expression of $P_{hsp-16.41}$*scFv::sfGFP::NLS* (*bcSi134*) whose expression can be induced by the heat-shock stress, the EGL-1 protein appears to become detectable, which is indicated by the bright GFP foci in the cytoplasm of certain cells (**Fig. 5.1B, C** on the right). These cells could represent cells programmed to die i.e. apoptotic cells. Importantly, such cytoplasmic GFP foci are not observed in wild-type embryos expressing only *scFv::sfGFP::NLS* (**Fig. 5.1C**, on the left). In addition, the unbound scFv::sfGFP::NLS protein localizes to the nucleus rather than the cytoplasm.

The 18 repeats of the SunTag fusion by themselves are ~40 kDa, which is four times higher in molecular weight than the EGL-1 protein (~10 kDa). The size of the 18xSunTag::EGL-1 fusion protein 'complex' can become much larger (~1,100 kDa) when 18xSunTag::EGL-1 is bound by 18 copies of scFv::sfGFP each ~60 kDa. Considering the large size, I determined whether the SunTag system disturbs *egl-1* function in *egl-1(bc449)* embryos/animals. First, I looked for cell corpses in embryos

to determine whether the SunTag::EGL-1 system blocks apoptosis. Surprisingly, cell corpses were frequently observed in *egl-1(bc449)* embryos without or with *scFv::sfGFP::NLS* co-expression (**Fig. 5.1D**), suggesting that *egl-1* function is not completely blocked by the formation of 18xSunTag::EGL-1 fusion protein complexes. To further determine the effect of 18xSunTag::EGL-1 fusion protein complexes on cells programmed to die through apoptosis, I determined the number of 'extra' (undead) cells in the anterior pharynx of *egl-1(bc449)* animals at the L3/L4 larval stage. Mutations that block apoptosis, such as strong lf mutations of *ced-3* or *egl-1*, result in the presence of ~12 extra cells, which are cells programmed to die but inappropriately survived, in the anterior pharynx (Conradt and Horvitz, 1998; Shaham et al., 1999). I found that that *egl-1(bc449)* animals had on average 2.7 (without *scFv::sfGFP::NLS* co-expression) or 4 (with *scFv::sfGFP::NLS* co-expression) extra cells in the anterior pharynx. By contrast, no extra cells were found in the wild-type or in animals that only expressed *scFv::sfGFP::NLS* (**Fig. 5.1D**). These results suggest that *egl-1* activity is partially blocked by the formation of 18xSunTag::EGL-1 fusion protein complexes.

Overall, the SunTag system seems to be working for imaging *egl-1* mRNA translation, while it partially disrupts *egl-1* function. Importantly, this method allows me to further investigate the translation of the *egl-1* mRNA at single-molecule resolution in specific cells in real time and to study its subcellular localization.

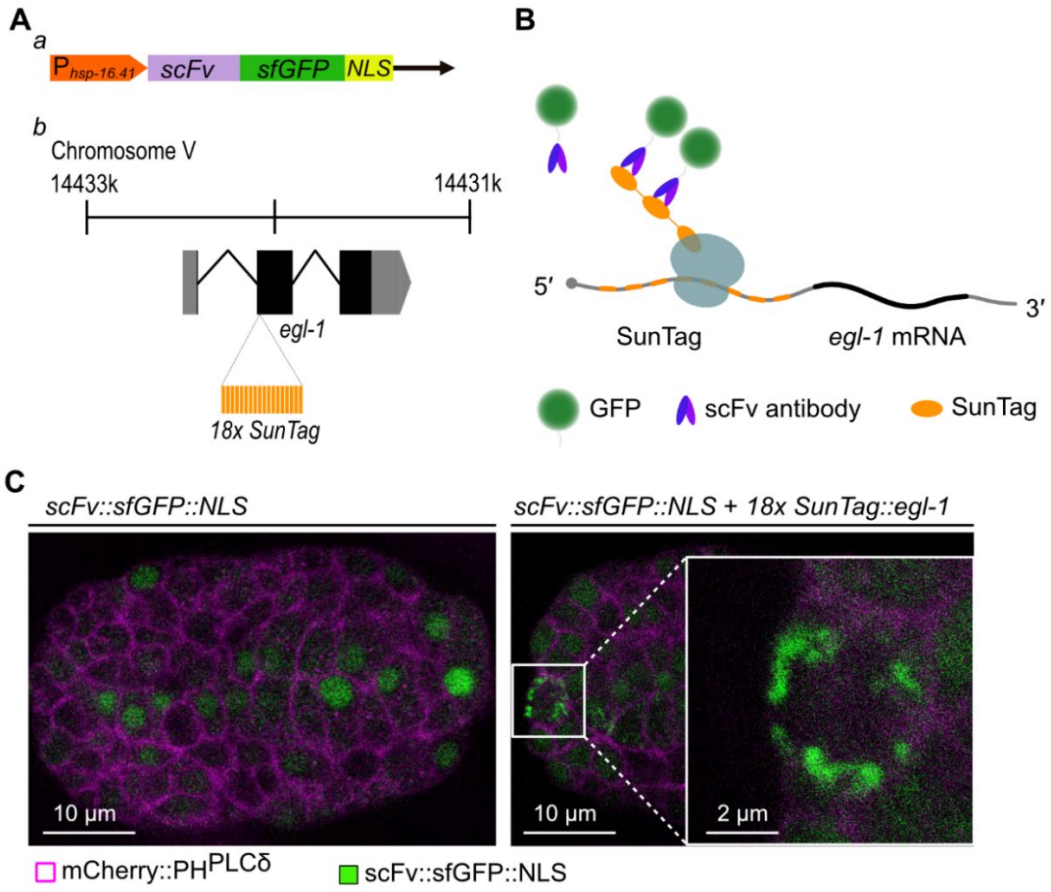

D

Genotype	Extra cells per pharynx #	Cell corpses in embryos	Large cell corpses in embryos
+/+	0 (15)*	Yes (10)	No (10)
egl-1(bc449)	2.7 ± 0.3 (18)	Yes (10)	No (10)
bcSi134(scFv::sfGFP)	0.3 ± 0.2 (10)	Yes (10)	No (10)
bcSi134(scFv::sfGFP); egl-1(bc449)	4.0 ± 0.4 (10)	Yes (10)	No (10)
egl-1(lf)	11.1 ± 1.5 (15)*	No (10)	No (10)

Figure 5.1 Establishment of the SunTag system for imaging *egl-1* mRNA translation in *C. elegans*. (A) Schematic diagram of the transgene $P_{hsp\text{-}16.41}$*scFv::sfGFP::NLS* (*bcSi134*) (*a*) and insertion of *18xSunTag* into the endogenous *egl-1* locus (*b*). (B) Diagram for the visualization of the 18xSunTag::EGL-1 protein in live cells. (C) Fluorescent microscopy images of embryos expressing *scFv::sfGFP::NLS* (control) or *scFv::sfGFP::NLS* and *18xSunTag::egl-1*. The EGL-1 protein is indicated by bright GFP foci (green color), and cell membrane is labeled by mCherry::$PH^{PLCdelta}$ (magenta color). Scale bars: 10 µm for images of embryos and 2 µm for the 4x enlarged inset. (D) Effect of the SunTag system on *egl-1* function. Data for the number of extra cells in the anterior pharynx are shown as mean ± SEM. The sample size (n) is shown in parenthesis. The assays for pharyngeal extra cells were performed by Barbara Conradt. The data for controls +/+ and *egl-1*(lf) are from Conradt and Horvitz (1998). The *egl-1*(lf) mutation used for pharyngeal extra cell assay is *egl-1(n1084 n3082)*. The *egl-1*(lf) mutation used for cell corpse detection is *egl-1(n3330)*.

5.2 Imaging *egl-1* mRNA translation in the RID lineage

After successfully establishing the SunTag system for imaging *egl-1* mRNA translation in live cells with high sensitivity, I sought to determine the time point at which *egl-1* mRNA translation is initiated in cell lineages in which apoptosis occurs. As example, the RID neuroblast (RIDnb) divides around 350 minutes after the first zygotic cleavage at 20°C to produce a daughter cell that survives and differentiates into the RID neuron and a daughter cell (RIDsc) that undergoes apoptosis during the 2nd wave of cell death (**Fig. 5.2A**) (Sulston et al., 1983). The transcription factor gene *unc-3* is expressed in the RIDnb and its daughter cells in embryos and a P$_{unc-3}$*unc-3::GFP* transgene can be used to identify this lineage in embryos (Wang et al., 2015). Our lab made a red version of this transgene, P$_{unc-3}$*unc-3::mScarlet* (*bcIs161*, made by Eric Lambie and Jimei Xu). Because the UNC-3::mScarlet protein localizes to the nucleus, the nuclear region can be marked (except for metaphase). With help of P$_{unc-3}$*unc-3::mScarlet* (*bcIs161)*, I was able to identify the RIDnb and its two daughter cells and detect *egl-1* mRNA translation in this cell lineage. The EGL-1 protein appears to be already synthesized in the mother RIDnb, indicated by a few bright GFP foci in the cytoplasm (**Fig. 5.2B**). The GFP foci in the dying RIDsc increase in numbers and become larger, indicating that more EGL-1 protein is synthesized in the dying RIDsc. By contrast, cytoplasmic GFP foci are not found in the surviving RID cell, indicating that EGL-1 protein is not synthesized in the RID neuron. GFP foci sometimes are also found in the nuclear region. This could be because of the high concentration of unbound scFv::sfGFP::NLS proteins that are enriched in the nucleus, which could form aggregates. Of note, these cells are very small in their size (~4 µm for the RIDnb and ~2 µm for the RIDsc); thus, the cytoplasmic region could not be easily identified.

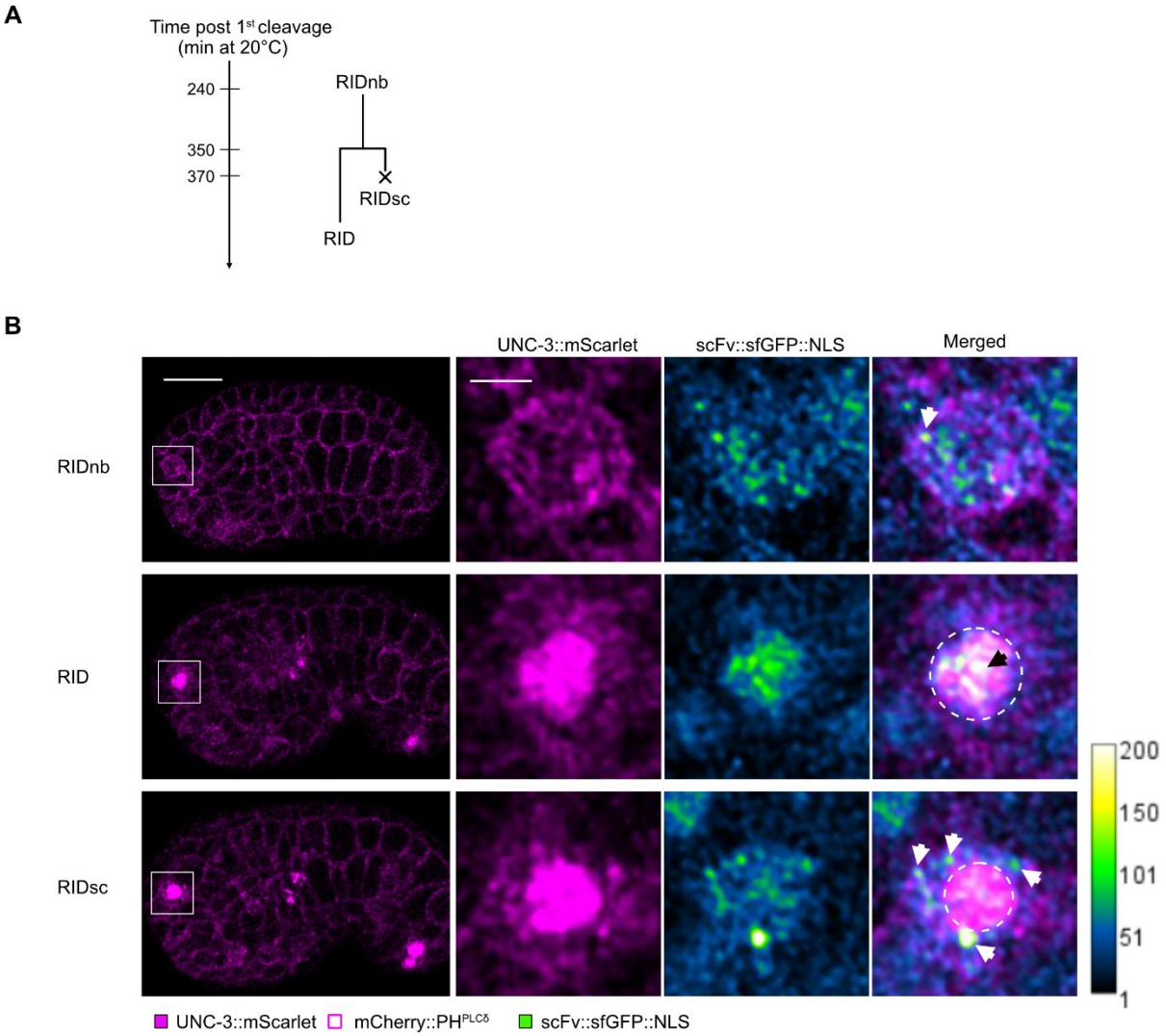

Figure 5.2 Imaging *egl-1* mRNA translation in the RID lineage. (A) Schematics showing the RID lineage. The RID neuroblast (RIDnb, *i.e.,* ABalappaap) is generated ~240 minutes post the first zygotic cleavage (at 20°C) and divides at ~350 min, generating two daughter cells: RID (*i.e.,* ABalappaapa) and the RID sister cell (RIDsc, *i.e.,* ABalappaapp). (B) Fluorescent microscopy images showing *egl-1* mRNA translation in the RIDnb and its two daughter cells. This lineage can be identified by the expression of transgene $P_{unc\text{-}3}$*unc-3::mScarlet* (*bcIs161).* The cell boundary is labeled by transgene $P_{pie\text{-}1}$ *mCherry::PH*^{PLCdelta} *(ltIs44)*. *18xSuntag::egl-1* (*bc449*) translation is labelled by $P_{hsp\text{-}16.41}$*scFv::sfGFP::NLS* (*bcSi134*). The representative images for the RIDnb and its daughters were obtained at 10 minutes before RIDnb division (metaphase) and 20 minutes after RIDnb division, respectively. The GFP channel is set to Green-Fire-Blue to make the signal more obvious. Cytoplasmic GFP foci for EGL-1 protein are indicated by white arrows. Nuclear scFv::GFP aggregates are indicated by black arrows and the nuclear region is indicated by the white circle. Scale bars: 10 μm for images of embryos and 2 μm for 5x enlarged cells.

Discussion

Chapter 6 Discussion

6.1 *cis*-acting elements in the *egl-1* 3′ UTR contribute to the repression of *egl-1* expression

egl-1 transcription is predominantly activated in cell death lineages during *C. elegans* development (Conradt et al., 2016). The smRNA FISH data show that within cell death lineages there is a low number of the *egl-1* mRNA in mother cells, a high number in daughters programmed to die, and essentially zero in daughters programmed to survive (Sherrard et al., 2017). The EGL-1 protein level in the mother cell is presumably below the threshold necessary to trigger cell death. To prevent it from going over this threshold thereby causing precocious cell death, *egl-1* expression must be highly controlled at the post-transcriptional level. Our lab and others have previously demonstrated that the miR-35 and miR-58 families of microRNAs repress *egl-1* expression. These microRNAs bind to their binding sites located in the *egl-1* 3′ UTR and promote mRNA turnover (Sherrard et al., 2017; Tran et al., 2019; Yang et al., 2020). In this study, I have identified additional elements in the *egl-1* 3′ UTR that might contribute to the repression of *egl-1* gene expression at the post-transcriptional level.

6.1.1 TPTE in the *egl-1* 3′ UTR contributes to the repression of *egl-1* expression

The last 33 nt of the *egl-1* 3′ UTR are conserved among *egl-1* orthologs in *Caenorhabditis* species. Based on the minimum free energy structure prediction, this 3′ terminal element (referred to as the TPTE) likely forms a stem-loop structure. This study demonstrates that the TPTE within the *egl-1* 3′ UTR likely contributes to the repression of *egl-1* expression and therefore the control of apoptosis. Disruption of the TPTE leads to the de-repression of the expression of the *egl-1* 3′ UTR reporter $P_{mai\text{-}2}$*gfp::h2b::egl-1 3′ UTR*. In addition, the disruption of the TPTE in the endogenous *egl-1* gene may result in precocious or ectopic cell death, which is indicated by the appearance of large cell corpses during embryo development. It has been reported that precocious or ectopic cell death during embryo development results in large cell corpses, because compared to cells that are programmed to die, these cells are larger

in size (Sherrard et al., 2017). However, without determining the identities of large cell corpses found in *egl-1* TPTE mutant embryos, I cannot rule out the possibility that these large cell corpses are formed by the 'normal death' of cells programmed to die. For example, if the asymmetric mother cell division becomes more symmetric, the cell corpse formed from the dying daughter could be larger. In addition, the function of the *egl-1* TPTE on the stability and translational efficiency of the *egl-1* mRNA remains to be determined in cell death lineages.

In general, the regulation of gene expression by *cis*-acting elements in an mRNA is mediated by the associated regulatory factors (proteins). The *egl-1* TPTE is predicted to form a stem-loop structure. Staufen protein is a double-stranded-RNA- and tubulin-binding protein, which forms ribonucleoprotein complexes (RNPs) that play critical roles in the localization, translational repression and turnover of mRNAs (LeGendre et al., 2013; Wickham et al., 1999). My data suggests that *C. elegans* Staufen protein STAU-1 might not be involved in the repression of *egl-1* expression. The loss of *stau-1* neither affects *egl-1* reporter gene expression nor causes the appearance of large cell corpses during embryo development. This would be consistent with the previous finding that STAU-1 does not bind to the *egl-1* mRNA (LeGendre et al., 2013). The *egl-1* TPTE contains an AU-rich element (ARE) and could potentially interact with ARE-binding RBPs, such as hnRNP (Geuens et al., 2016), CELF1 (Barreau et al., 2006), HuR (Ripin et al., 2019), and TIA1/TIAL1 proteins (Izquierdo, 2010) (listed in **Table 3.2**). However, only ETR-1 (ortholog of human CELF1) and HRPA-1 (ortholog of human hnRNP A1/3) weakly repress *egl-1* expression. ETR-1 and HRPA-1 are identified as repressor candidates of the *egl-1* in my genetic screen (described in **Chapter 4.2**). The *trans*-acting factors that regulate *egl-1* expression by associating with the *egl-1* TPTE remain to be uncovered.

The 3′ terminal stem-loop structure is commonly found in the 3′ UTR of mRNAs and is involved in diverse processes of mRNA regulation. The 3′ terminal stem-loop structure is thought to function in intrinsic transcription termination in both eukaryotes and prokaryotes (Proudfoot, 2016; You et al., 2023). The hairpin loop in an mRNA causes the RNA polymerase to become dissociated from the DNA template strand. The ability of the stem-loop structure to signal transcription termination depends on sequence specificity and secondary structure. The canonical termination signal is composed of

a GC-rich inverted stem sequence followed by a U-rich sequence (U stretch) (Gusarov and Nudler, 1999). The 3′ terminal stem-loop also functions in mRNA processing, export of mRNAs from the nucleus to the cytoplasm, and regulation of mRNA stability and translation (Gallie et al., 1996; Gorgoni et al., 2005; Marzluff and Koreski, 2017; Tan et al., 2013; Zhang et al., 2014). For example, mRNAs of Histone genes that are expressed during DNA replication usually lack a poly(A) tail. Instead, the regulation of mRNA processing and metabolism depends on a highly conserved stem-loop structure and the associated stem-loop binding proteins (SLBP, also called hairpin-binding protein, HBP) (Marzluff and Koreski, 2017). This element is functionally similar to a poly(A) tail and is important for maintaining mRNA stability as well as translation initiation. The canonical stem-loop in histone mRNAs contains a GC-rich sequence in the stem portion. The AU-rich 3′ terminal stem-loop structure has also been proposed to play a role in mRNA localization. For example, an AU-rich stem-loop structure is identified in the 3′ UTR of mouse *c-myc* mRNA (Chabanon et al., 2005). Mutating this element prevents the perinuclear localization of the *c-myc* mRNA. Distinctly, the results from my work suggest a novel role of the 3′ terminal stem-loop structure, namely repression of gene expression. Mutating the 3′ terminal stem-loop structure in the *egl-1* 3′ UTR (i.e. *egl-1* TPTE) up-regulates the expression of the *egl-1* 3′ UTR reporter. The underlying molecular mechanism remains to be determined. The RBPs that associate with the *egl-1* TPTE to repress *egl-1* expression can be identified by biochemical work, for example RNA pulldown coupled with mass spectrometry. Besides, whether the binding of these RBPs to the *egl-1* TPTE affects the stability of *egl-1* mRNA can be determined by smRNA FISH.

6.1.2 FBEs in the *egl-1* 3′ UTR contribute to the repression of *egl-1* reporter expression

FBF-1 and FBF-2 (collectively referred to as ‘FBF’) are two nearly identical *C. elegans* PUF family RBPs, which are required for germ stem cell maintenance and which regulate the mitosis/meiosis switch in the *C. elegans* germline (Crittenden et al., 2002; Haupt et al., 2020; Lamont et al., 2004; Merritt and Seydoux, 2010). FBF-1 and FBF-2 are redundant, and the mRNA sequences of *fbf-1* and *fbf-2* are 93% identical (Zhang et al., 1997). FBF proteins repress target gene expression by binding to FBF binding elements (FBEs) in the 3′ UTR of target mRNAs (Zhang et al., 1997). The *egl-1* mRNA

has been previously identified as a target of FBF proteins (Kershner and Kimble, 2010; Porter et al., 2019). My study presents evidence that FBEs identified in the *egl-1* 3′ UTR likely contribute to the repression of *egl-1* expression. Disruption of these FBEs in the *egl-1* 3′ UTR de-represses the expression of the *egl-1* 3′ UTR reporter $P_{mai\text{-}2}$*gfp::h2b::egl-1 3′ UTR*. However, FBF proteins do not seem to have an inhibitory effect on *egl-1* expression because the loss of both *fbf-1* and *fbf-2* does not affect the expression of the *egl-1* 3′ UTR reporter and does not result in a large cell corpse phenotype indicative of precocious or ectopic cell death. The effect of the loss of FBEs on the expression of the *egl-1* 3′ UTR reporter may be caused by changes in the binding accessibility of other regulators to the *egl-1* 3' UTR. In fact, the FBE1 is very close to and structurally interacts with the binding site of the miR-35 family microRNAs in the *egl-1* 3′ UTR. Therefore, mutating the FBE1 in the *egl-1* 3' UTR probably affects the binding of miR-35 microRNAs to the *egl-1* mRNA. Otherwise, the absence of a phenotype upon the loss of *fbf1* and *fbf2* could also be because of the presence of other functionally redundant RBPs. The partial redundancy of the function of FBF1/2 and PUF-3 /11 in germ stem cells has been reported (Haupt et al., 2020). An *fbf-1 fbf-2; puf-3 puf-11* quadruple null mutant has a stronger defect in germ stem cells compared to *fbf-1 fbf-2* or *puf-3 puf-11* double mutants. For this reason, in the future, the quadruple mutant should be tested for phenotypes with respect to *egl-1* expression and apoptosis.

6.2 Diverse RBPs might act coordinatively to regulate *egl-1* expression and the robustness of the cell death fate

By screening for effects on the expression of the P_{mai-2}*gfp::h2b::egl-1 3′ UTR* transgene as well as apoptosis-related phenotypes after individually knocking down the 660 genes that are predicted to encode RBPs, I identified five repressor candidates (VHA-10, SWSN-7, RACK-1, ETR-1, and HRPA-1) and two activator candidates (EIF-3.H and HRPR-1) of *egl-1*.

VHA-10 is an ortholog of subunit G of the cytoplasmic (V1) domain of human Vacuolar (H+)-ATPase. It is involved in the acidification of intracellular organelles and the regulation of cellular pH at the expense of ATP (Lee et al., 2010; Sun et al., 2020; Syntichaki et al., 2005). VHA-10 has previously been shown to be present in poly(A)-containing mRNA complexes by an RNA pull down experiment (Matia-Gonzalez et al., 2015). However, it does not seem to contain a traditional RNA-binding domain. Of note, only knocking down of *vha-10* up-regulates the expression of the P_{mai-2}*gfp::h2b::egl-1 3′ UTR* transgene, but knocking down of the other Vacuolar (H+)-ATPase genes does not (data not shown). This suggests that this effect is not caused by the decrease in Vacuolar (H+)-ATPase activity but due to the loss of *vha-10* by itself. How VHA-10 is involved in the repression of *egl-1* expression remains to be determined. The effect of VHA-10 on *egl-1* mRNA stability can be determined by smRNA FISH experiment. As far as I know, this is the first evidence that VHA-10 possibly regulates gene expression. Because VHA-10 does not contain any known RNA-binding domain, it could regulate the stability or translation of target mRNAs by indirectly interacting with them. This speculation can be determined by the immunoprecipitation experiment or electrophoretic mobility shift assay (EMSA).

SWSN-7 is an ortholog of human BAF200 (also known as ARID2), which is a component of the SWI/SNF nucleosome remodeling complex. SWSN-7 protein carries an AT-rich interaction domain 2 (ARID2) at the N-terminus and C2H2-type Zinc fingers at the C-terminus (Large and Mathies, 2014; Tamburino et al., 2013). These domains were originally identified as DNA-binding domains, but they were later proposed to interact also with mRNAs (Korn and Schlundt, 2022; Tamburino et al., 2013). I provide evidence that SWSN-7 possibly contributes to the repression of *egl-1* at the post-transcriptional level. This effect could be mediated by binding to the *egl-1* mRNA

through ARID2 or Zinc fingers present in SWSN-7. This possibility can be confirmed by biochemical experiments in future work. It is also possible that the regulation of *egl-1* expression by SWSN-7 is mediated by the SWI/SNF complex through remodeling the chromatin structure and affecting *egl-1*'s transcription activity. To this end, the effect of the other components of the SWI/SNF complex on *egl-1* expression needs to be determined.

RACK-1 is an ortholog of human Receptor of Activated C Kinase 1 protein (RACK1), which is a scaffold for the protein kinase C (PKC) by bringing the activated PKC to various substrates (Birikh et al., 2003). RACK1 is a multifaceted scaffolding protein (Adams et al., 2011; Gandin et al., 2013). It anchors various protein at particular locations in a cell (Adams et al., 2011). It has been demonstrated that *C. elegans* RACK-1 regulates axon pathfinding and cell migration by physically interacting with the actin-binding protein UNC-115 (Demarco and Lundquist, 2010). Besides, RACK1 is also thought to be a ribosomal protein (Thompson et al., 2016). It has been shown to associate with poly(A)-containing mRNAs in neurons (Angenstein et al., 2002). But it does not seem to contain a traditional RNA-binding domain. For this reason, it is possible that RACK-1 is involved in the repression of *egl-1* mRNA translation by indirectly interacting with the *egl-1* mRNA. The potential interaction between RACK-1 and *egl-1* mRNA can be determined by the immunoprecipitation experiment or electrophoretic mobility shift assay (EMSA). Whether RACK-1 represses *egl-1* mRNA translation can be determined using the novel method for live imaging *egl-1* mRNA translation that has been established in this work.

ETR-1 is an ELAV-like family RBP (an ortholog of human CELF1). CELF1 has been shown to promote mRNA decay by binding to the GU-rich element (GRE) in target mRNAs (Goraczniak and Gunderson, 2008; Vlasova-St Louis and Bohjanen, 2011; Vlasova et al., 2008). CELF1 is also predicted to bind the AU-rich element (ARE) in the 3' UTR of target mRNAs by UniPro (www.uniprot.org). I provide evidence that ETR-1 possibly contributes to the repression of *egl-1* expression. Consistent with my finding, knocking down of *etr-1* increases the number of cell corpses in *C. elegans* germline (Boateng et al., 2017). Future studies need to determine whether ETR-1 regulates *egl-1* mRNA decay by binding to the ARE within the *egl-1* 3' UTR. The potential interaction between ETR-1 and *egl-1* mRNA can be determined by the immunoprecipitation

experiment or electrophoretic mobility shift assay (EMSA). The effect of ETR-1 on *egl-1* mRNA stability can be determined by smRNA FISH.

HRPA-1 (also known as HRP-1) is an ortholog of human hnRNP A1/3, which regulates various RNA metabolic processes, including transcription, alternative splicing of pre-mRNA, translation, and mRNA stability (Feng et al., 2022). hnRNP A1/3 proteins can bind to the poly(A)-containing mRNAs in the nucleus and cytoplasm (Mili et al., 2001). It has been reported that hnRNP A1 can repress mRNA translation by binding to the ARE in mRNAs (Buxade et al., 2005). I provide evidence that *C. elegans* HRPA-1 possibly contributes to the repression of *egl-1* expression. A possible mechanism is that HRPA-1 could bind to the ARE found in the *egl-1* 3' UTR and thereby regulate its translation. However, this speculation needs to be confirmed in future studies. The potential effect on *egl-1* mRNA translation can be determined using the novel method for live imaging *egl-1* mRNA translation that has been established in this work.

EIF-3.H is an ortholog of human EIF3H, which functions in translational activation or repression of mRNAs of cell proliferation genes (Lee et al., 2015). It has been shown that EIF3H regulates target gene translation by targeting specific mRNAs to polysomes during embryogenesis in zebrafish (Choudhuri et al., 2013). In *C. elegans*, EIF-3.H was reported to regulate axon formation (Schmitz et al., 2007). My results show that *C. elegans* EIF-3.H possibly acts as an activator of *egl-1*. It would be interesting to determine whether EIF-3.H regulates *egl-1* mRNA translation by recruiting the *egl-1* mRNA to polysomes in future studies. The potential effect on *egl-1* mRNA translation can be determined using the novel method for live imaging *egl-1* mRNA translation that has been established in this work.

HRPR-1 (also known as HRP-2) is an ortholog of human hnRNP R, hnRNP Q (Syncrip), and ACF protein. hnRNP R is supposed to modulate mRNA abundance in the axon. *C. elegans* HRPR-1 contains three RNA-recognition motifs (RRM) and a C-terminal RG/RGG repeats element, indicating that it has RNA-binding activity (Kinnaird et al., 2004). My results show that HRPR-1 possibly enhances *egl-1* expression and hereby promotes apoptosis. In *C. elegans,* HRPR-1 is widely expressed and localized

in the nucleus during embryogenesis and larval development. HRPR-1 has been reported to regulate mRNA splicing by binding to UCUAUC splicing regulatory elements in target mRNAs, which include *unc-52* and *lin-10* (Kabat et al., 2009). In line with my results, RNAi knockdown of *hrpr-1* leads to embryonic lethality (Kinnaird et al., 2004). By contrast, *hrpr-1* (RNAi) in adult animals did not show discernible phenotypes, indicating that *hrpr-1* is essential for developmental processes but not for the maintenance of tissues (Kinnaird et al., 2004). In mammalian neurons, hnRNP R shuttles between the nucleus and cytosol (Dombert et al., 2014; Glinka et al., 2010). For example, hnRNP R directs the localization of *β-actin* mRNAs to axons by binding to the 3′ UTR of *β-actin* mRNA (Glinka et al., 2010; Rossoll et al., 2003). Very recently, hnRNP R has also been reported to negatively regulate transcription by associating with its interactor non-coding RNA 7SK (Ji et al., 2022). hnRNP Q has been reported to regulate mRNA splicing (Chen et al., 2008a), transport (McDermott et al., 2012), translation (Svitkin et al., 2013) and stability (Grosset et al., 2000). For example, hnRNP Q regulates the usage of exon 7 in the survival motor neuron 2 gene *SMN2* (Chen et al., 2008a). In addition, hnRNP Q has been reported to control the selectivity of microRNA loading into exosomes (Hobor et al., 2018; Santangelo et al., 2016). The microRNA sorting by hnRNP Q implies coordinated recognition of an hEXO (GGCU/A) sequence in target miRNAs by its N-terminal unit for RNA recognition (NURR, a non-canonical RNA-binding domain) and binding of its RRM domains to microRNAs at the site 5′ to the hEXO sequence. Surprisingly, hnRNP Q is predominantly localized in the cytoplasm (Chen et al., 2008a). It seems plausible that hnRNP Q can shuttle between the nucleus and cytosol to exert its distinct function in the two compartments. HRPR-1 is possibly involved in all aspects of *egl*-1 mRNA regulation. Whether HRPR-1 regulates the splicing, stability, or translation of *egl*-1 mRNA needs to be investigated in future studies. The potential effect on *egl-1* mRNA stability can be determined by smRNA FISH. The potential effect on *egl-1* mRNA translation can be determined using the novel method for live imaging *egl-1* mRNA translation that has been established in this work.

Although this study provides useful information for our understanding of the control of *egl-1* expression and apoptosis, there are some unavoidable weaknesses in my

genetic screen. First, the relevant phonotypes I observed were quite subtle. It is plausible that the apoptosis pathway is regulated by a large class of functionally redundant factors to ensure the robustness of the cell death fate. Removing one of the regulators might not cause a big disturbance to the apoptosis pathway and not lead to abnormal cell death events. However, removing a second regulator could increase the workload too much and increase developmental defects. Second, I believe some important regulators were unavoidably omitted from this screen (during the re-screen for apoptosis-related phenotypes) due to the limitations of the RNAi knockdown efficiency in cell death lineages. We have already known that some cells (e.g., some neurons and neuroblasts) show resistance to RNAi due to a lack of factors in the RNAi pathway (Calixto et al., 2010). And most of the somatic apoptotic cells are generated from neuronal precursor lineages (Sulston and Horvitz, 1977; Sulston et al., 1983); thus, it is plausible that RNAi is not efficient enough in these lineages to cause a strong effect. In addition, the major evidence for *egl-1* repressor candidates is from the analyses of the expression of the 3' UTR reporter $P_{mai\text{-}2}$*gfp::h2b::egl-1 3′ UTR* and the appearance of the large cell corpse. This reporter is artificial and might not completely reflect the effect of these candidates on *egl-1* expression in cell death lineages. Most of the cells programmed to die in *C. elegans* are generated by asymmetric cell division and are smaller in size compared to surviving cells. It has been shown that precocious or ectopic cell death of cells that should normally survive generates larger cell corpses (Sherrard et al., 2017). However, without determining the identities of these large cell corpses, I cannot rule out the possibility that they are generated from cells that are programmed to die. The size of cell corpses might become larger because the mother cell division occurs more symmetrically.

Based on the current data, the *cis*-acting elements in the *egl-1* 3′ UTR and associated *trans*-acting factors, such as miRNAs and RBPs, likely contribute to the spatiotemporal control of *egl-1* expression and, hence, apoptotic cell death, to ensure proper cell number homeostasis during *C. elegans* development (**Fig. 6.1**).

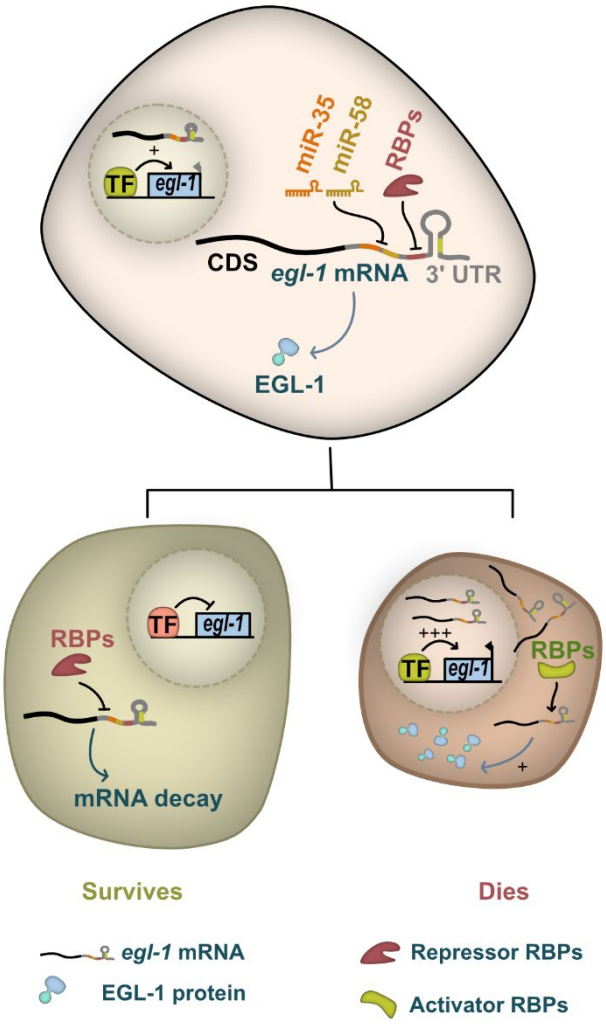

Figure 6.1 Model for the regulation of *egl-1* expression in a cell death lineage. In the mother cell, *egl-1* gene is moderately transcribed, but the translation is largely repressed by posttranscriptional mechanisms involving miRNAs and repressor RBPs through binding to the *egl-1* 3′ UTR. In the smaller daughter cell, *egl-1* expression is remarkably increased due to increased transcription regulated by transcription activators and increased translation regulated by activator RBPs, which eventually leads to apoptotic cell death. In the larger daughter, *egl-1* transcription is inhibited, and inherited *egl-1* mRNAs are eliminated by destabilization regulated by miRNAs and repressor RBPs.

6.3 Live imaging reveals spatiotemporal *egl-1* mRNA translation

The smRNA FISH data show that, within cell death lineages, there is a low number of *egl-1* mRNAs in mother cells, a high number in daughters programmed to die, and essentially zero in daughters programmed to survive (Sherrard et al., 2017). But the visualization of *egl-1* mRNA translation has been challenging. It could be because there are probably very few copies of *egl-1* mRNAs compared to other genes and the half-life of the EGL-1 protein is possibly short.

In this study, I established a novel method for live imaging *egl-1* mRNA translation using SunTag-based signal amplification. Though fusing 18xSunTag peptide repeats to EGL-1 and co-expressing the SunTag antibody fused to sfGFP (i.e., scFv::sfGFP), as many as eighteen copies of GFP could potentially be enriched at a single EGL-1 protein. This can dramatically increase the signal from a single EGL-1 protein. Taking advantage of this approach, I show that, in the RID lineage (ABalappaap, a cell death lineage), *egl-1* mRNA translation is already initiated in the mother cell (RIDnb, ABalappaap) and increases in the daughter cell that is programmed to die (RIDsc, ABalappaapp). This finding is in line with the evidence that EGL-1 activity is already present at a certain low level in the mothers of the NSM and QL.p cell death lineages and that *egl-1* is necessary for the asymmetric division in mothers (Chakraborty et al., 2015; Mishra et al., 2018). Upon the loss of EGL-1, mother cell division becomes more symmetric, and the daughter cell that is programmed to die increases in its size. Although whether *egl-1* is necessary for the asymmetric division in the RIDnb has not been determined, *egl-1* mRNAs are detectable in the RIDnb.

The levels of *egl-1* mRNA translation could have a high variance among different cell death lineages. It is well established that EGL-1 activity is regulated by transcription factors in a lineage-specific manner (Conradt et al., 2016; Nehme and Conradt, 2008). In line with this, it has been shown that *egl-1* mRNA copy number is higher in the MSpaapp cell (programmed to die during the first cell death wave) than that in the RIDsc (programmed to die during the second cell death wave) (Sherrard et al., 2017). Of note, the MSpaapp cell is larger than the RIDsc in size. I speculate that larger cells may need more EGL-1 proteins to go over the concentration threshold that is necessary to trigger apoptosis. In this context, it would be interesting to determine

whether the level of *egl-1* mRNA translation is higher in cell death lineages where cells have a larger size.

The SunTag system is a very bright genetically encoded fluorescent labeling system available so far, and it has several advantages compared to other translation imaging methods. First, it shows a very high sensitivity, so that a low expression level of the target protein is sufficient for imaging, which avoids problems caused by protein overexpression using a transgene. This makes it a suitable solution for imaging *egl-1* mRNA translation. Second, labeling of protein molecules with bright signals allows imaging using a much lower laser intensity, which could minimize phototoxicity and photobleaching during long term imaging with multiple time series. However, this system does have several limitations. Loading of 18 copies of scFv::sfGFP (~1,100 kDa) makes the target protein very huge, which could disturb the function of the target protein. Besides, fusing such a long tag (1.2 kb) without codon optimization for *C. elegans* to the 5′ end of the target mRNA possibly decreases the translation efficiency. In my study, this system causes a partial loss of *egl-1* function and partially blocks apoptosis. Finally, It is important to control the expression stoichiometry between SunTag::EGL-1 and its binding module scFv::GFP, so that there is neither incomplete labeling nor too much background from excessive scFv::GFP. In my study, the expression *scFv::sfGFP::NLS* is under the control of the promoter of the heat-shock responsive gene *hsp-16.41*. Using this strategy, I can manipulate the expression level of the scFv::sfGFP::NLS by heat-shock treatment and localize the unbound scFv::sfGFP::NLS to the nuclear region to gain a better signal/noise ratio. But the inducible promoter also raises an issue. Because the expression level of scFv::sfGFP::NLS is variable among different cells and different embryos at different time series during imaging, it is not very reliable for quantitative analysis. Using a promoter that is moderately but consistently active could minimize this variance.

6.4 Conclusions

My work shows that the conserved *cis*-acting elements (including TPTE and FBEs) in the *egl-1* 3′ UTR likely contribute to the repression of *egl-1* expression and the repression of apoptosis.

Additionally, five repressor candidates and two activator candidates of *egl-1* are identified in a genetic screen by RNAi.

Finally, by establishing a novel method for imaging *egl-1* mRNA translation, its spatiotemporal pattern can now be revealed during *C. elegans* development.

The *cis*-acting elements in the *egl-1* 3′ UTR and associated *trans*-acting factors, such as miRNAs and RBPs, likely contribute to the spatiotemporal control of *egl-1* expression and, hence, apoptotic cell death, to ensure proper cell number homeostasis during *C. elegans* development. It seems plausible that these regulatory mechanisms have redundancies, and that they cooperatively control *egl-1* expression to ensure the highly reproducible and robust survival and death pattern.

6.5 Future works

Several questions remain to be answered.

First, the identities of large cell corpses observed in embryos of the *egl-1* TPTE mutant as well as upon the loss of identified repressor candidates of *egl-1* remain to be determined by lineaging analysis. This will answer the question whether they are from precocious or ectopic cell death of cells that should normally survive or from cells programmed to die.

Second, biochemical work needs to be performed to determine whether the identified *egl-1* regulators could directly bind the *egl-1* mRNA. The identified RBP regulators can be immunoprecipitated and the associated mRNAs can be subsequently examined by qPCR.

Additionally, the *trans*-acting factors that associate with the *egl-1* TPTE to repress *egl-1* expression remain to be further investigated. ETR-1 and HRPA-1 are identified to contribute to the repression of *egl-1* expression, and they are thought to bind the AU-rich element (ARE). Interestingly, the *egl-1* TPTE contains an ARE. Whether ETR-1 and HRPA-1 repress *egl-1* expression by binding the *egl-1* TPTE should be confirmed.

Finally, through combining with the labeling of cell organelles, the SunTag system established in this study can be used to study the subcellular localization of the EGL-1 protein. Based on findings from previous studies, the EGL-1 protein presumably localizes to mitochondria to exert its pro-apoptotic function, through binding to the CED-9 protein located on the outer mitochondrial membrane. In addition, to answer the question where the *egl-1* mRNA is translated in a cell, the SunTag system can be coupled with the MS2-MCP system to simultaneously label the nascent EGL-1 protein and the *egl-1* mRNA.

References

References

Abraham, M.C., Lu, Y., and Shaham, S. (2007). A morphologically conserved nonapoptotic program promotes linker cell death in Caenorhabditis elegans. Dev Cell *12*, 73-86.

Adams, D.R., Ron, D., and Kiely, P.A. (2011). RACK1, A multifaceted scaffolding protein: Structure and function. Cell Commun Signal *9*, 22.

Ameisen, J.C. (2002). On the origin, evolution, and nature of programmed cell death: a timeline of four billion years. Cell Death Differ *9*, 367-393.

Anderson, P., and Kedersha, N. (2008). Stress granules: the Tao of RNA triage. Trends Biochem Sci *33*, 141-150.

Anderson, P., and Kedersha, N. (2009). RNA granules: post-transcriptional and epigenetic modulators of gene expression. Nat Rev Mol Cell Biol *10*, 430-436.

Angenstein, F., Evans, A.M., Settlage, R.E., Moran, S.T., Ling, S.C., Klintsova, A.Y., Shabanowitz, J., Hunt, D.F., and Greenough, W.T. (2002). A receptor for activated C kinase is part of messenger ribonucleoprotein complexes associated with PolyA-mRNAs in neurons. J Neurosci *22*, 8827-8837.

Ast, G. (2004). How did alternative splicing evolve? Nature Reviews Genetics *5*, 773-782.

Audhya, A., Hyndman, F., McLeod, I.X., Maddox, A.S., Yates, J.R., Desai, A., and Oegema, K. (2005). A complex containing the Sm protein CAR-1 and the RNA helicase CGH-1 is required for embryonic cytokinesis in Caenorhabditis elegans. J Cell Biol *171*, 267-279.

Bachorik, J.L., and Kimble, J. (2005). Redundant control of the Caenorhabditis elegans sperm/oocyte switch by PUF-8 and FBF-1, two distinct PUF RNA-binding proteins. Proceedings of the National Academy of Sciences of the United States of America *102*, 10893-10897.

Bailly, A., and Gartner, A. (2013). Germ Cell Apoptosis and DNA Damage Responses. Adv Exp Med Biol *757*, 249-276.

Bakhshi, A., Jensen, J.P., Goldman, P., Wright, J.J., McBride, O.W., Epstein, A.L., and Korsmeyer, S.J. (1985). Cloning the chromosomal breakpoint of t(14;18) human lymphomas: clustering around JH on chromosome 14 and near a transcriptional unit on 18. Cell *41*, 899-906.

Baltz, A.G., Munschauer, M., Schwanhausser, B., Vasile, A., Murakawa, Y., Schueler, M., Youngs, N., Penfold-Brown, D., Drew, K., Milek, M.*, et al.* (2012). The mRNA-Bound Proteome and Its Global Occupancy Profile on Protein-Coding Transcripts. Mol Cell *46*, 674-690.

Bao, C., Zhu, M.Y., Nykonchuk, I., Wakabayashi, H., Mathews, D.H., and Ermolenko, D.N. (2022). Specific length and structure rather than high thermodynamic stability enable regulatory mRNA stem-loops to pause translation. Nature Communications *13*.

Barondeau, D.P., Putnam, C.D., Kassmann, C.J., Tainer, J.A., and Getzoff, E.D. (2003). Mechanism and energetics of green fluorescent protein chromophore synthesis revealed by trapped intermediate structures. Proc Natl Acad Sci U S A *100*, 12111-12116.

Barreau, C., Paillard, L., and Osborne, H.B. (2005). AU-rich elements and associated factors: are there unifying principles? Nucleic Acids Res *33*, 7138-7150.

Barreau, C., Watrin, T., Osborne, H.B., and Paillard, L. (2006). Protein expression is increased by a class III AU-rich element and tethered CUG-BP1. Biochem Biophys Res Commun *347*, 723-730.

Bartel, D.P. (2009). MicroRNAs: target recognition and regulatory functions. Cell *136*, 215-233.

Baum, J.S., St George, J.P., and McCall, K. (2005). Programmed cell death in the germline. Semin Cell Dev Biol *16*, 245-259.

Bava, F.A., Eliscovich, C., Ferreira, P.G., Minana, B., Ben-Dov, C., Guigo, R., Valcarcel, J., and Mendez, R. (2013). CPEB1 coordinates alternative 3'-UTR formation with translational regulation. Nature *495*, 121-125.

Becker, K., Bluhm, A., Casas-Vila, N., Dinges, N., Dejung, M., Sayols, S., Kreutz, C., Roignant, J.Y., Butter, F., and Legewie, S. (2018). Quantifying post-transcriptional regulation in the development of Drosophila melanogaster. Nat Commun *9*, 4970.

Beckmann, B.M., Horos, R., Fischer, B., Castello, A., Eichelbaum, K., Alleaume, A.M., Schwarzl, T., Curk, T., Foehr, S., Huber, W.*, et al.* (2015). The RNA-binding proteomes from yeast to man harbour conserved enigmRBPs. Nature Communications *6*.

Bentley, D.L. (2014). Coupling mRNA processing with transcription in time and space. Nat Rev Genet *15*, 163-175.

Berkovits, B.D., and Mayr, C. (2015). Alternative 3 ' UTRs act as scaffolds to regulate membrane protein localization. Nature *522*, 363-+.

Bertheloot, D., Latz, E., and Franklin, B.S. (2021). Necroptosis, pyroptosis and apoptosis: an intricate game of cell death. Cell Mol Immunol *18*, 1106-1121.

Birikh, K.R., Sklan, E.H., Shoham, S., and Soreq, H. (2003). Interaction of "readthrough" acetylcholinesterase with RACK1 and PKCbeta II correlates with intensified fear-induced conflict behavior. Proc Natl Acad Sci U S A *100*, 283-288.

Boateng, R., Nguyen, K.C.Q., Hall, D.H., Golden, A., and Allen, A.K. (2017). Novel functions for the RNA-binding protein ETR-1 in Caenorhabditis elegans reproduction and engulfment of germline apoptotic cell corpses. Dev Biol *429*, 306-320.

Boersma, S., Khuperkar, D., Verhagen, B.M.P., Sonneveld, S., Grimm, J.B., Lavis, L.D., and Tanenbaum, M.E. (2019). Multi-Color Single-Molecule Imaging Uncovers Extensive Heterogeneity in mRNA Decoding. Cell *178*, 458-472 e419.

Boo, S.H., and Kim, Y.K. (2020). The emerging role of RNA modifications in the regulation of mRNA stability. Experimental and Molecular Medicine *52*, 400-408.

Brenner, S. (1974). The genetics of Caenorhabditis elegans. Genetics *77*, 71-94.

Broughton, J.P., and Pasquinelli, A.E. (2013). Identifying Argonaute binding sites in Caenorhabditis elegans using iCLIP. Methods *63*, 119-125.

Buxade, M., Parra, J.L., Rousseau, S., Shpiro, N., Marquez, R., Morrice, N., Bain, J., Espel, E., and Proud, C.G. (2005). The Mnks are novel components in the control of TNF alpha biosynthesis and phosphorylate and regulate hnRNP A1. Immunity *23*, 177-189.

Cabantous, S., Terwilliger, T.C., and Waldo, G.S. (2005). Protein tagging and detection with engineered self-assembling fragments of green fluorescent protein. Nat Biotechnol *23*, 102-107.

Calixto, A., Chelur, D., Topalidou, I., Chen, X.Y., and Chalfie, M. (2010). Enhanced neuronal RNAi in C. elegans using SID-1. Nat Methods *7*, 554-U102.

Castello, A., Fischer, B., Frese, C.K., Horos, R., Alleaume, A.M., Foehr, S., Curk, T., Krijgsveld, J., and Hentze, M.W. (2016). Comprehensive Identification of RNA-Binding Domains in Human Cells. Mol Cell *63*, 696-710.

Chabanon, H., Mickleburgh, I., Burtle, B., Pedder, C., and Hesketh, J. (2005). An AU-rich stem-loop structure is a critical feature of the perinuclear localization signal of c-myc mRNA. Biochem J *392*, 475-483.

Chakraborty, S., Lambie, E.J., Bindu, S., Mikeladze-Dvali, T., and Conradt, B. (2015). Engulfment pathways promote programmed cell death by enhancing the unequal segregation of apoptotic potential. Nat Commun *6*, 10126.

Chartron, J.W., Hunt, K.C.L., and Frydman, J. (2016). Cotranslational signal-independent SRP preloading during membrane targeting. Nature *536*, 224-+.

Chattopadhyay, A., Chiang, C.W., and Yang, E. (2001). BAD/BCL-[X(L)] heterodimerization leads to bypass of G0/G1 arrest. Oncogene *20*, 4507-4518.

Chen, C.Y., Gherzi, R., Ong, S.E., Chan, E.K.L., Raijmakers, R., Pruijn, G.J.M., Stoecklin, G., Moroni, C., Mann, M., and Karin, M. (2001). AU binding proteins recruit the exosome to degrade ARE-containing mRNAs. Cell *107*, 451-464.

Chen, F., Hersh, B.M., Conradt, B., Zhou, Z., Riemer, D., Gruenbaum, Y., and Horvitz, H.R. (2000). Translocation of C. elegans CED-4 to nuclear membranes during programmed cell death. Science *287*, 1485-1489.

Chen, H.H., Chang, J.G., Lu, R.M., Peng, T.Y., and Tarn, W.Y. (2008a). The RNA Binding Protein hnRNP Q Modulates the Utilization of Exon 7 in the Survival Motor Neuron 2 (SMN2) Gene. Mol Cell Biol *28*, 6929-6938.

Chen, K.X., Song, F.J., Calin, G.A., Wei, Q.Y., Hao, X.S., and Zhang, W. (2008b). Polymorphisms in microRNA targets: a gold mine for molecular epidemiology. Carcinogenesis *29*, 1306-1311.

Chen, L., Willis, S.N., Wei, A., Smith, B.J., Fletcher, J.I., Hinds, M.G., Colman, P.M., Day, C.L., Adams, J.M., and Huang, D.C.S. (2005). Differential targeting of prosurvival Bcl-2 proteins by their BH3-only ligands allows complementary apoptotic function. Mol Cell *17*, 393-403.

Chinnaiyan, A.M., O'Rourke, K., Lane, B.R., and Dixit, V.M. (1997). Interaction of CED-4 with CED-3 and CED-9: a molecular framework for cell death. Science *275*, 1122-1126.

Choudhuri, A., Maitra, U., and Evans, T. (2013). Translation initiation factor eIF3h targets specific transcripts to polysomes during embryogenesis. Proceedings of the National Academy of Sciences of the United States of America *110*, 9818-9823.

Cleary, M.L., and Sklar, J. (1985). Nucleotide sequence of a t(14;18) chromosomal breakpoint in follicular lymphoma and demonstration of a breakpoint-cluster region near a transcriptionally active locus on chromosome 18. Proc Natl Acad Sci U S A *82*, 7439-7443.

Colby, D.W., Garg, P., Holden, T., Chao, G., Webster, J.M., Messer, A., Ingram, V.M., and Wittrup, K.D. (2004). Development of a human light chain variable domain (V(L)) intracellular antibody specific for the amino terminus of huntingtin via yeast surface display. J Mol Biol *342*, 901-912.

Colgan, D.F., and Manley, J.L. (1997). Mechanism and regulation of mRNA polyadenylation. Genes Dev *11*, 2755-2766.

Conrad, T., Albrecht, A.S., Costa, V.R.D., Sauer, S., Meierhofer, D., and Orom, U.A. (2016). Serial interactome capture of the human cell nucleus. Nature Communications *7*.

Conradt, B., and Horvitz, H.R. (1998). The C-elegans protein EGL-1 is required for programmed cell death and interacts with the Bcl-2-like protein CED-9. Cell *93*, 519-529.

Conradt, B., and Horvitz, H.R. (1999). The TRA-1A sex determination protein of C. elegans regulates sexually dimorphic cell deaths by repressing the egl-1 cell death activator gene. Cell *98*, 317-327.

Conradt, B., Wu, Y.C., and Xue, D. (2016). Programmed Cell Death During Caenorhabditis elegans Development. Genetics *203*, 1533-1562.

Crittenden, S.L., Bernstein, D.S., Bachorik, J.L., Thompson, B.E., Gallegos, M., Petcherski, A.G., Moulder, G., Barstead, R., Wickens, M., and Kimble, J. (2002). A conserved RNA-binding protein controls germline stem cells in Caenorhabditis elegans. Nature *417*, 660-663.

Danial, N.N. (2008). BAD: undertaker by night, candyman by day. Oncogene *27*, S53-S70.

Danial, N.N., Gramm, C.F., Scorrano, L., Zhang, C.Y., Krauss, S., Ranger, A.M., Datta, S.R., Greenberg, M.E., Licklider, L.J., Lowell, B.B.*, et al.* (2003). BAD and glucokinase reside in a mitochondrial complex that integrates glycolysis and apoptosis. Nature *424*, 952-956.

Danial, N.N., Walensky, L.D., Zhang, C.Y., Choi, C.S., Fisher, J.K., Molina, A.J.A., Datta, S.R., Pitter, K.L., Bird, G.H., Wikstrom, J.D.*, et al.* (2008). Dual role of proapoptotic BAD in insulin secretion and beta cell survival. Nat Med *14*, 144-153.

Datta, S.R., Katsov, A., Hu, L., Petros, A., Fesik, S.W., Yaffe, M.B., and Greenberg, M.E. (2000). 14-3-3 proteins and survival kinases cooperate to inactivate BAD by BH3 domain phosphorylation. Mol Cell *6*, 41-51.

Dekkers, M.P.J., Nikoletopoulou, V., and Barde, Y.A. (2013). Death of developing neurons: New insights and implications for connectivity. J Cell Biol *203*, 385-393.

Demarco, R.S., and Lundquist, E.A. (2010). RACK-1 acts with Rac GTPase signaling and UNC-115/abLIM in Caenorhabditis elegans axon pathfinding and cell migration. PLoS Genet *6*, e1001215.

Dickinson, D.J., Pani, A.M., Heppert, J.K., Higgins, C.D., and Goldstein, B. (2015). Streamlined Genome Engineering with a Self-Excising Drug Selection Cassette. Genetics *200*, 1035-1049.

Dombert, B., Sivadasan, R., Simon, C.M., Jablonka, S., and Sendtner, M. (2014). Presynaptic localization of Smn and hnRNP R in axon terminals of embryonic and postnatal mouse motoneurons. PLoS One *9*, e110846.

Dreze, M., Charloteaux, B., Milstein, S., Vidalain, P.O., Yildirim, M.A., Zhong, Q., Svrzikapa, N., Romero, V., Laloux, G., Brasseur, R.*, et al.* (2009). 'Edgetic' perturbation of a C. elegans BCL2 ortholog. Nat Methods *6*, 843-849.

Dufourt, J., Bellec, M., Trullo, A., Dejean, M., De Rossi, S., Favard, C., and Lagha, M. (2021). Imaging translation dynamics in live embryos reveals spatial heterogeneities. Science *372*, 840-844.

Duncan, C.D.S., and Mata, J. (2011). Widespread Cotranslational Formation of Protein Complexes. PLoS Genet *7*.

Eckner, R., Ellmeier, W., and Birnstiel, M.L. (1991). Mature mRNA 3' end formation stimulates RNA export from the nucleus. EMBO J *10*, 3513-3522.

Edgley, M.L., and Riddle, D.L. (2001). LG II balancer chromosomes in Caenorhabditis elegans: mT1(II;III) and the mIn1 set of dominantly and recessively marked inversions. Mol Genet Genomics *266*, 385-395.

El Mouali, Y., and Balsalobre, C. (2019). 3'untranslated regions: regulation at the end of the road. Curr Genet *65*, 127-131.

Elkon, R., Ugalde, A.P., and Agami, R. (2013). Alternative cleavage and polyadenylation: extent, regulation and function. Nat Rev Genet *14*, 496-506.

Ellis, H.M., and Horvitz, H.R. (1986). Genetic control of programmed cell death in the nematode C. elegans. Cell *44*, 817-829.

Feng, J.G., Zhou, J.L., Lin, Y.X., and Huang, W.H. (2022). hnRNP A1 in RNA metabolism regulation and as a potential therapeutic target. Frontiers in Pharmacology *13*.

Fernandez-Cardenas, L.P., Villanueva-Chimal, E., Salinas, L.S., Jose-Nunez, C., Tuena de Gomez Puyou, M., and Navarro, R.E. (2017). Caenorhabditis elegans ATPase inhibitor factor 1 (IF1) MAI-2 preserves the mitochondrial membrane potential (Deltapsim) and is important to induce germ cell apoptosis. PLoS One *12*, e0181984.

Filipowicz, W., Bhattacharyya, S.N., and Sonenberg, N. (2008). Mechanisms of post-transcriptional regulation by microRNAs: are the answers in sight? Nature Reviews Genetics *9*, 102-114.

Franks, T.M., and Lykke-Andersen, J. (2008). The control of mRNA decapping and P-body formation. Mol Cell *32*, 605-615.

Frokjaer-Jensen, C., Davis, M.W., Ailion, M., and Jorgensen, E.M. (2012). Improved Mos1-mediated transgenesis in C. elegans. Nat Methods *9*, 117-118.

Frokjaer-Jensen, C., Davis, M.W., Hopkins, C.E., Newman, B.J., Thummel, J.M., Olesen, S.P., Grunnet, M., and Jorgensen, E.M. (2008). Single-copy insertion of transgenes in Caenorhabditis elegans. Nat Genet *40*, 1375-1383.

Fuchs, Y., and Steller, H. (2015). Live to die another way: modes of programmed cell death and the signals emanating from dying cells. Nature Reviews Molecular Cell Biology *16*, 329-344.

Gallie, D.R., Lewis, N.J., and Marzluff, W.F. (1996). The histone 3'-terminal stem-loop is necessary for translation in Chinese hamster ovary cells. Nucleic Acids Res *24*, 1954-1962.

Gallo, C.M., Munro, E., Rasoloson, D., Merritt, C., and Seydoux, G. (2008). Processing bodies and germ granules are distinct RNA granules that interact in C. elegans embryos. Dev Biol *323*, 76-87.

Gallo, S., Ricciardi, S., Manfrini, N., Pesce, E., Oliveto, S., Calamita, P., Mancino, M., Maffioli, E., Moro, M., Crosti, M.*, et al.* (2018). RACK1 Specifically Regulates Translation through Its Binding to Ribosomes. Mol Cell Biol *38*.

Gandin, V., Senft, D., Topisirovic, I., and Ronai, Z.A. (2013). RACK1 Function in Cell Motility and Protein Synthesis. Genes Cancer *4*, 369-377.

Geuens, T., Bouhy, D., and Timmerman, V. (2016). The hnRNP family: insights into their role in health and disease. Hum Genet *135*, 851-867.

Ghanta, K.S., Ishidate, T., and Mello, C.C. (2021). Microinjection for precision genome editing in Caenorhabditis elegans. STAR Protoc *2*, 100748.

Gilks, N., Kedersha, N., Ayodele, M., Shen, L., Stoecklin, G., Dember, L.M., and Anderson, P. (2004). Stress granule assembly is mediated by prion-like aggregation of TIA-1. Molecular Biology of the Cell *15*, 5383-5398.

Gimenez-Cassina, A., and Danial, N.N. (2015). Regulation of mitochondrial nutrient and energy metabolism by BCL-2 family proteins. Trends Endocrinol Metab *26*, 165-175.

Glinka, M., Herrmann, T., Funk, N., Havlicek, S., Rossoll, W., Winkler, C., and Sendtner, M. (2010). The heterogeneous nuclear ribonucleoprotein-R is necessary for axonal beta-actin mRNA translocation in spinal motor neurons. Hum Mol Genet *19*, 1951-1966.

Glisovic, T., Bachorik, J.L., Yong, J., and Dreyfuss, G. (2008). RNA-binding proteins and post-transcriptional gene regulation. Febs Lett *582*, 1977-1986.

Goldblatt, Z.E., Cirka, H.A., and Billiar, K.L. (2021). Mechanical Regulation of Apoptosis in the Cardiovascular System. Ann Biomed Eng *49*, 75-97.

Goraczniak, R., and Gunderson, S.I. (2008). The regulatory element in the 3'-untranslated region of human papillomavirus 16 inhibits expression by binding CUG-binding protein 1. J Biol Chem *283*, 2286-2296.

Gorgoni, B., Andrews, S., Schaller, A., Schumperli, D., Gray, N.K., and Muller, B. (2005). The stem-loop binding protein stimulates histone translation at an early step in the initiation pathway. RNA *11*, 1030-1042.

Gross, A., and Katz, S.G. (2017). Non-apoptotic functions of BCL-2 family proteins. Cell Death Differ *24*, 1348-1358.

Gross, A., McDonnell, J.M., and Korsmeyer, S.J. (1999). BCL-2 family members and the mitochondria in apoptosis. Genes Dev *13*, 1899-1911.

Grosset, C., Chen, C.Y.A., Xu, N.H., Sonenberg, N., Jacquemin-Sablon, H., and Shyu, A.B. (2000). A mechanism for translationally coupled mRNA turnover: Interaction between the poly(A) tail and a c-fos RNA coding determinant via a protein complex. Cell *103*, 29-40.

Grosswendt, S., Filipchyk, A., Manzano, M., Klironomos, F., Schilling, M., Herzog, M., Gottwein, E., and Rajewsky, N. (2014). Unambiguous Identification of miRNA: Target Site Interactions by Different Types of Ligation Reactions. Mol Cell *54*, 1042-1054.

Guhaniyogi, J., and Brewer, G. (2001). Regulation of mRNA stability in mammalian cells. Gene *265*, 11-23.

Gumienny, T.L., Lambie, E., Hartwieg, E., Horvitz, H.R., and Hengartner, M.O. (1999). Genetic control of programmed cell death in the Caenorhabditis elegans hermaphrodite germline. Development *126*, 1011-1022.

Gusarov, I., and Nudler, E. (1999). The mechanism of intrinsic transcription termination. Mol Cell *3*, 495-504.

Hatzold, J., and Conradt, B. (2008). Control of apoptosis by asymmetric cell division. PLoS Biol *6*, 771-784.

Haupt, K.A., Law, K.T., Enright, A.L., Kanzler, C.R., Shin, H., Wickens, M., and Kimble, J. (2020). A PUF Hub Drives Self-Renewal in Caenorhabditis elegans Germline Stem Cells. Genetics *214*, 147-161.

Heinrich, S., Sidler, C.L., Azzalin, C.M., and Weis, K. (2017). Stem-loop RNA labeling can affect nuclear and cytoplasmic mRNA processing. RNA *23*, 134-141.

Hengartner, M.O., Ellis, R.E., and Horvitz, H.R. (1992). Caenorhabditis elegans gene ced-9 protects cells from programmed cell death. Nature *356*, 494-499.

Hilleren, P., McCarthy, T., Rosbash, M., Parker, R., and Jensen, T.H. (2001). Quality control of mRNA 3 '-end processing is linked to the nuclear exosome. Nature *413*, 538-542.

Hirose, T., Galvin, B.D., and Horvitz, H.R. (2010). Six and Eya promote apoptosis through direct transcriptional activation of the proapoptotic BH3-only gene egl-1 in Caenorhabditis elegans. Proceedings of the National Academy of Sciences of the United States of America *107*, 15479-15484.

Hirose, T., and Horvitz, H.R. (2013). An Sp1 transcription factor coordinates caspase-dependent and -independent apoptotic pathways. Nature *500*, 354-+.

Hobor, F., Dallmann, A., Ball, N.J., Cicchini, C., Battistelli, C., Ogrodowicz, R.W., Christodoulou, E., Martin, S.R., Castello, A., Tripodi, M.*, et al.* (2018). A cryptic RNA-binding domain mediates Syncrip recognition and exosomal partitioning of miRNA targets. Nature Communications *9*.

Hockenbery, D., Nunez, G., Milliman, C., Schreiber, R.D., and Korsmeyer, S.J. (1990). Bcl-2 Is an Inner Mitochondrial-Membrane Protein That Blocks Programmed Cell-Death. Nature *348*, 334-336.

Hodgkin, J. (1987). A genetic analysis of the sex-determining gene, tra-1, in the nematode Caenorhabditis elegans. Genes Dev *1*, 731-745.

Horvitz, H.R. (1999). Genetic control of programmed cell death in the nematode Caenorhabditis elegans. Cancer Res *59*, 1701s-1706s.

Hughes, R., Gilley, J., Kristiansen, M., and Ham, J. (2011). The MEK-ERK pathway negatively regulates

expression through the 3′ UTR in sympathetic neurons. BMC Neurosci *12*.

Ichikawa, N., Ando, C., and Fumino, M. (2006). Caenorhabditis elegans MAI-1 protein, which is similar to mitochondrial ATPase inhibitor (IF1), can inhibit yeast F0F1-ATPase but cannot be transported to yeast mitochondria. J Bioenerg Biomembr *38*, 93-99.

Inohara, N., Ding, L.Y., Chen, S., and Nunez, G. (1997). harakiri, a novel regulator of cell death, encodes a protein that activates apoptosis and interacts selectively with survival-promoting proteins Bcl-2 and Bcl-X-L. EMBO J *16*, 1686-1694.

Izquierdo, J.M. (2010). Heterogeneous ribonucleoprotein C displays a repressor activity mediated by T-cell intracellular antigen-1-related/like protein to modulate Fas exon 6 splicing through a mechanism involving Hu antigen R. Nucleic Acids Res *38*, 8001-8014.

Ji, C., Deng, C., Antor, K., Bischler, T., Schneider, C., Fischer, U., Sendtner, M., and Briese, M. (2022). hnRNP R negatively regulates transcription by modulating the association of P-TEFb with 7SK and BRD4. EMBO Rep *23*, e55432.

Jiang, H.S., and Wu, Y.C. (2014). LIN-3/EGF Promotes the Programmed Cell Death of Specific Cells in Caenorhabditis elegans by Transcriptional Activation of the Pro-apoptotic Gene egl-1. PLoS Genet *10*.

Jiang, Y., Adhikari, D., Li, C., and Zhou, X. (2023). Spatiotemporal regulation of maternal mRNAs during vertebrate oocyte meiotic maturation. Biol Rev Camb Philos Soc *98*, 900-930.

Jurado, A.R., Tan, D., Jiao, X., Kiledjian, M., and Tong, L. (2014). Structure and function of pre-mRNA 5'-end capping quality control and 3'-end processing. Biochemistry *53*, 1882-1898.

Kabat, J.L., Barberan-Soler, S., and Zahler, A.M. (2009). HRP-2, the Caenorhabditis elegans Homolog of Mammalian Heterogeneous Nuclear Ribonucleoproteins Q and R, Is an Alternative Splicing Factor That Binds to UCUAUC Splicing Regulatory Elements. J Biol Chem *284*, 28490-28497.

Kamath, R.S., and Ahringer, J. (2003). Genome-wide RNAi screening in Caenorhabditis elegans. Methods *30*, 313-321.

Kamath, R.S., Fraser, A.G., Dong, Y., Poulin, G., Durbin, R., Gotta, M., Kanapin, A., Le Bot, N., Moreno, S., Sohrmann, M.*, et al.* (2003). Systematic functional analysis of the Caenorhabditis elegans genome using RNAi. Nature *421*, 231-237.

Kamer, I., Sarig, R., Zaltsman, Y., Niv, H., Oberkovitz, G., Regev, L., Haimovich, G., Lerenthal, Y., Marcellus, R.C., and Gross, A. (2005). Proapoptotic BID is an ATM effector in the DNA-damage response. Cell *122*, 593-603.

Kedersha, N.L., Gupta, M., Li, W., Miller, I., and Anderson, P. (1999). RNA-binding proteins TIA-1 and TIAR link the phosphorylation of eIF-2 alpha to the assembly of mammalian stress granules. J Cell Biol *147*, 1431-1442.

Kerr, J.F.R., Wyllie, A.H., and Currie, A.R. (1972). Apoptosis - Basic Biological Phenomenon with Wide-Ranging Implications in Tissue Kinetics. Br J Cancer *26*, 239-+.

Kershner, A.M., and Kimble, J. (2010). Genome-wide analysis of mRNA targets for Caenorhabditis elegans FBF, a conserved stem cell regulator. Proceedings of the National Academy of Sciences of the United States of America *107*, 3936-3941.

Kim, K., Colosimo, M.E., Yeung, H., and Sengupta, P. (2005). The UNC-3 Olf/EBF protein represses alternate neuronal programs to specify chemosensory neuron identity. Dev Biol *286*, 136-148.

Kinnaird, J.H., Maitland, K., Walker, G.A., Wheatley, I., Thompson, F.J., and Devaney, E. (2004). HRP-2, a heterogeneous nuclear ribonucleoprotein, is essential for embryogenesis and oogenesis in Caenorhabditis elegans. Exp Cell Res *298*, 418-430.

Komili, S., and Silver, P.A. (2008). Coupling and coordination in gene expression processes: a systems biology view. Nat Rev Genet *9*, 38-48.

Korn, S.M., and Schlundt, A. (2022). Structures and nucleic acid-binding preferences of the eukaryotic ARID domain. Biol Chem *403*, 731-747.

Kratsios, P., Stolfi, A., Levine, M., and Hobert, O. (2012). Coordinated regulation of cholinergic motor neuron traits through a conserved terminal selector gene. Nat Neurosci *15*, 205-214.

Lai, C.H., Chou, C.Y., Ch'ang, L.Y., Liu, C.S., and Lin, W. (2000). Identification of novel human genes evolutionarily conserved in Caenorhabditis elegans by comparative proteomics. Genome Res *10*, 703-713.

Lamont, L.B., Crittenden, S.L., Bernstein, D., Wickens, M., and Kimble, J. (2004). FBF-1 and FBF-2 regulate the size of the mitotic region in the C-elegans germline. Dev Cell *7*, 697-707.

Large, E.E., and Mathies, L.D. (2014). Caenorhabditis elegans SWI/SNF subunits control sequential developmental stages in the somatic gonad. G3 (Bethesda) *4*, 471-483.

Lecerf, J.M., Shirley, T.L., Zhu, Q., Kazantsev, A., Amersdorfer, P., Housman, D.E., Messer, A., and Huston, J.S. (2001). Human single-chain Fv intrabodies counteract in situ huntingtin aggregation in cellular models of Huntington's disease. Proc Natl Acad Sci U S A *98*, 4764-4769.

Lee, A.S.Y., Kranzusch, P.J., and Cate, J.H.D. (2015). eIF3 targets cell-proliferation messenger RNAs for translational activation or repression. Nature *522*, 111-U292.

Lee, S.K., Li, W., Ryu, S.E., Rhim, T., and Ahnn, J. (2010). Vacuolar (H+)-ATPases in Caenorhabditis elegans: What can we learn about giant H+ pumps from tiny worms? Biochimica Et Biophysica Acta-Bioenergetics *1797*, 1687-1695.

Lee, Y., and Rio, D.C. (2015). Mechanisms and Regulation of Alternative Pre-mRNA Splicing. Annu Rev Biochem *84*, 291-323.

LeGendre, J.B., Campbell, Z.T., Kroll-Conner, P., Anderson, P., Kimble, J., and Wickens, M. (2013). RNA Targets and Specificity of Staufen, a Double-stranded RNA-binding Protein in Caenorhabditis elegans. J Biol Chem *288*, 2532-2545.

Letai, A. (2017). Apoptosis and Cancer. Annual Review of Cancer Biology, Vol 1 *1*, 275-294.

Licatalosi, D.D., Mele, A., Fak, J.J., Ule, J., Kayikci, M., Chi, S.W., Clark, T.A., Schweitzer, A.C., Blume, J.E., Wang, X.N.*, et al.* (2008). HITS-CLIP yields genome-wide insights into brain alternative RNA processing. Nature *456*, 464-U422.

Liu, H.R., Strauss, T.J., Potts, M.B., and Cameron, S. (2006). Direct regulation of egl-1 and of programmed cell death by the Hox protein MAB-5 and by CEH-20, a C-elegans homolog of Pbx1. Development *133*, 641-650.

Lizcano, J.M., Morrice, N., and Cohen, P. (2000). Regulation of BAD by cAMP-dependent protein kinase is mediated via phosphorylation of a novel site, Ser(155). Biochem J *349*, 547-557.

Lomonosova, E., and Chinnadurai, G. (2008). BH3-only proteins in apoptosis and beyond: an overview. Oncogene *27 Suppl 1*, S2-19.

Lutje Hulsik, D., Liu, Y.Y., Strokappe, N.M., Battella, S., El Khattabi, M., McCoy, L.E., Sabin, C., Hinz, A., Hock, M., Macheboeuf, P.*, et al.* (2013). A gp41 MPER-specific llama VHH requires a hydrophobic CDR3 for neutralization but not for antigen recognition. PLoS Pathog *9*, e1003202.

Maduro, M., and Pilgrim, D. (1995). Identification and cloning of unc-119, a gene expressed in the Caenorhabditis elegans nervous system. Genetics *141*, 977-988.

Maniatis, T., and Reed, R. (2002). An extensive network of coupling among gene expression machines. Nature *416*, 499-506.

Mansfield, K.D., and Keene, J.D. (2012). Neuron-specific ELAV/Hu proteins suppress HuR mRNA during neuronal differentiation by alternative polyadenylation. Nucleic Acids Res *40*, 2734-2746.

Martin, K.C., and Ephrussi, A. (2009). mRNA localization: gene expression in the spatial dimension. Cell *136*, 719-730.

Marzluff, W.F., and Koreski, K.P. (2017). Birth and Death of Histone mRNAs. Trends Genet *33*, 745-759.

Marzluff, W.F., Wagner, E.J., and Duronio, R.J. (2008). Metabolism and regulation of canonical histone mRNAs: life without a poly(A) tail. Nature Reviews Genetics *9*, 843-854.

Matia-Gonzalez, A.M., Laing, E.E., and Gerber, A.P. (2015). Conserved mRNA-binding proteomes in eukaryotic organisms. Nat Struct Mol Biol *22*, 1027-1033.

Matoulkova, E., Michalova, E., Vojtesek, B., and Hrstka, R. (2012). The role of the 3' untranslated region in post-transcriptional regulation of protein expression in mammalian cells. RNA Biol *9*, 563-576.

Matsui, H., Asou, H., and Inaba, T. (2007). Cytokines direct the regulation of Bim mRNA stability by heat-shock cognate protein 70. Mol Cell *25*, 99-112.

Mayr, C. (2017). Regulation by 3'-Untranslated Regions. Annu Rev Genet *51*, 171-194.

McDermott, S.M., Meignin, C., Rappsilber, J., and Davis, I. (2012). Drosophila Syncrip binds the gurken mRNA localisation signal and regulates localised transcripts during axis specification. Biology Open *1*, 488-497.

Mcdonnell, T.J., and Korsmeyer, S.J. (1991). Progression from Lymphoid Hyperplasia to High-Grade Malignant-Lymphoma in Mice Transgenic for the T(14, 18). Nature *349*, 254-256.

McHugh, C.A., Russell, P., and Guttman, M. (2014). Methods for comprehensive experimental identification of RNA-protein interactions. Genome Biol *15*, 203.

Merritt, C., and Seydoux, G. (2010). The Puf RNA-binding proteins FBF-1 and FBF-2 inhibit the expression of synaptonemal complex proteins in germline stem cells. Development *137*, 1787-1798.

Mili, S., Shu, H.J., Zhao, Y., and Pinol-Roma, S. (2001). Distinct RNP complexes of shuttling hnRNP proteins with pre-mRNA and mRNA: candidate intermediates in formation and export of mRNA. Mol Cell Biol *21*, 7307-7319.

Mishra, N., Wei, H., and Conradt, B. (2018). Caenorhabditis elegans ced-3 Caspase Is Required for Asymmetric Divisions That Generate Cells Programmed To Die. Genetics *210*, 983-998.

Miska, E.A., Alvarez-Saavedra, E., Abbott, A.L., Lau, N.C., Hellman, A.B., McGonagle, S.M., Bartel, D.P., Ambros, V.R., and Horvitz, H.R. (2007). Most Caenorhabditis elegans microRNAs are individually not essential for development or viability. PLoS Genet *3*, 2395-2403.

Mok, C.L., Gil-Gomez, G., Williams, O., Coles, M., Taga, S., Tolaini, M., Norton, T., Kioussis, D., and Brady, H.J.M. (1999). Bad can act as a key regulator of T cell apoptosis and T cell development. J Exp Med *189*, 575-586.

Morisaki, T., Lyon, K., DeLuca, K.F., DeLuca, J.G., English, B.P., Zhang, Z.J., Lavis, L.D., Grimm, J.B., Viswanathan, S., Looger, L.L., *et al.* (2016). Real-time quantification of single RNA translation dynamics in living cells. Science *352*, 1425-1429.

Nachtergaele, S., and He, C. (2018). Chemical Modifications in the Life of an mRNA Transcript. Annual Review of Genetics, Vol 52 *52*, 349-+.

Nagata, S. (2018). Apoptosis and Clearance of Apoptotic Cells. Annual Review of Immunology, Vol 36 *36*, 489-517.

Nehme, R., and Conradt, B. (2008). egl-1: a key activator of apoptotic cell death in C-elegans. Oncogene *27*, S30-S40.

Nilsson, J., Sengupta, J., Frank, J., and Nissen, P. (2004). Regulation of eukaryotic translation by the RACK1 protein: a platform for signalling molecules on the ribosome. EMBO Rep *5*, 1137-1141.

Noma, K., and Jin, Y. (2016). Optogenetic Random Mutagenesis Using Histone-miniSOG in C. elegans. J Vis Exp.

Noma, K., and Jin, Y. (2018). Rapid Integration of Multi-copy Transgenes Using Optogenetic Mutagenesis in Caenorhabditis elegans. G3 (Bethesda) *8*, 2091-2097.

Ochs, M.E., Josephson, M.P., and Lundquist, E.A. (2020). The Predicted RNA-Binding Protein ETR-1/CELF1 Acts in Muscles To Regulate Neuroblast Migration in Caenorhabditis elegans. G3 (Bethesda) *10*, 2365-2376.

Oda, E., Ohki, R., Murasawa, H., Nemoto, J., Shibue, T., Yamashita, T., Tokino, T., Taniguchi, T., and Tanaka, N. (2000). Noxa, a BH3-only member of the Bcl-2 family and candidate mediator of p53-induced apoptosis. Science *288*, 1053-1058.

Okouchi, M., Ekshyyan, O., Maracine, M., and Aw, T.Y. (2007). Neuronal apoptosis in neurodegeneration. Antioxid Redox Signal *9*, 1059-1096.

Opferman, J.T., and Korsmeyer, S.J. (2003). Apoptosis in the development and maintenance of the immune system. Nat Immunol *4*, 410-415.

Pan, Q., Shai, O., Lee, L.J., Frey, B.J., and Blencowe, B.J. (2008). Deep surveying of alternative splicing complexity in the human transcriptome by high-throughput sequencing. Nat Genet *40*, 1413-1415.

Perez-Garijo, A., and Steller, H. (2015). Spreading the word: non-autonomous effects of apoptosis during development, regeneration and disease. Development *142*, 3253-3262.

Pestova, T.V., Kolupaeva, V.G., Lomakin, I.B., Pilipenko, E.V., Shatsky, I.N., Agol, V.I., and Hellen, C.U.T. (2001). Molecular mechanisms of translation initiation in eukaryotes. Proceedings of the National Academy of Sciences of the United States of America *98*, 7029-7036.

Pinto, P.A., Henriques, T., Freitas, M.O., Martins, T., Domingues, R.G., Wyrzykowska, P.S., Coelho, P.A., Carmo, A.M., Sunkel, C.E., Proudfoot, N.J.*, et al.* (2011). RNA polymerase II kinetics in polo polyadenylation signal selection. EMBO J *30*, 2431-2444.

Porter, D.F., Prasad, A., Carrick, B.H., Kroll-Connor, P., Wickens, M., and Kimble, J. (2019). Toward Identifying Subnetworks from FBF Binding Landscapes in Caenorhabditis Spermatogenic or Oogenic Germlines. G3-Genes Genomes Genetics *9*, 153-165.

Pourkarimi, E., Greiss, S., and Gartner, A. (2012). Evidence that CED-9/Bcl2 and CED-4/Apaf-1 localization is not consistent with the current model for C. elegans apoptosis induction. Cell Death Differ *19*, 406-415.

Prasad, A., Porter, D.F., Kroll-Conner, P.L., Mohanty, I., Ryan, A.R., Crittenden, S.L., Wickens, M., and Kimble, J. (2016). The PUF binding landscape in metazoan germ cells. RNA *22*, 1026-1043.

Prasher, D.C., Eckenrode, V.K., Ward, W.W., Prendergast, F.G., and Cormier, M.J. (1992). Primary structure of the Aequorea victoria green-fluorescent protein. Gene *111*, 229-233.

Proudfoot, N.J. (2016). Transcriptional termination in mammals: Stopping the RNA polymerase II juggernaut. Science *352*, aad9926.

Ramanathan, A., Robb, G.B., and Chan, S.H. (2016). mRNA capping: biological functions and applications. Nucleic Acids Res *44*, 7511-7526.

Ramat, A., and Simonelig, M. (2021). Functions of PIWI Proteins in Gene Regulation: New Arrows Added to the piRNA Quiver. Trends Genet *37*, 188-200.

Ran, F.A., Hsu, P.D., Wright, J., Agarwala, V., Scott, D.A., and Zhang, F. (2013). Genome engineering using the CRISPR-Cas9 system. Nat Protoc *8*, 2281-2308.

Reddien, P.W., Andersen, E.C., Huang, M.C., and Horvitz, H.R. (2007). DPL-1 DP, LIN-35 Rb and EFL-1 E2F act with the MCD-1 zinc-finger protein to promote programmed cell death in Caenorhabditis elegans. Genetics *175*, 1719-1733.

Redemann, S., Schloissnig, S., Ernst, S., Pozniakowsky, A., Ayloo, S., Hyman, A.A., and Bringmann, H. (2011). Codon adaptation-based control of protein expression in C. elegans. Nat Methods *8*, 250-252.

Ren, Z.J., Veksler-Lublinsky, I., Morrissey, D., and Ambros, V. (2016). Staufen Negatively Modulates MicroRNA Activity in Caenorhabditis elegans. G3-Genes Genom Genet *6*, 1227-1237.

Richard, J.P., Zuryn, S., Fischer, N., Pavet, V., Vaucamps, N., and Jarriault, S. (2011). Direct in vivo cellular reprogramming involves transition through discrete, non-pluripotent steps. Development *138*, 1483-1492.

Rieckher, M., and Tavernarakis, N. (2017). Generation of Caenorhabditis elegans Transgenic Animals by DNA Microinjection. Bio-Protocol *7*.

Ripin, N., Boudet, J., Duszczyk, M.M., Hinniger, A., Faller, M., Krepl, M., Gadi, A., Schneider, R.J., Sponer, J., Meisner-Kober, N.C*., et al.* (2019). Molecular basis for AU-rich element recognition and dimerization by the HuR C-terminal RRM. Proceedings of the National Academy of Sciences of the United States of America *116*, 2935-2944.

Roegiers, F., and Jan, Y.N. (2000). Staufen: a common component of mRNA transport in oocytes and neurons? Trends Cell Biol *10*, 220-224.

Rogalska, M.E., Vivori, C., and Valcarcel, J. (2023). Regulation of pre-mRNA splicing: roles in physiology and disease, and therapeutic prospects. Nature Reviews Genetics *24*, 251-269.

Rolland, S.G., Schneid, S., Schwarz, M., Rackles, E., Fischer, C., Haeussler, S., Regmi, S.G., Yeroslaviz, A., Habermann, B., Mokranjac, D.*, et al.* (2019). Compromised Mitochondrial Protein Import Acts as a Signal for UPR^{mt}. Cell reports *28*, 1659-1669.e1655.

Rose, L., and Gonczy, P. (2014). Polarity establishment, asymmetric division and segregation of fate determinants in early C. elegans embryos. WormBook, 1-43.

Rossoll, W., Jablonka, S., Andreassi, C., Kroning, A.K., Karle, K., Monani, U.R., and Sendtner, M. (2003). Smn, the spinal muscular atrophy-determining gene product, modulates axon growth and localization of beta-actin mRNA in growth cones of motoneurons. J Cell Biol *163*, 801-812.

Roufayel, R., Younes, K., Al-Sabi, A., and Murshid, N. (2022). BH3-Only Proteins Noxa and Puma Are Key Regulators of Induced Apoptosis. Life (Basel) *12*.

Rowley, J.D. (1973). Letter: A new consistent chromosomal abnormality in chronic myelogenous leukaemia identified by quinacrine fluorescence and Giemsa staining. Nature *243*, 290-293.

Rowley, J.D. (1988). Chromosome studies in the non-Hodgkin's lymphomas: the role of the 14;18 translocation. J Clin Oncol *6*, 919-925.

Rual, J.F., Ceron, J., Koreth, J., Hao, T., Nicot, A.S., Hirozane-Kishikawa, T., Vandenhaute, J., Orkin, S.H., Hill, D.E., van den Heuvel, S.*, et al.* (2004). Toward improving Caenorhabditis elegans phenome mapping with an ORFeome-based RNAi library. Genome Res *14*, 2162-2168.

Sanchez, R., and Marzluff, W.F. (2002). The stem-loop binding protein is required for efficient translation of histone mRNA in vivo and in vitro. Mol Cell Biol *22*, 7093-7104.

Sandberg, R., Neilson, J.R., Sarma, A., Sharp, P.A., and Burge, C.B. (2008). Proliferating cells express mRNAs with shortened 3' untranslated regions and fewer microRNA target sites. Science *320*, 1643-1647.

Santangelo, L., Giurato, G., Cicchini, C., Montaldo, C., Mancone, C., Tarallo, R., Battistelli, C., Alonzi, T., Weisz, A., and Tripodi, M. (2016). The RNA-Binding Protein SYNCRIP Is a Component of the Hepatocyte Exosomal Machinery Controlling MicroRNA Sorting. Cell Reports *17*, 799-808.

Scherrer, T., Mittal, N., Janga, S.C., and Gerber, A.P. (2010). A screen for RNA-binding proteins in yeast indicates dual functions for many enzymes. PLoS One *5*, e15499.

Schindelin, J., Arganda-Carreras, I., Frise, E., Kaynig, V., Longair, M., Pietzsch, T., Preibisch, S., Rueden, C., Saalfeld, S., Schmid, B.*, et al.* (2012). Fiji: an open-source platform for biological-image analysis. Nat Methods *9*, 676-682.

Schmitz, C., Kinge, P., and Hutter, H. (2007). Axon guidance genes identified in a large-scale RNAi screen using the RNAi -hypersensitive Caenorhabditis elegans strain nre-1(hd20) lin-15b(hd126). Proceedings of the National Academy of Sciences of the United States of America *104*, 834-839.

Schnabel, R., Bischoff, M., Hintze, A., Schulz, A.K., Hejnol, A., Meinhardt, H., and Hutter, H. (2006). Global cell sorting in the C. elegans embryo defines a new mechanism for pattern formation. Dev Biol *294*, 418-431.

Schnabel, R., Hutter, H., Moerman, D., and Schnabel, H. (1997). Assessing normal embryogenesis in Caenorhabditis elegans using a 4D microscope: variability of development and regional specification. Dev Biol *184*, 234-265.

Schwanhausser, B., Busse, D., Li, N., Dittmar, G., Schuchhardt, J., Wolf, J., Chen, W., and Selbach, M. (2011). Global quantification of mammalian gene expression control. Nature *473*, 337-342.

Shaham, S., Reddien, P.W., Davies, B., and Horvitz, H.R. (1999). Mutational analysis of the Caenorhabditis elegans cell-death gene ced-3. Genetics *153*, 1655-1671.

Shamas-Din, A., Brahmbhatt, H., Leber, B., and Andrews, D.W. (2011). BH3-only proteins: Orchestrators of apoptosis. Biochim Biophys Acta *1813*, 508-520.

Shan, J., Munro, T.P., Barbarese, E., Carson, J.H., and Smith, R. (2003). A molecular mechanism for mRNA trafficking in neuronal dendrites. J Neurosci *23*, 8859-8866.

Sherrard, R., Luehr, S., Holzkamp, H., McJunkin, K., Memar, N., and Conradt, B. (2017). miRNAs cooperate in apoptosis regulation during C. elegans development. Genes Dev *31*, 209-222.

Shi, Y. (2012). Alternative polyadenylation: new insights from global analyses. RNA *18*, 2105-2117.

Shimabukuro, M., Ishida, M., Yagi, S., Fukuda, D., Soeki, T., and Sata, M. (2014). Post-transcriptional regulation of adiponectin by microRNA-378 in adipose tissue: a novel mechanism for hypoadiponectinemia. Eur Heart J *35*, 272-272.

Shukla, K.K., Mahdi, A.A., and Rajender, S. (2012). Apoptosis, spermatogenesis and male infertility. Front Biosci (Elite Ed) *4*, 746-754.

Souers, A.J., Leverson, J.D., Boghaert, E.R., Ackler, S.L., Catron, N.D., Chen, J., Dayton, B.D., Ding, H., Enschede, S.H., Fairbrother, W.J.*, et al.* (2013). ABT-199, a potent and selective BCL-2 inhibitor, achieves antitumor activity while sparing platelets. Nat Med *19*, 202-208.

Steber, H.S., Gallante, C., O'Brien, S., Chiu, P.L., and Mangone, M. (2019). The C. elegans 3' UTRome v2 resource for studying mRNA cleavage and polyadenylation, 3'-UTR biology, and miRNA targeting. Genome Res *29*, 2104-2116.

Sulston, J.E., and Horvitz, H.R. (1977). Post-embryonic cell lineages of the nematode, Caenorhabditis elegans. Dev Biol *56*, 110-156.

Sulston, J.E., Schierenberg, E., White, J.G., and Thomson, J.N. (1983). The Embryonic-Cell Lineage of the Nematode Caenorhabditis-Elegans. Dev Biol *100*, 64-119.

Sun, Y.N., Li, M.J., Zhao, D.F., Li, X., Yang, C.L., and Wang, X.C. (2020). Lysosome activity is modulated by multiple longevity pathways and is important for lifespan extension in C. elegans. Elife *9*.

Surova, O., and Zhivotovsky, B. (2013). Various modes of cell death induced by DNA damage. Oncogene *32*, 3789-3797.

Susor, A., Jansova, D., Cerna, R., Danylevska, A., Anger, M., Toralova, T., Malik, R., Supolikova, J., Cook, M.S., Oh, J.S.*, et al.* (2015). Temporal and spatial regulation of translation in the mammalian oocyte via the mTOR-eIF4F pathway. Nature Communications *6*.

Svitkin, Y.V., Yanagiya, A., Karetnikov, A.E., Alain, T., Fabian, M.R., Khoutorsky, A., Perreault, S., Topisirovic, I., and Sonenberg, N. (2013). Control of Translation and miRNA-Dependent Repression by a Novel Poly(A) Binding Protein, hnRNP-Q. PLoS Biol *11*.

Syntichaki, P., Samara, C., and Tavernarakis, N. (2005). The vacuolar H+ -ATPase mediates intracellular acidification required for neurodegeneration in C. elegans. Curr Biol *15*, 1249-1254.

Sze, J.Y., Victor, M., Loer, C., Shi, Y., and Ruvkun, G. (2000). Food and metabolic signaling defects in a Caenorhabditis elegans serotonin-synthesis mutant. Nature *403*, 560-564.

Tamburino, A.M., Ryder, S.P., and Walhout, A.J. (2013). A compendium of Caenorhabditis elegans RNA binding proteins predicts extensive regulation at multiple levels. G3 (Bethesda) *3*, 297-304.

Tan, D.Z., Marzluff, W.F., Dominski, Z., and Tong, L. (2013). Structure of Histone mRNA Stem-Loop, Human Stem-Loop Binding Protein, and 3 ' hExo Ternary Complex. Science *339*, 318-321.

Tan, F.J., Fire, A.Z., and Hill, R.B. (2007). Regulation of apoptosis by C. elegans CED-9 in the absence of the C-terminal transmembrane domain. Cell Death Differ *14*, 1925-1935.

Tan, Y., Demeter, M.R., Ruan, H., and Comb, M.J. (2000). BAD Ser-155 phosphorylation regulates BAD/Bcl-XL interaction and cell survival. J Biol Chem *275*, 25865-25869.

Tanenbaum, M.E., Gilbert, L.A., Qi, L.S., Weissman, J.S., and Vale, R.D. (2014). A protein-tagging system for signal amplification in gene expression and fluorescence imaging. Cell *159*, 635-646.

Tang, D., Kang, R., Berghe, T.V., Vandenabeele, P., and Kroemer, G. (2019). The molecular machinery of regulated cell death. Cell Res *29*, 347-364.

Taylor, R.C., Cullen, S.P., and Martin, S.J. (2008). Apoptosis: controlled demolition at the cellular level. Nature Reviews Molecular Cell Biology *9*, 231-241.

Thellmann, M., Hatzold, J., and Conradt, B. (2003). The Snail-like CES-1 protein of C-elegans can block the expression of the BH3-only cell-death activator gene egl-1 by antagonizing the function of bHLH proteins. Development *130*, 4057-4071.

Thompson, M.K., Rojas-Duran, M.F., Gangaramani, P., and Gilbert, W.V. (2016). The ribosomal protein Asc1/RACK1 is required for efficient translation of short mRNAs. Elife *5*.

Tran, A.T., Chapman, E.M., Flamand, M.N., Yu, B., Krempel, S.J., Duchaine, T.F., Eroglu, M., and Derry, W.B. (2019). MiR-35 buffers apoptosis thresholds in the C. elegans germline by antagonizing both MAPK and core apoptosis pathways. Cell Death Differ *26*, 2637-2651.

Tse, C., Shoemaker, A.R., Adickes, J., Anderson, M.G., Chen, J., Jin, S., Johnson, E.F., Marsh, K.C., Mitten, M.J., Nimmer, P.*, et al.* (2008). ABT-263: a potent and orally bioavailable Bcl-2 family inhibitor. Cancer Res *68*, 3421-3428.

Tsujimoto, Y., Finger, L.R., Yunis, J., Nowell, P.C., and Croce, C.M. (1984). Cloning of the chromosome breakpoint of neoplastic B cells with the t(14;18) chromosome translocation. Science *226*, 1097-1099.

Tsvetanova, N.G., Klass, D.M., Salzman, J., and Brown, P.O. (2010). Proteome-wide search reveals unexpected RNA-binding proteins in Saccharomyces cerevisiae. PLoS One *5*.

Valencia-Sanchez, M.A., Liu, J.D., Hannon, G.J., and Parker, R. (2006). Control of translation and mRNA degradation by miRNAs and siRNAs. Genes Dev *20*, 515-524.

Van Nostrand, E.L., Pratt, G.A., Shishkin, A.A., Gelboin-Burkhart, C., Fang, M.Y., Sundararaman, B., Blue, S.M., Nguyen, T.B., Surka, C., Elkins, K.*, et al.* (2016). Robust transcriptome-wide discovery of RNA-binding protein binding sites with enhanced CLIP (eCLIP). Nat Methods *13*, 508-514.

Vaux, D.L., Cory, S., and Adams, J.M. (1988). Bcl-2 gene promotes haemopoietic cell survival and cooperates with c-myc to immortalize pre-B cells. Nature *335*, 440-442.

Verma, S., Zhao, L.J., and Chinnadurai, G. (2001). Phosphorylation of the pro-apoptotic protein BIK: mapping of phosphorylation sites and effect on apoptosis. J Biol Chem *276*, 4671-4676.

Vlasova-St Louis, I., and Bohjanen, P.R. (2011). Coordinate regulation of mRNA decay networks by GU-rich elements and CELF1. Curr Opin Genet Dev *21*, 444-451.

Vlasova, I.A., Tahoe, N.M., Fan, D., Larsson, O., Rattenbacher, B., Sternjohn, J.R., Vasdewani, J., Karypis, G., Reilly, C.S., Bitterman, P.B.*, et al.* (2008). Conserved GU-rich elements mediate mRNA decay by binding to CUG-binding protein 1. Mol Cell *29*, 263-270.

Wahl, M.C., Will, C.L., and Luhrmann, R. (2009). The Spliceosome: Design Principles of a Dynamic RNP Machine. Cell *136*, 701-718.

Wang, E.T., Sandberg, R., Luo, S., Khrebtukova, I., Zhang, L., Mayr, C., Kingsmore, S.F., Schroth, G.P., and Burge, C.B. (2008). Alternative isoform regulation in human tissue transcriptomes. Nature *456*, 470-476.

Wang, J.B., Chitturi, J., Ge, Q.L., Laskova, V., Wang, W., Li, X., Ding, M., Zhen, M., and Huang, X. (2015). The C-elegans COE transcription factor UNC-3 activates

lineage-specific apoptosis and affects neurite growth in the RID lineage. Development *142*, 1447-1457.

Wang, X., Zhao, Y., Wong, K., Ehlers, P., Kohara, Y., Jones, S.J., Marra, M.A., Holt, R.A., Moerman, D.G., and Hansen, D. (2009). Identification of genes expressed in the hermaphrodite germ line of C. elegans using SAGE. BMC Genomics *10*, 213.

Wei, H., Yan, B., Gagneur, J., and Conradt, B. (2017). Caenorhabditis elegans CES-1 Snail Represses pig-1 MELK Expression To Control Asymmetric Cell Division. Genetics *206*, 2069-2084.

Wickham, L., Duchaine, T., Luo, M., Nabi, I.R., and DesGroseillers, L. (1999). Mammalian Staufen is a double-stranded-RNA- and tubulin-binding protein which localizes to the rough endoplasmic reticulum. Mol Cell Biol *19*, 2220-2230.

Wu, B., Qiu, W., Wang, P., Yu, H., Cheng, T., Zambetti, G.P., Zhang, L., and Yu, J. (2007). p53 independent induction of PUMA mediates intestinal apoptosis in response to ischaemia-reperfusion. Gut *56*, 645-654.

Yan, B., Memar, N., Gallinger, J., and Conradt, B. (2013). Coordination of Cell Proliferation and Cell Fate Determination by CES-1 Snail. PLoS Genet *9*.

Yan, N., Chai, J.J., Lee, E.S., Gu, L.C., Liu, Q., He, J.Q., Wu, J.W., Kokel, D., Li, H.L., Hao, Q.*, et al.* (2005). Structure of the CED-4-CED-9 complex provides insights into programmed cell death in Caenorhabditis elegans. Nature *437*, 831-837.

Yan, X., Hoek, T.A., Vale, R.D., and Tanenbaum, M.E. (2016). Dynamics of Translation of Single mRNA Molecules In Vivo. Cell *165*, 976-989.

Yang, B., Schwartz, M., and McJunkin, K. (2020). In vivo CRISPR screening for phenotypic targets of the mir-35-42 family in C. elegans. Genes Dev *34*, 1227-1238.

Yin, X.M. (2006). Bid, a BH3-only multi-functional molecule, is at the cross road of life and death. Gene *369*, 7-19.

Yoo, H., Cha, H.J., Lee, J., Yu, E.O., Bae, S., Jung, J.H., Sohn, I., Lee, S.J., Yang, K.H., Woo, S.H.*, et al.* (2008). Specific proteolysis of the A-kinase-anchoring protein 149 at the Asp582 residue by caspases during apoptosis. Oncol Rep *19*, 1577-1582.

You, L.L., Omollo, E.O., Yu, C.Z., Mooney, R.A., Shi, J., Shen, L.Q., Wu, X.X., Wen, A.J., He, D.W., Zeng, Y.*, et al.* (2023). Structural basis for intrinsic transcription termination. Nature.

Zetsche, B., Gootenberg, J.S., Abudayyeh, O.O., Slaymaker, I.M., Makarova, K.S., Essletzbichler, P., Volz, S.E., Joung, J., van der Oost, J., Regev, A.*, et al.* (2015). Cpf1 Is a Single RNA-Guided Endonuclease of a Class 2 CRISPR-Cas System. Cell *163*, 759-771.

Zha, J.P., Harada, H., Yang, E., Jockel, J., and Korsmeyer, S.J. (1996). Serine phosphorylation of death agonist BAD in response to survival factor results in binding to 14-3-3 not BGL-X(L). Cell *87*, 619-628.

Zhang, B.L., Gallegos, M., Puoti, A., Durkin, E., Fields, S., Kimble, J., and Wickens, M.P. (1997). A conserved RNA-binding protein that regulates sexual fates in the C-elegans hermaphrodite germ line. Nature *390*, 477-484.

Zhang, H., Lee, J.Y., and Tian, B. (2005). Biased alternative polyadenylation in human tissues. Genome Biol *6*, R100.

Zhang, J., Tan, D.Z., DeRose, E.F., Perera, L., Dominski, Z., Marzluff, W.F., Tong, L., and Hall, T.M.T. (2014). Molecular mechanisms for the regulation of histone mRNA stem-loop-binding protein by phosphorylation. Proceedings of the National Academy of Sciences of the United States of America *111*, E2937-E2946.

Zhao, N., Kamijo, K., Fox, P.D., Oda, H., Morisaki, T., Sato, Y., Kimura, H., and Stasevich, T.J. (2019). A genetically encoded probe for imaging nascent and mature HA-tagged proteins in vivo. Nat Commun *10*, 2947.

Zhu, H., Zhou, H.L., Hasman, R.A., and Lou, H. (2007). Hu proteins regulate polyadenylation by blocking sites containing U-rich sequences. J Biol Chem *282*, 2203-2210.

Zinkel, S.S., Hurov, K.E., Ong, C., Abtahl, F.M., Gross, A., and Korsmeyer, S.J. (2005). A role for proapoptotic BID in the DNA-damage response. Cell *122*, 579-591.

Zisoulis, D.G., Lovci, M.T., Wilbert, M.L., Hutt, K.R., Liang, T.Y., Pasquinelli, A.E., and Yeo, G.W. (2010). Comprehensive discovery of endogenous Argonaute binding sites in Caenorhabditis elegans. Nat Struct Mol Biol *17*, 173-U176.